VIBRATIONAL SUM-FREQUENCY SPECTROSCOPY INVESTIGATIONS OF CARBOXYLIC ACID BASED SURFACTANTS AND POLYMERS AT THE OIL-WATER INTERFACE

by

DANIEL KEITH BEAMAN

A DISSERTATION

Presented to the Department of Chemistry
and the Graduate School of the University of Oregon
in partial fulfillment of the requirements
for the degree of
Doctor of Philosophy

September 2010

University of Oregon Graduate School

Confirmation of Approval and Acceptance of Dissertation prepared by:

Daniel Beaman

Title:

"Vibrational Sum-Frequency Spectroscopy Investigations of Carboxylic Acid Based Surfactants and Polymers at the Oil-Water Interface"

This dissertation has been accepted and approved in partial fulfillment of the requirements for the degree in the Department of Chemistry by:

Thomas Dyke, Chairperson, Chemistry
Geraldine Richmond, Advisor, Chemistry
John Hardwick, Member, Chemistry
Jeffrey Cina, Member, Chemistry
J. Andrew Berglund, Member, Chemistry
John Conery, Outside Member, Computer & Information Science

and Richard Linton, Vice President for Research and Graduate Studies/Dean of the Graduate School for the University of Oregon.

September 4, 2010

Original approval signatures are on file with the Graduate School and the University of Oregon Libraries.

An Abstract of the Dissertation of

Daniel Keith Beaman for the degree of Doctor of Philosophy

in the Department of Chemistry to be taken September 2010

Title: VIBRATIONAL SUM-FREQUENCY SPECTROSCOPY INVESTIGATIONS OF CARBOXYLIC ACID BASED SURFACTANTS AND POLYMERS AT THE OIL-WATER INTERFACE

Approved: _____
Dr. Geraldine L. Richmond

Aqueous solutes next to hydrophobic interfaces are prevalent in a multitude of chemical and biological systems throughout the world. Their presence ranges from environmental processes such as soil and water remediation to biological processes such as ion transport, membrane formation, and enzyme activity. In these and other examples, the interface is an integral part of the system. Understanding these chemically complex systems requires that a molecular level picture be built as a starting basis. In this dissertation, vibrational sum-frequency spectroscopy (VSFS), a surface selective non-linear optical technique, is used to obtain a fundamental

understanding of the interfacial properties of carboxylic acid based surfactants and polymers at the oil-water interface.

Interfacial studies of the solvating environment around a carboxylate headgroup surfactant are presented first. By utilizing different VSFS polarization schemes, the carboxylate vibrational stretching region was used to monitor the headgroup environment. Results showed the oil-water interface provides a unique environment for adsorption and structuring, and distinct differences exist from the air-water and solid-water interface.

With the information gained in the first study, the binding of metal ions to carboxylate headgroups is investigated using VSFS. Mg^{2+}, Ca^{2+}, Mn^{2+}, Ni^{2+}, Cu^{2+}, and Zn^{2+} were used to perturb the headgroup vibrations to further our understanding of the types of interactions and the binding strength between the ion and headgroup. The results show each ion to have a different interaction characteristics with the strongest being bi-dentate in nature and the weakest having ionic character.

The final work presented involves moving VSFS studies towards macromolecular assemblies at the oil-water interface to model inherently complex biomolecular systems. These studies present adsorption structure and dynamics of poly(acrylic-acid) as a function of pH, molecular weight, concentration, and the presence of mono and divalent salts. Poly(acrylic-acid) was found to have ordered adsorption characteristics that were highly dependent on the pH and the presence of aqueous salts.

This dissertation includes unpublished co-authored materials.

CURRICULUM VITAE

NAME OF AUTHOR: Daniel Keith Beaman

GRADUATE AND UNDERGRADUATE SCHOOLS ATTENDED:

University of Oregon, Eugene, Oregon
California Polytechnic State University, San Luis Obispo, California

DEGREES AWARDED:

Doctor of Philosophy in Chemistry, 2010, University of Oregon
Bachelor of Science in Chemistry, 2002, California Polytechnic State University

AREAS OF SPECIAL INTEREST:

Interfacial chemistry, structure and adsorption
Instrumentation design and construction
Laser spectroscopy of interfaces
Utilizing computer programming for scientific problems

PROFESSIONAL EXPERIENCE:

Graduate Research Assistant, Department of Chemistry, University of Oregon, Eugene, Oregon, 2004–2010
Graduate Teaching Fellow, Department of Chemistry, University of Oregon, Eugene, Oregon, 2003–2004

PUBLICATIONS:

C. L. McFearin, D. K. Beaman, F. G. Moore, and G. L. Richmond, *From Franklin to today: Toward a molecular level understanding of bonding and adsorption at the oil-water interface*, J. Phys. Chem. C **113**, 1171 (2009).

D. E. Gragson, D. Beaman, R. Porter, *Using compression isotherms of phospholipid monolayers to explore critical phenomena: A biophysical chemistry experiment*, J. Chem. Ed. **85** 272 (2008).

D. K. Hore, D. K. Beaman, and G. L. Richmond, *Surfactant headgroup orientation at the air-water interface*, J. Am. Chem. Soc. **127** 9356 (2005).

D. K. Hore, D. K. Beaman, D. H. Parks, and G. L. Richmond, *Whole molecule approach for determining orientation at isotropic surfaces by nonlinear vibrational spectroscopy*, J. Phys. Chem. B **109** 16846 (2005).

ACKNOWLEDGEMENTS

There are many people who have contributed to the end of this chapter of my life, both directly and in passing. To thank them all would be a gesture in futility, so for those not mentioned, you are also appreciated.

I would first like to thank Professor Geri Richmond for her continued support throughout my time in her lab. She is a role model as both a scientist and in her balance of life. Geri juggles more in a day than I can fathom, while at the same time being an integral member of her family, something I know she is proud of. Geri helps her students to excel in science, but also extends the same allowances for balance in life, and for both of these things, I am truly grateful.

To the Richmond lab members, both past and present. We rely on each other both scientifically and socially. It would not be possible to get through this without all of you. Dennis, your enthusiasm for science was inspiring and I couldn't have asked for a better friend and mentor when I joined the lab. Cathryn, it was a pleasure sharing an office with you, I will always remember the times we had together. To everyone else in the lab, thank you for your support, discussions, and patience, we wouldn't be anywhere without each other.

To my parents, siblings, and extended family, I have always appreciated your continued support. RG, I don't know where I would be had it not been for your guiding hand.

Most importantly, to Jill and Joe, you are my family and my life. There is no way I could have gotten through this without you. Your continued love and support keeps me going everyday and my most cherished memories and smiles are a result of our lives together.

For Jill and Joe

TABLE OF CONTENTS

LIST OF FIGURES

Figure Page

LIST OF TABLES

CHAPTER I

INTRODUCTION

Water covers nearly two-thirds of our planet, and water next to hydrophobic surfaces constitute some of the most important interfacial boundaries in both the natural and man made world. At first glance the interface seems inconsequential as it makes up such a small portion of the total liquid volume. However, it is one of the most important aspects of a chemical system and plays an integral role in processes such as the stabilization of biomolecules[1], polymer and nanoparticle synthesis[2–4], oil recovery[5], and environmental remediation of soil and water[6].

In order to understand these and other important processes that dictate our biological and chemical makeup and the environment around us, molecular level detail of the interfacial region is needed. With the advent of the laser and non-linear optics, the realization of molecular level detail was possible. However, of all the spectroscopies developed over the last 50 years, very few provide surface detail on a molecular level. Of these, vibrational sum-frequency spectroscopy (VSFS), a second order non-linear technique, can supply the interfacial molecular information that is sought[7–9]. VSFS is inherently surface specific, and thus the acquired data is not subject to complications from bulk interferences. Surface tensiometry, another interface specific method, complements VSFS experiments and provides a

more complete picture of the interfacial region. Chapter II presents an overview of VSFS theory and the experimental details, as well as a brief description of the interfacial tension measurements. Chapters III, IV, and V discuss the use of both of these techniques to investigate the interfacial structure of adsorbates at the oil-water boundary.

Chapter III presents a study of the solvating environment around Na-dodecanoate, a carboxylate headgroup surfactant. Headgroup structure and molecular composition play an important role in a surfactant's ability to undergo reactions at the aqueous interface, as well as having an effect on the surfactant's surface activity and orientation. These interfacial properties are relevant to industrial, biological, and environmental processes where carboxylate surfactants are prevalent and play an important role. Adsorption of these medium chain length carboxylate surfactants leads to unique findings on the orientation adopted by the headgroup as well as the hydrogen bonding environment surrounding the headgroup. Variations in concentration and pH show a number of differences between the oil-water interface and the more commonly studied air-water interface. Based on data from different polarization schemes and isotopic substitution, it was found that Na-dodecanoate adopts a wide variety of orientations at the oil-water interface and as a result, a large variety of hydrogen bonding configurations exist for the headgroup. The main differences between the two types of interfaces are attributed in large part to the solvating environment around the chains, which permits a more disordered monolayer and hence allows

the headgroups to adopt a wider variety of orientations at the interface and a larger variety of hydrogen bonding scenarios. E. J. Robertson assisted in acquiring interfacial tension measurements as an REU.

A vibrational sum-frequency spectroscopy study of divalent metal cations chelating with carboxylate surfactants at the oil-water interface is discussed in chapter IV. Binding of metal ions are relevant to a number of biological and environmental systems and play an integral role in the macrostructure of a number of biomolecules, as well as an important catalysis role in one-third of all enzyme reactions. The effects of Mg^{2+}, Ca^{2+}, Mn^{2+}, Ni^{2+}, Cu^{2+}, and Zn^{2+} on the adsorption and orientation of Na-decanoate are investigated in both the carboxylate and methyl vibrational stretching regions. Different polarization combinations are used to probe the carboxylate functional group and how the distribution of orientations changes with the addition of metal ions, as well as how the hydrogen bonding structure of the headgroup changes. The methyl and methylene vibrations are monitored to track the ordering of the alkyl chains when metal salts are added. Each metal salt was found to have a distinct affect on the carboxylate headgroup and the alkyl chain ordering. In addition, the strength of the ion-headgroup interaction based on the vibrational frequency shifts and amplitudes was classified by both relative strength and the type of interaction taking place. E. J. Robertson contributed interfacial tension results in this chapter.

In chapter V, a study of polyelectrolytes adsorbed to the oil-water interface under a variety of conditions is presented. Polyelectrolytes are pervasive throughout

industrial, environmental, and biological systems. In the environment, polyelectrolytes such as humic substances have strong chelating abilities due to their high carboxylic acid content and thus play a role in the transport of nutrients and toxins through soil. Biological polyelectrolytes, such as proteins and DNA, have folding, binding, and transport processes that have conformational and charge density dependence on the pH of the surrounding solution. These and other processes often occur at interfaces, which present different molecular characteristics and effects on adsorbates than the corresponding bulk aqueous solutions, and thus warrant further investigation. The common denominator in these systems is that they involve charged macromolecules adsorbed to an interface. The oil-water interface is an excellent platform for studying macromolecular conformation due to its highly fluid nature. Poly(acrylic acid), a weak polyelectrolyte, is an ideal model to study adsorption of environmentally and biologically relevant macromolecules at the oil-water interface due to its high carboxylic acid content and simple repeat unit structure. In these studies, poly(acrylic acid) was used as a model system and found to adsorb strongly to the oil-water interface at low pH. Raising the pH led to rapid desorption of the polymer. In its wake, a nearly neat interfacial region is observed indicating no polymer adsorption occurs above a critical pH level. Above this critical pH, adsorption was found to occur in the presence of metal ions, which act to bind the charged groups, displace solvating water molecules, and drive the polymer to the interface. In addition, interesting dynamical differences were observed between the interfacial tension and

the vibrational sum-frequency spectroscopy measurements, indicating the presence of a multi-step adsorption process where orientation and adsorption don't always occur simultaneously. E. J. Robertson contributed interfacial tension results in this chapter.

In each of the chapters discussed here, an aspect of adsorption to the oil-water interface is addressed and a molecular level picture is proposed for the interfacial region based on the data presented. Each chapter makes an important contribution to what is known about adsorbate structure at the oil-water interface. These experiments show that the oil-water interface is a unique environment and it should not be assumed that it will provide the same type of interfacial results as the solid-liquid or air-water interface. It is also shown that VSFS is a viable probe of macromolecular complexes at the oil-water interface, a system that no other technique has the ability to probe with the same level of detail.

CHAPTER II

EXPERIMENTAL TECHNIQUES AND THEORY

In this chapter, vibrational sum-frequency spectroscopy (VSFS) will be described from a standpoint of light interacting with matter and the response of the surface molecules. Following this, experimental considerations and the spectroscopic technique will be covered, including treatment of the data. In addition, interfacial tension measurements, as they are related to the work within this dissertation, will be described. Vibrational sum-frequency spectroscopy (VSFS) is a surface specific non-linear optical technique that allows one to probe molecular vibrations of interfacial molecules. Linear spectroscopic experiments such as infrared reflection absorption spectroscopy (IRRAS) can be used to probe surfaces. However, the signal is dependent on the penetration depth of the electromagnetic field and is usually on the order of microns. VSFS is unique in this respect due to its signal dependence on the structure and number density at the interface. Signal is acquired only to the depth at which a net orientation of molecules exists. This depth of orientation is commonly used to define the width of an interfacial region in MD studies, which is on the order of 6-9 Å[10, 11]. Given this interfacial depth, IR spectroscopies are sampling several orders of magnitude greater depth than what is sampled in the VSFS experiments. In addition, this dissertation is focused on studies at the oil-water interface, which

are experimentally difficult to access with IR experiments due to the shallow angles required.

Vibrational Sum Frequency Spectroscopy

When a weak electric field ($\mathbf{E}$) interacts with a molecule an oscillating dipole is induced, which is expressed as

$$\mathbf{p}_{\text{ind}} = \mathbf{p}_0 + \alpha\mathbf{E} \tag{II.1}$$

where $\mathbf{p}_0$ is the permanent dipole of the molecule, and α is the polarizability. For a macroscopic system, the dipole per unit volume is considered and is known as the induced polarization ($\mathbf{P}_{\text{ind}}$). Ignoring $\mathbf{p}_o$ in Equation II.1 due to the lack of a static dipole in most materials, the polarization is written as

$$\mathbf{P}_{\text{ind}} = \epsilon_0\boldsymbol{\chi}^{(1)}\mathbf{E} \tag{II.2}$$

where $\chi^{(1)}$ is the first order susceptibility and is the macroscopic average of the polarizability (α), and ϵ_0 is the vacuum permittivity. The dipole oscillation induced in the material is the same frequency as the driving incident electric field, and is the basis for linear spectroscopy and processes such as reflection and refraction.

Non-linear spectroscopy however, requires strong electric fields such as those provided by pulsed lasers. As a result, the expression for the dipole moment of a molecule must be expanded in a power series to include non-linear terms as shown by

$$\mathbf{p}_{\text{ind}} = \alpha\mathbf{E} + \frac{1}{2}\alpha^{(2)}\mathbf{EE} + \frac{1}{6}\alpha^{(3)}\mathbf{EEE} + \cdots + \frac{1}{n!}\alpha^{(n)}\mathbf{E}^n \tag{II.3}$$

where $\alpha^{(2)}$ and $\alpha^{(3)}$ are often replace by β and γ respectively, and are the first and second order hyperpolarizabilities. Expanding the microscopic description to a macroscopic system, analogous to Equation II.2, gives the induced polarization ($\mathbf{P}$) and is written as

$$\mathbf{P}_{\text{ind}} = \mathbf{P}^{(1)} + \mathbf{P}^{(2)} + \mathbf{P}^{(3)} + \cdots \tag{II.4}$$

$$\mathbf{P}_{\text{ind}} = \varepsilon_o \boldsymbol{\chi}^{(1)}\mathbf{E} + \frac{1}{2}\varepsilon_o \boldsymbol{\chi}^{(2)}\mathbf{E}\mathbf{E} + \frac{1}{6}\varepsilon_o \boldsymbol{\chi}^{(3)}\mathbf{E}\mathbf{E}\mathbf{E} + \cdots + \frac{1}{n!}\varepsilon_o \boldsymbol{\chi}^{(n)}\mathbf{E}^n \tag{II.5}$$

where $\boldsymbol{\chi}^{(2)}$ and $\boldsymbol{\chi}^{(3)}$ are the second and third order nonlinear susceptibilites. The focus of this dissertation exclusively deals with $\mathbf{P}^{(2)}$, where two electric fields are incident on the sample, and the radiated output consists of components in addition to the two incident fields[12–15]. These two electric fields, $\mathbf{E}_1(\omega_1)$ and $\mathbf{E}_2(\omega_2)$, can result in several different processes depending on the incident field wavelengths. When $\omega_1 = \omega_2$ the result is second harmonic generation and the output is at 2ω. When $\omega_1 \neq \omega_2$, one possible output is radiation at $\omega_1 + \omega_2$ and is called sum-frequency generation, which is the focus of this dissertation.

From the second order terms in Equations II.3 and II.5 an expression can be obtained that relates the microscopic and macroscopic quantities of the material and is shown by

$$\boldsymbol{\chi}^{(2)} = \frac{\mathrm{N}}{\varepsilon_o}\langle\beta\rangle \tag{II.6}$$

where N is the volume number density, and the brackets around the molecular hyperpolarizability denote it is an orientational average over the macroscopic system. Under the electric dipole approximation, a simplified expression for the microscopic

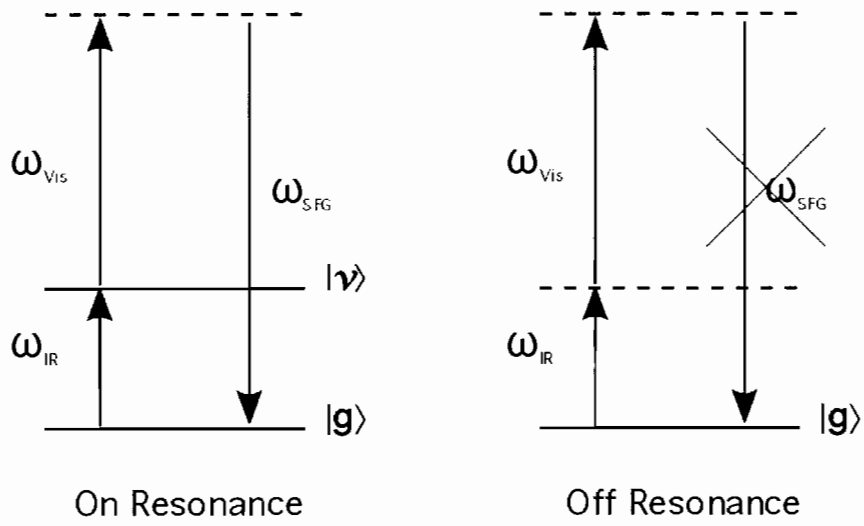

Figure 2.1. Energy level diagrams for VSFS showing on and off resonant processes. Solid lines represent distinct ground or excited vibrational states, whereas dashed lines are any other state.

hyperpolarizability, β, where the IR frequency is vibrational resonant and the visibile frequency is far from an electronic resonance, can be expressed as

$$\beta(\omega_{\mathrm{IR}}) = \frac{\langle g|\hat{\alpha}|\nu\rangle\langle\nu|\hat{\mu}|g\rangle}{\omega_{\mathrm{IR}} - \omega_o + \mathrm{i}\Gamma_{\mathrm{h}}} \tag{II.7}$$

where $\langle\hat{\alpha}\rangle$ and $\langle\hat{\mu}\rangle$ are the Raman polarizability and IR dipole moment operators, $|g\rangle$ and $|\nu\rangle$ are the vibrational ground and excited states, ω_o is the frequency of the vibrational mode, ω_{IR} is the frequency of the infrared beam which is tuned over the vibrational resonances, and Γ_{h} is the homogenous line width. From these equations, two main fundamental certainties of VSFS are found. The first is that for a vibrational mode to be sum-frequency active, it must have a change in dipole moment *and* a change in polarizability, i.e. it must be both IR and Raman active. Energy level diagrams for on and off resonance VSFS are shown in Figure 2.1. The

second noteworthy point is that the VSFS signal is sensitive to both number density and orientation of the surface molecules. This means that changes in either of these two variables can lead to enhancement or depletion of signal. It also means that even if there are molecules of interest at the interface, they will only give VSFS signal if there is a net orientation, ie. if $\chi^{(2)}$ does not cancel[13, 15].

Polarization Schemes

VSFS is uniquely significant due to the fact that all 27 elements of the third rank tensor, $\chi^{(2)}$, must equal zero in centrosymmetric media. In such an environment, inversion symmetry dictates that $\chi^{(2)}_{ijk} = \chi^{(2)}_{-i-j-k} = -\chi^{(2)}_{ijk}$[15]. The only solution to satisfy this is for $\chi^{(2)}_{ijk} = 0$. The outcome of this result is that VSFS is only allowed where a break in symmetry of the media is experienced. The interface is the dominant case where this break in symmetry occurs for liquids, which are the main focus of this dissertation.

Liquid interfaces are in general $C_{\infty}v$ in the plane of the interface, meaning that a majority of the 27 elements of the third rank tensor $\chi^{(2)}$ are equal to zero. To arrive at this conclusion the reader is referred to Table 2.1 where the 27 elements along with the seven non-zero elements of $\chi^{(2)}$ are displayed. The non-zero elements are found by applying the operators that compose $C_{\infty}v$ symmetry to each element of $\chi^{(2)}_{ijk}$. If the operations applied yield a non-zero result, then that is a valid polarization scheme for the interface. Of the seven non-zero elements, only four are unique because a liquid

Table 2.1. $C_{\infty}v$ symmetry applied to the 27 elements of $\chi^{(2)}_{ijk}$ showing the 7 non-zero elements for a liquid interface.

27 Elements $\chi^{(2)}_{ijk}$			Applying $C_{\infty}v$		
xxx	yyy	zzz	~~xxx~~	~~yyy~~	zzz
xxy	yyx	zzx	~~xxy~~	~~yyx~~	~~zzx~~
xyx	yxy	zxz	~~xyx~~	~~yxy~~	~~zxz~~
yxx	xyy	xzz	~~yxx~~	~~xyy~~	~~xzz~~
xxz	yyz	zzy	xxz	yyz	~~zzy~~
xzx	yzy	zyz	xzx	yzy	~~zyz~~
zxx	zyy	yzz	zxx	zyy	~~yzz~~
xyz	yxz	zxy	~~xyz~~	~~yxz~~	~~zxy~~
xzy	yzx	zyx	~~xzy~~	~~yzx~~	~~zyx~~

is isotropic within the plane of the interface and thus x = y. The four elements of the rank two tensor that are applicable to liquid interfaces are $\chi^{(2)}_{yyz} = \chi^{(2)}_{xxz}$, $\chi^{(2)}_{yzy} = \chi^{(2)}_{xzx}$, $\chi^{(2)}_{zyy} = \chi^{(2)}_{zxx}$, and $\chi^{(2)}_{zzz}$. These four can be reduced even further because $\chi^{(2)}_{yzy}$ and $\chi^{(2)}_{zyy}$ are equivalent due to the visible wavelength in the experiment being far from any electronic resonance, and $\alpha_{lm} = \alpha_{ml}$, ie. the polarizability tensor is symmetric. The three unique non-zero elements of $\chi^{(2)}$ that are left can be experimentally probed using linearly polarized light with ssp, sps, and ppp polarization schemes, where s polarization is perpendicular to the plane of incidence and its component lies only in the plane of the interface, whereas p is parrallel to the plane of incidence and has components in both the x=y and z plane, as shown in Figure 2.2. The polarization scheme notation follows the wavelength of the three beams in increasing order, ie. sum-frequency, visible, infrared. Each polarization scheme probes a different element of $\chi^{(2)}$ and a different component of the dipole moment at the interface. For example, ssp is used to probe the $\chi^{(2)}_{yyz}$element and components of the dipole that lie normal to

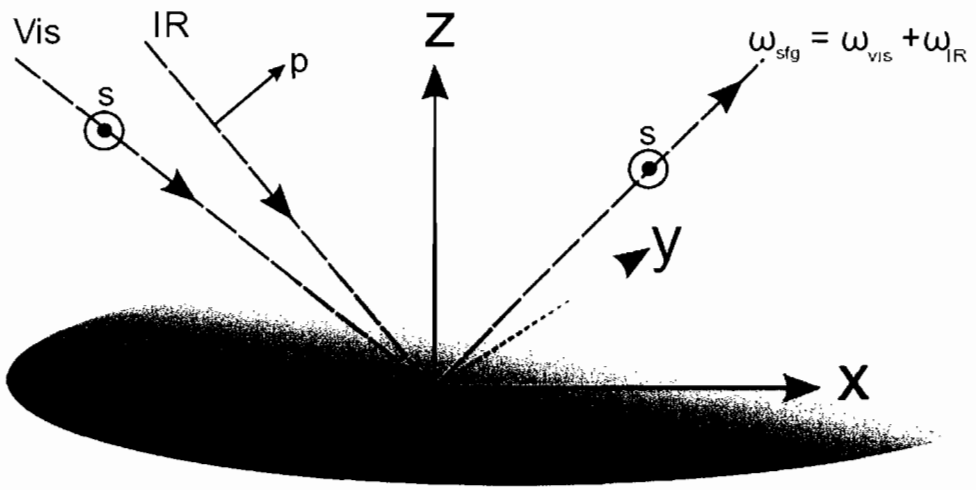

Figure 2.2. Laboratory axis system used to describe the incident polarizations that make up the VSFS experiments. The figure shown omits the reflected visible and IR beams for clarity. The polarization scheme shown is ssp.

the interfacial plane and sps is used to probe the $\chi^{(2)}_{yzy}$element and components of the dipole that are in the plane of the interface. However, ppp is sensitive to components that are both in and out of the plane of the interface, and as a result, four elements of $\chi^{(2)}$ contribute to the ppp polarization scheme. By utilizing multiple polarization schemes in an experiment, it is possible to gain an understanding of the orientation of the molecule, as well as the distribution of orientations.

For the VSFS experiments in this dissertation, two laser pulses, one a fixed visible wavelength and the other a tunable IR, are overlapped spatially and temporally at an interface. The result is a generated pulse at the sum of the two incident frequencies. The intensity of the generated sum-frequency is proportional to the square of the effective second order susceptibility $\chi^{(2)}_{eff}$ and the intensity of the incident IR and

visible electric fields as shown by

$$\mathrm{I}(\omega_{\mathrm{sf}}) \propto |\chi^{(2)}_{\mathrm{eff}}|^2 \mathrm{I}(\omega_{\mathrm{vis}})\mathrm{I}(\omega_{\mathrm{IR}}) \tag{II.8}$$

The second order susceptibility, $\chi^{(2)}$, as shown in Equation II.6 and the effective second order susceptibility from Equation II.8 are related through the fresnel coefficients (L) and unit polarization vectors ($\hat{e}$) shown by

$$\chi^{(2)}_{\mathrm{eff}} = [\hat{e}(\omega) \cdot L(\omega)] \cdot \chi^{(2)} : [L(\omega_{\mathrm{vis}}) \cdot \hat{e}(\omega_{\mathrm{vis}})]\,[L(\omega_{\mathrm{IR}}) \cdot \hat{e}(\omega_{\mathrm{IR}})] \tag{II.9}$$

The Fresnel coefficients (L) determine reflection and transmission of a field at an interface and the unit polarization vectors $\hat{e}$ take into account the experimental geometry of the incident and reflected beams in the laboratory frame[12, 16].

When an adsorbate is placed on a substrate that gives no SFG response, Equation II.6 is adequate to describe the response of the adsorbate. However, as is most often the case, the substrate, be it liquid or solid, often yields a small response in addition to the adsorbate. In this case, there are two contributions to $\chi^{(2)}$ as shown by

$$\chi^{(2)} = \chi^{(2)}_{\mathrm{NR}} + \sum_{\nu} \chi^{(2)}_{\mathrm{R}_\nu} \tag{II.10}$$

which contains a non-resonant component and the sum of all the resonant components. This affects the treatment of the data and needs to be accounted for in the fitting expression when it is present[17].

Data Analysis

Interpretation of VSFS data is not straightforward like linear spectroscopies due to the intensity of the signal being equal to the square of $\chi^{(2)}_{\text{eff}}$ as shown in Equation II.8. This dictates that interferences will exist between the non-resonant and resonant contributions to $\chi^{(2)}$, as well as between different resonant modes in the spectra, leading to constructive and destructive interferences, as well as asymmetric line shapes. In addition, $\chi^{(2)}$ is complex so there is both a phase and an amplitude associated with each resonant mode, as well as with the non-resonant signal. These complications to the shape of the spectra necessitate using a fitting routine to accurately determine amplitudes, phases, frequencies, and widths of the modes. The expression used for fitting was first proposed by Bain and coworkers[17] and implemented by Prof. Fred Moore[18]. The expression is

$$|\chi^{(2)}(\omega_{\text{SF}})|^2 = \left|\chi^{(2)}_{\text{NR}} + \int_{-\infty}^{\infty} \frac{A_\nu}{\omega_{\text{L}} - \omega_{\text{IR}} + i\Gamma_{\text{L}}} \exp\left[-\frac{(\omega_{\text{L}} - \omega_\nu)^2}{\Gamma_\nu^2}\right] \mathrm{d}\omega_{\text{L}}\right|^2 \qquad \text{(II.11)}$$

and fits the spectra to a Lorentzian convoluted with a Gaussian to account for homogeneous and inhomogeneous broadening. There are five parameters that are fit for each vibrational mode. They are the center frequency, amplitude, phase, Lorentzian width, and Gaussian width. In addition, there is a non-resonant amplitude and phase for each spectrum. The Lorentzian width can be fixed at 2 $\text{cm}^{-1}$to account for homogenous broadening which leaves only four parameters to fit. In most cases, the center frequency is known within a range based on literature values and can thus

be highly constrained. One is then left with amplitude, phase, and the Gaussian width to fit. Obviously, the number of parameters grows rapidly, and with n modes there are 5n+2 parameters to be fit. For the liquid-liquid interface however, there is not an observed non-resonant component so those parameters are generally not applicable. The remaining parameter space is still large and one must be careful to achieve appropriate fits. To rely less on intuitive logic for fits, more confidence can be achieved by using global fitting routines to simultaneously fit series of spectra where applicable. This forces fits for multiple data sets to agree on certain parameters such as center frequency, width, or phase, which shouldn't change as certain experimental parameters are changed.

Spectroscopic Measurements

All measurements in this dissertation were made on a commercially available VSFS system designed and built by Ekspla in Vilnius, Lithuania. Modifications to the system were made to accommodate the inverted sample geometries necessary to study the oil-water interface. Due to the angle changes of the non-linear optical crystals while tuning across IR wavelength regions, small amounts of beam movement are unavoidable. To track the IR beam location, a motorized mirror was placed in the incident IR beam line with programs to track spot locations for different regions of interest. Figure 2.3 shows a schematic of the laser system. A Nd:YAG laser (model PL2143A) outputs 1064 nm light with ≈30 ps pulse lengths at 10 Hz with peak

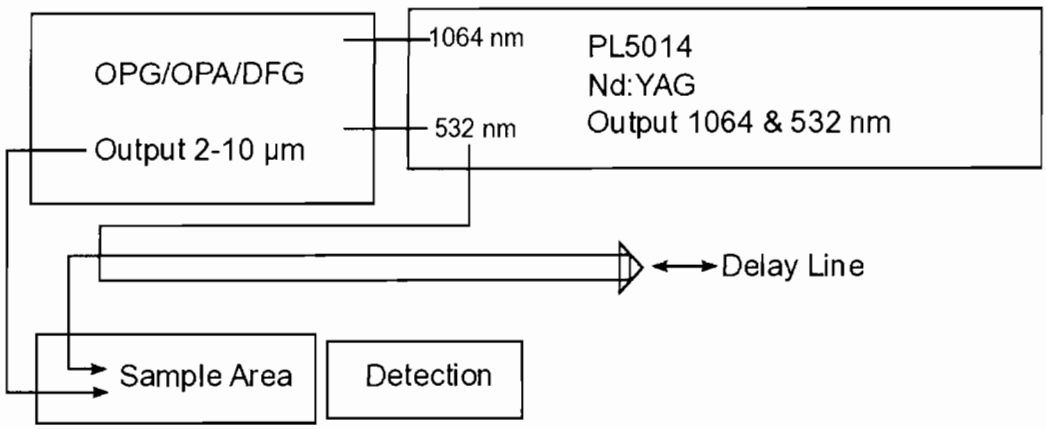

Figure 2.3. A schematic of the laser system used for the work in this dissertation. The laser consists of both visible and IR generation stages as well as a sample area and detection stage. Details of the system are left out of the schematic for clarity.

energies up to 600 μJ per pulse. Within the laser, seed pulses are generated with a flash lamp pumped Nd:YAG rod. Active and passive mode locking using a Pockel cell, polarizers and a solid state modulator, allow for good stability in both energy and time. Introducing losses to the cavity gives bandwidth stabilized pulses with $\approx$10 μJ, which make roughly 200 round trips within the cavity before they are sent to the next stage. When pulses are selected out by another Pockel cell and polarizer, they enter an intra-cavity regenerative amplifier, which increases the pulse energy to $\approx$500 μJ without damaging the solid state modulator. Once a set number of round trips occurs, the pulses are selected out by yet another Pockel cell and polarizer and sent to a double pass amplifier which consists of a dual flash lamp pumped Nd:YAG rod. Here the pulses are amplified through flash lamp timing to get output in the tens of mJ. However, to preserve the non-linear optical crystals, output does not usually exceed around 8 mJ. Once these high energy 1064 nm pulses are made, the light is split

into two lines and one line is frequency doubled in a KDP (potassium dideuterium phosphate) crystal to give 532 nm light. A small portion of the 532 nm line is then split off and used as the visible portion at the interface. This visible line is spatially filtered and collimated and has a relatively long path length with a delay stage built in so that these pulses may be overlapped temporally with the pulses exiting the IR generation box.

The remainder of the 532 nm line and the 1064 nm line are used to generate tunable infrared light via a series of parametric processes (model PG501/DFG2-10P). First, the 532 nm light is split into two lines, one of which is double passed through a heated BBO crystal for optical parametric generation (OPG). The parametric beam is then reflected off a grating to narrow the spectral bandwidth. The other 532 nm line and the spectrally narrowed OPG generated seed are then sent to another double pass BBO stage for optical parametric amplification (OPA). After the OPA stage, the signal and idler are separated via a Glan prism polarizer and the idler is sent to the difference frequency generation (DFG) stage where it is mixed with the 1064 nm light to generate tunable IR from 2-10 microns.

In these experiments, all data was taken with the beams at their respective TIR angles for the CCl_4-water interface. The angles for incident beams were 23.5° from the plane of the interface for the visible, and 15-17° for the IR. Polarization changes of the IR beam were accomplished using periscopes on magnetic mounts. Polarization changes of the visible line were accomplished using a wave-plate and polarizer. In

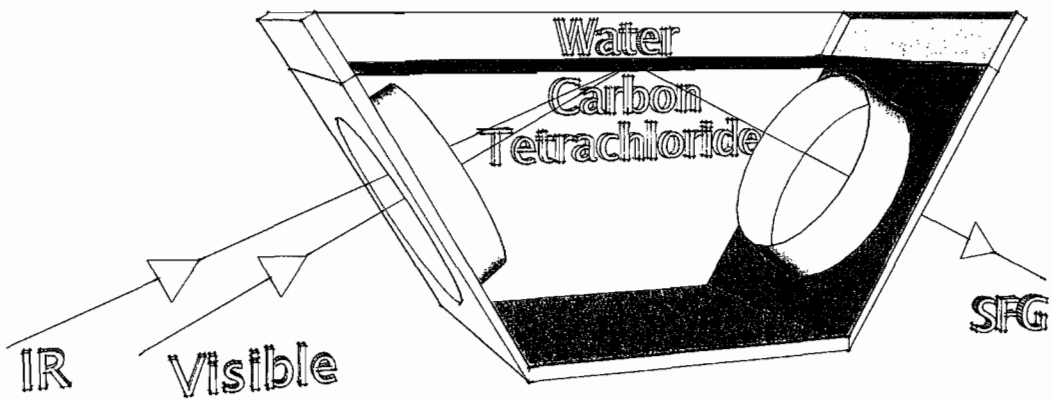

Figure 2.4. A schematic of the sample cell showing a cutaway from the side view with the incident and outgoing beams.

the detection line a wave-plate and polarizer are used to select the cleanest polarized signal for detection.

The sample cell was designed from a solid piece of Kel-f and contains two windows set normal to the incident and outgoing 532 nm beam and are sealed with Dupont Kalrez® perfluoropolymer O-rings. The input window was CaF_2 or BaF_2 and the output window was BK-7 glass as it only needed to transmit the generated visible sum-frequency light and it was more robust towards the aggressive cleaning process used. All glassware, the cell, the BK-7 window, and the O-rings were soaked in concentrated sulfuric acid with No-Chromix for a minimum of 6 hours and then each piece was rinsed under water from an 18 MΩ Nanopure filtration system for at at least 20 minutes. The CaF_2 window was allowed to soak in the same acidic solution for 15-20 minutes and then copiously rinsed. The BaF_2 window was used as is after gently wiping with lense tissue soaked with methanol. A schematic of the sample cell is shown in Figure 2.4, which also shows the incident and outgoing beams. Data

acquisition started immediately after the interface was made and usually continued for approximately an hour for each prepared interface. All spectra shown in these experiments is an average of at least 300 laser shots per data point. Post data processing included averaging spectra and normalizing by dividing by gold or the IR profile.

Interfacial Tension

Interfacial tension measurements provide a quantitative method to monitor the number density of solutes at the oil-water interface. The data gathered from this technique complements the VSFS data and allows one to conclude whether changes in SFG spectral amplitudes are due to changes in number density or changes in orientation, since both contribute to the spectra as shown in the above section. Interfacial tension experiments were carried out on two different types of tensiometers made by KSV. The first is a balance type and uses the Wilhelmy plate method and the other is an optical tensiometer and uses the pendant drop method. Both types of tensiometers give equivalent results, however, depending on experimental conditions and the types of data desired, one is often better than the other.

The Wilhelmy plate method consists of using a platinum plate that is cleaned by dipping in sulfuric acid, then water, then heated over a bunsen burner until glowing orange. The plate is allowed to cool, and then is placed on the balance, and lowered into the interfacial region as shown in Figure 2.5. To take a measurement, a neat CCl_4-

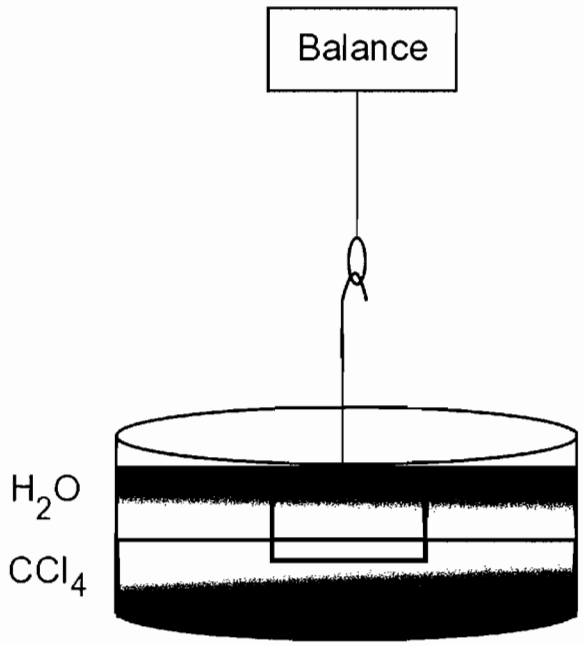

Figure 2.5. A schematic of the Wilhelmy plate method used for gathering interfacial tension data in this dissertation.

water interfacial tension value is obtained and verified over time with the balance. Then using this same prepared interface, pH adjustments were made to bring the water phase to the desired pH. To obtain interfacial data for different surfactant concentrations, aliquots of a stock solution of surfactant that was pH adjusted, were added to the aqueous phase and allowed to equilibrate. Interfacial tension data was recorded when the surface tension didn't drift more than 0.2 mN/m for 5 minutes.

Analysis of the data is straightforward. If one is simply comparing the effect of different adsorbates on the interfacial tension, then the equilibrium values of each interface are used to define which adsorbate causes the greatest change in the interfacial tension. If data on a particular adsorbate, a surfactant for example, is

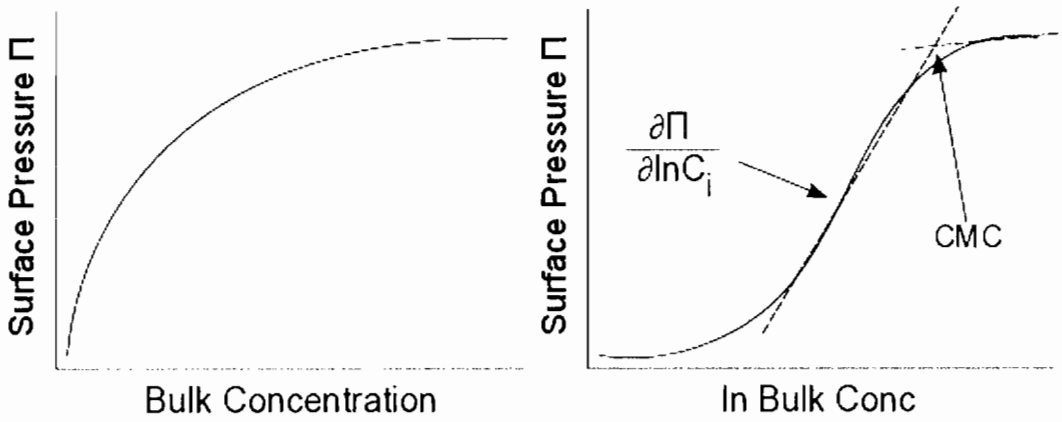

Figure 2.6. Typical surface pressure plot for a surfactant at the oil-water interface.

required in more detail, then a concentration series of the surfactant would be taken. The equilibrium interfacial tension value will be obtained for each concentration and plotted with respect to bulk concentration. An example of what this would like is shown in Figure 2.6, where the surface pressure is the interfacial tension of the adsorbate subtracted from the neat interfacial tension value (γ_o - γ_i). From the plot in Figure 2.6, a number of properties of the adsorbate can be calculated such as the critical micelle concetration (CMC), the minimum surface area per molecule, surface excess as a function of bulk concentration, as well as a number of thermodynamic properties like the free energy of adsorption. In order to calculate the CMC, one simply plots the surface tension as a function of the natural log of the bulk concentration. The plot will generally show a clear break in the slope of the data, and this concentration is where the CMC is. To calculate the surface excess, the Gibbs equation is used which relates the bulk concentration (C) to the surface concentration Γ, which is defined as the concentration of a solute at the interface in

excess of the concentration if the bulk concentration were at the interface. The Gibbs equation is used in the form

$$\Gamma_l = \frac{1}{n_i RT}\left(\frac{\partial \Pi}{\partial \ln a_i}\right) \tag{II.12}$$

where Γ_l is the limiting surface excess, n_i is the number of species, and Π is the interfacial pressure, and a_i is the activity which can be replaced by concentration under dilute surfactant conditions[19]. As seen in Equation II.12 the slope of the plot used to find the CMC is all that is needed to calculate the limiting surface excess (the maximum surface coverage). The surface excess coverage can now be obtained using the Frumkin isotherm expression as follows

$$\Pi_i = -\Gamma_l \ln\left[1 - \frac{\Gamma_i}{\Gamma_l}\right] \tag{II.13}$$

where Π_i is the interfacial pressure at the i^{th} concentration, Γ_l is from Equation II.12, and Γ_i is the surface excess at the i^{th} concentration[20]. Under dilute surfactant conditions, the surface excess is considered equivalent to the surface concentration.

Interfacial tension experiments were also carried out on a KSV optical tensiometer using the pendant drop method. Interfaces were prepared by filling a cuvette with CCl_4. A hooked needle on a syringe containing the aqueous solution was then inserted into the cuvette and a drop was formed as shown in Figure 2.7. Data acquisition was started upon formation of the drop. When acquiring data of aqueous polymer solutions, a neat CCl_4-water interface was always prepared first and the interfacial tension value verified against the known value of CCl_4-water, which is 44 mN/m

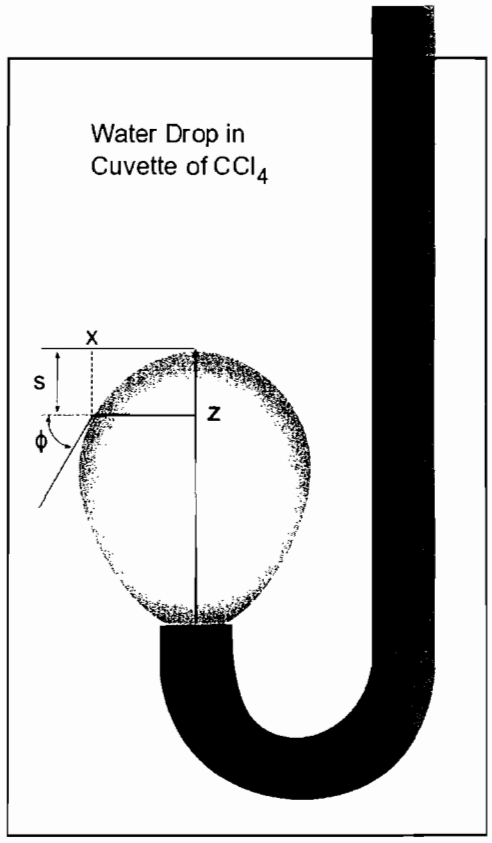

Figure 2.7. The pendant drop method as used for interfacial tension measurements.

[21, 22]. Once the correct neat interfacial tension value was achieved, the syringe was filled with the polymer solution of interest and a pendant drop was made. Data were recorded until an equilibrium interfacial tension value was achieved, or in the cases of the long time acquisitions, there was drop failure. Interfacial tension values were calculated from the acquired images using the KSV software. Calculations were accomplished using the Young-Laplace equation expressed as three dimensionless first order equations in the form

$$\frac{dx}{ds} = cos\phi \tag{II.14}$$

$$\frac{dz}{ds} = sin\phi \tag{II.15}$$

$$\frac{d\phi}{ds} = 2 + \beta z - \frac{(sin\phi)}{x} \tag{II.16}$$

to find the shape factor, β. Then Equation II.17,

$$\gamma = \frac{\Delta\rho g R_o^2}{\beta} \tag{II.17}$$

can be used, which relates the surface tension (γ) to the drop shape through the difference in the density of the fluids at the interface ($\Delta\rho$), the gravitational constant (g), the radius of the drop curvature at the apex (R_o), and the shape factor (β)[23].

Both methods for gathering interfacial tension data were found to give overlapping data and the plots shown in this dissertation contain data from both instruments, and will be specified as needed.

CHAPTER III

INVESTIGATING THE SOLVATION STRUCTURE AND HYDROGEN BONDING OF CARBOXYLATE SURFACTANTS

In this chapter, vibrational sum-frequency spectroscopy and surface tensiometry are used to study the adsorption of Na-dodecanoate and Na-octanoate as a function of concentration and pH to gain a fundamental understanding of the carboxylate headgroup structure at the CCl_4-water interface. While studies of the alkyl chains of surfactants at oil-water interfaces are numerous, there is still very little known regarding the structure of surfactant headgroups at this interface. This study aims to understand not only how the headgroup is structured at the interface, but also to learn about how water orients around the headgroup, the hydrogen bonding scenarios that are possible, and how the hydrogen bonding and headgroup structure are linked. Different polarization schemes are used to probe the dipole components of the headgroup both parallel and perpendicular to the interface and are used in the interpretation of the molecular structure. It was determined that water adopts a wide variety of hydrogen bonding structures with the headgroup. Along with the solvation of the alkyl chains by the oil phase, the headgroup exists in broad distribution of orientations from having its dipole perpendicular to the interface, to having one of its C=O in the plane of the interface. E. J. Robertson assisted with surface tension.

Introduction

Carboxylic acids are the some of the most ubiquitous organic functional groups in both environmental chemistry and biological systems. They are present in all amino acids and are thus an integral part of every biological molecule made from these building blocks. Due to their overwhelming presence, their ability to be charged or neutral, and their hydrogen bonding character, they play an important role in many biological processes such as peptidyl transferase[24] and protein dynamics[25]. Environmentally, carboxylates play an important role in the transport of nutrients and toxins in soils in the form of humic and formic substances[26–28]. Small COOH compounds are some of the most abundant organics found in fine particulate matter in the atmosphere and thus their surface activity and ability to hydrogen bond at the surface of water droplets plays an important role in atmospheric chemistry[29–31]. It is therefore of great importance to understand the aqueous solvating environment surrounding these functional groups at a wide variety of interfaces.

Carboxylic acid and carboxylate containing molecules at both the air-water[29, 32–38] and the solid-liquid[39–42] interface have received much interest over the last two decades using surface specific techniques. IRRAS work by Gericke and coworkers involved the study of long chain carboxylic acids under a variety of conditions using a number of different metals to study binding affects and monolayer conformation[36, 43]. Johann et al. used PMIRRAS to study similar monolayers as a function of pH[44].

While both of these studies were able to see splitting of the C=O vibrational mode into three distinct peaks due to hydrogen bonding structure, limited information was available about how the charged carboxylate headgroup was solvated at the air-water interface due to small carboxylate signal. Additionally, splitting of the asymmetric and symmetric carboxylate vibrational modes was seen by Johann et al., but there was no explanation as to why this occurred. Miranda and coworkers studied long chain carboxylic acids with vibrational sum-frequency spectroscopy (VSFS) at the air-water interface and found that the surface pKa is much different than what is normally found in bulk liquid[33]. Confirmation of this was found by Eisenthal and coworkers who showed that surface pKa is not equal to bulk pKa in their VSFS work on phenolate ions at the air-water interface[38]. The presence of Na^+ and K^+ under a monolayer of long chain carboxylates produced frequency shifts due to binding of the ions with the carboxylates[32]. Tyrode et al. have completed a number of studies on carboxylates at the air-water interface, studying fluorinated carboxylate surfactants[34], acetic acid[45, 46], and formic acid[35]. More recently in this group, investigations of hexanoic acid at the air-water interface found interesting time dependent effects for the formed monolayer[29]. This time dependence was observed to disappear upon the addition of salts. Also in this group were a number of investigations of carboxylate surfactants at the fluorite-water interface[39, 41]. While many of these studies have observed the headgroup vibrational modes, there has been little evidence for the types of hydrogen bonding character surrounding the charged

carboxylate headgroup. In addition, the oil-water interface often proves to be unique when compared with the air-water or solid-liquid interface[47, 48]. From the past studies described here, it is clear that surfactant headgroup vibrational modes in the mid infrared region are rich in information and are often the most important functionality on a molecule. This is due to the headgroup being the primary location for water and salt interactions, and thus continuing studies can provide interesting information regarding the interfacial chemistry, particularly at the oil-water interface where little is known regarding the headgroup structure and orientation.

The oil-water interface has long held the interest of scientists and it has been used as a model for a wide variety of chemical systems ranging from environmental to biological in nature. It has shown over time to have unique interfacial properties related to adsorption and orientation of surfactants[49–53], phospholipids[54–56], and simple ions[57, 58]. Although there is knowledge of surfactants at the oil-water interface, the body of knowledge regarding headgroup structure and binding has not caught up with what is known about headgroups at the air-water interface. This work attempts to start filling this gap with a study of medium chain length carboxylate surfactants at the CCl_4-interface. It is found that the headgroup exists in a broad distribution of orientations and direct evidence is provided for a multitude of coexisting hydrogen bonding coordinations that act to solvate the charged carboxylate head group at the CCl_4-water interface. The surfactants of interest are Na-dodecanoate (Na-Laurate) and Na-octanoate. Figure 3.1 shows these surfactants in their various

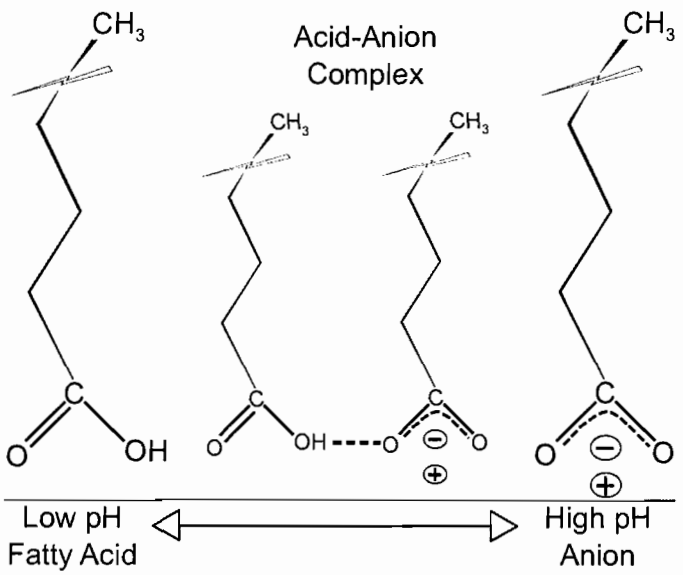

Figure 3.1.. Carboxylate/carboxylic acid surfactants at low and high pH.

states at different pHs. Literature reports give the pKa of fatty acids in bulk water as ≈4-6[32, 33, 40, 59, 60]. Below the pKa, the molecule exists as a fatty acid; above it exists in its anionic form. pH values near the pKa produce an equilibrium between the charged and uncharged headgroup that can lead to acid-anion complexes. These acid-anion complexes are known to exist when the surface area per headrgoup is small, such as when monolayers are compressed on Langmuir troughs. According to the interfacial tension data presented later in this work, the small area per headgroup required for inter-headgroup interactions is not approached by a factor of 2-3, thus acid-anion complexes are not relevant to these experiments. In addition, all work done in this chapter is at a fixed pH of 10, well above the pKa to ensure the surfactant is in its fully deprotonated state.

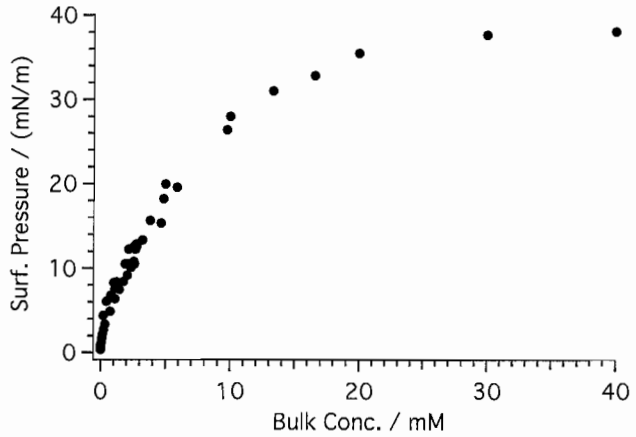

Figure 3.2. Surface Pressure of Na-dodecanoate at the CCl_4-water interface taken with the Whilhelmy plate method and the pendant drop method.

Interfacial Tension

Interfacial tension measurements were made with both the Wilhelmy plate method and the pendant drop method and were found to agree within error. The interfacial tension of Na-dodecanoate at the CCl_4-water interface is shown in the inset in Figure 3.2 and is typical when compared with other surfactants adsorbed at the the oil-water interface. The data shown gives a CMC value of ≈27 mM which is in line with past literature CMC values for Na-dodecanoate[20, 61]. From the interfacial tension data the maximum surface coverage Γ_m can be calculated as a good indicator of *effectiveness of adsorption*[20]. Γ_m for Na-dodecanoate at the CCl_4-water interface was calculated at ≈ 67 $Å^2$/molecule, which is somewhat larger than other carboxylate surfactants at neutral pH[20]. The main reason for this larger than normal value is solutions in these experiments are adjusted to pH 10, which gives a solution of

surfactant where the headgroup is primarily in its anionic form. This results in repulsion between headgroups leading to a larger surface area per molecule. In addition, it is unknown whether there is a preference for the adsorption of the charged vs. uncharged molecules at the interface. In other studies completed near the pKa where an equilibrium exists between charged and uncharged headgroups in bulk solution, there could actually be a preference for the protonated uncharged headgroup at the interface, leading to further differences between between these and other studies. Interfacial tension studies in this work unambiguously show that for a solution of fully charged carboxylate surfactants, the area per headgroup is larger than what is normally reported in the literature for the air-water or hexane-water interface. This is attributed to the dominance of the charge-charge repulsion forces between headgroups in the interfacial region as this acts to keep the area per molecule large, and the solvation of the chains by the CCl_4 allowing a more disordered monolayer.

From the interfacial tension data the surface excess (surface concentration), Γ_i, can be calculated as a function of bulk concentration. Figure 3.3 shows the surface excess for Na-dodecanoate at the CCl_4-water interface. In the figure, it is observed that a full monolayer is achieved at $\approx$ 4.5 mM bulk concentration. Beyond this bulk concentration, no additional adsorption of the surfactant at the interface is observed. This data is important for the VSFS experiments because a decrease in signal can occur for a variety of reasons such as loss of orientation, decrease in number density at the interface, or signal cancellation from the formation of a

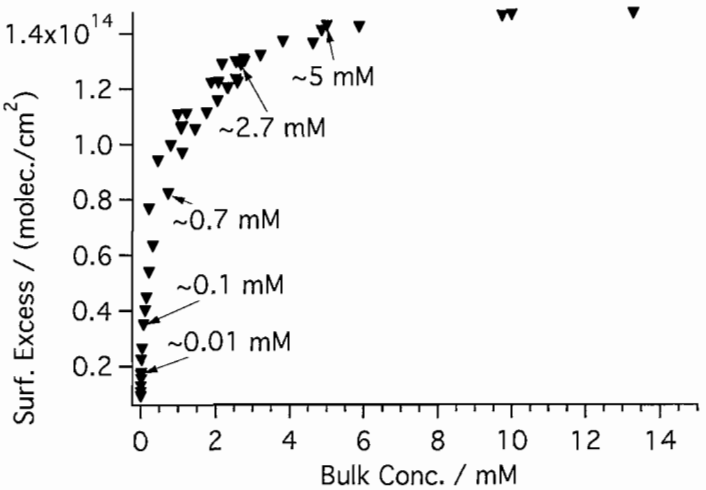

Figure 3.3. Surface concentration as a function of bulk concentration for Na-dodecanoate at the CCl_4-water interface as calculated from the inset surface pressure data. The data points that are marked correspond to the concentrations used in the spectroscopy experiments.

bilayer at the interface. Combining the spectroscopic data with the interfacial tension results allows a complete picture of the formation of a monolayer to be built. For the spectroscopy studies, five bulk concentrations (shown in Figure 3.3) have been chosen to allow investigation of the dilute surface concentration regime, up to the full monolayer regime. Choosing concentrations in this range makes it possible to use the spectroscopy to identify how the conformation of the monolayer is changing while the surface excess is increasing.

VSFS of Na-dodecanoate at CCl_4-Water Interface

Bulk concentrations obtained from the surface excess data in Figure 3.3 were used to probe the interface with VSFS at different levels of surface coverage. Previous

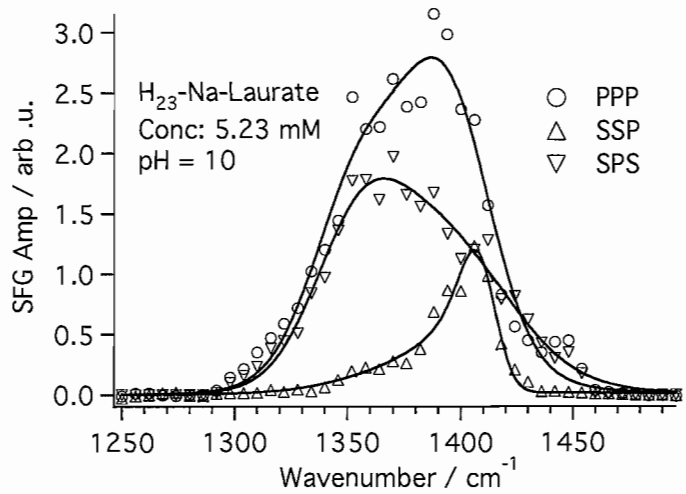

Figure 3.4. Polarization schemes ppp (○), ssp (△), and sps (▽) of Na-dodecanoate with a fully protonated chain at a concentration of 5.23 mM which is equivalent to a full monolayer at the interface according to our interfacial tension data. Solid lines are two-peak fits to the data.

literature suggests the COO^- ν_s is centered at $\approx$1410 cm^{-1} at the air-water interface[34, 62–65]. Polarizations ssp, sps, and ppp spectra can be seen plotted against each other at full monolayer coverage in Figure 3.4. These three polarization schemes show two distinct modes in the spectral window. In ssp, there is clearly a mode at $\approx$ 1405 cm^{-1} with a tailing shoulder at lower frequency, whereas in sps polarization, the lower frequency is dominant and the higher frequency tails off. In addition, because sps is sensitive to components of the dipole parallel to the interface, it can be seen that the lower frequency mode has a significant dipole contribution in that plane due to its larger amplitude in sps than in ssp. The ssp polarization spectra show the opposite amplitude trend as seen in sps and this is as expected given that it is sensitive to dipole components normal to the plane of the interface. Due to selection

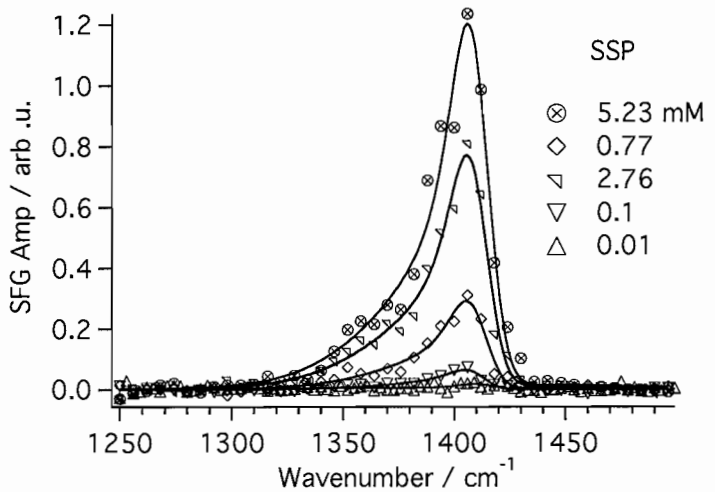

Figure 3.5. Concentration series of Na-dodecanoate in the ssp polarization scheme at pH 10. Equivalent concentrations in this figure and Figure 3.6 have the same data symbols. 0.01 mM (△) was not able to be fit accurately due to the very low signal count obtained. Solid lines are two-peak fits to the data.

rules, ppp is a combination of four elements of $\chi^{(2)}_{ijk}$ and shows both the low and high frequency vibrational modes with a different trend than what is seen in ssp or sps. The ssp (sps) spectra show a small amount of the low frequency (high frequency) mode because those contributing components of the dipole are not exclusively parallel (perpendicular) to the interface, thus they will have a small component projected into the perpendicular (parallel) plane which will be picked up by the ssp (sps) polarization scheme.

A concentration series for ssp polarization combination is shown in Figure 3.5 and a clear dominant mode is observed to grow in at $\approx$1405 cm^{-1} with a small shoulder on the low energy side at $\approx$1360 cm^{-1}. Spectra in the ppp polarization scheme can be seen in Figure 3.6 where the lower frequency mode is clearly seen and the modes

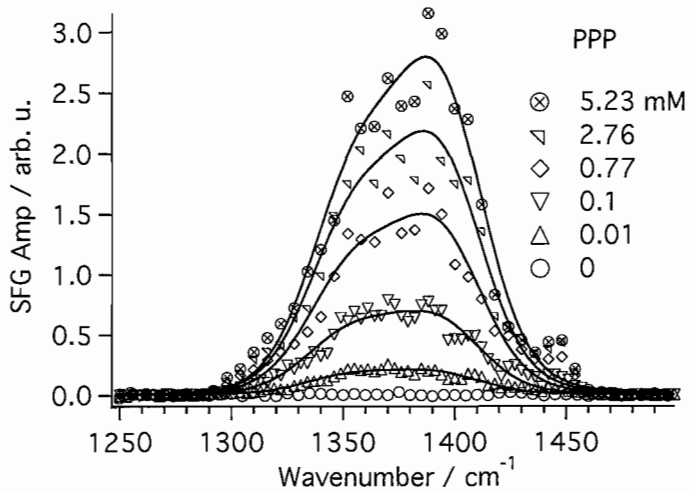

Figure 3.6. Spectral series showing a concentration range of Na-dodecanoate in the ppp polarization scheme at pH 10. Zero mM concentration (○) is added for reference to demonstrate a scan of the CCl_4-water interface in this region with no surfactant added. Solid lines are two-peak fits to the data.

together are very broad, spanning roughly 75 cm^{-1} FWHM. In ppp this sample gives more signal than ssp and the lower concentrations are more clearly resolved, which will have consequences for the spectral analysis discussed in the next section.

Spectral Fitting and Analysis

As shown in Equation II.10 VSFS spectral intensity is related to the square of $\chi^{(2)}_{NR}$ and $\chi^{(2)}_{R_\nu}$, and thus interferences can occur between the non-resonant background and the resonant modes, as well between different resonant modes like the case presented here where there are two modes in the spectra. Due to these interferences, the spectra must be fit in order to gain accurate information such as amplitudes, center position, and phase. In order to take a more rigorous approach to fitting, a global routine was

Table 3.1. Fixed, global, and variable parameters that were used in fitting the ssp, ppp, and sps VSFS data sets.

Fixed Param.	Γ_L	ϕ_{pk1}	ϕ_{pk2}	A_{NR}	ϕ_{NR}
All Pol	2	0	3.14	0	0

Glob. Param.	Pos1	$\Gamma_{\nu 1}$	Pos2	$\Gamma_{\nu 2}$
ssp	1385±7	35±3	1411±2	9±1
ppp	1345±3	24±1	1400±2	23±1
sps	1345±2	24±1	1405±2	34±1

ssp	$A_{\nu 1}$	$A_{\nu 2}$	ppp	$A_{\nu 1}$	$A_{\nu 2}$
0.01mM	-	-	0.01mM	0.43±0.04	0.45±0.04
0.1	0.17±0.04	0.36±0.06	0.1	0.76±0.03	0.82±0.03
0.77	0.35±0.04	0.80±0.09	0.77	1.05±0.05	1.23±0.04
2.76	0.57±0.07	1.3±0.1	2.76	1.24±0.06	1.49±0.04
5.23	0.69±0.08	1.6±0.1	5.23	1 .36±0.07	1.70±0.04
sps	$A_{\nu 1}$	$A_{\nu 2}$			
5.23mM	1.26±0.05	1.13±0.04	-	-	-

used for the ssp and ppp concentration series shown in Figure 3.5 and 3.6. In these cases all parameters are global except the amplitudes which allows a much higher confidence in the results versus fitting each individual spectra separately. The fitting parameters are shown for reference in Table 3.1

One of most useful parameters from the global fits is the amplitudes from the concentration series. From Equation II.6, it is clear that the two contributions to spectral intensity are number density of the molecules at the interface, and the average orientation of those molecules. By combining the resulting surface concentrations from the interfacial tension data and the amplitudes from the spectral global fits, it is possible to determine conformational changes during the formation of the monolayer. In Figure 3.7, the square root of the amplitude is plotted with respect to the surface concentration for both the low and high frequency peaks in the ssp spectral series.

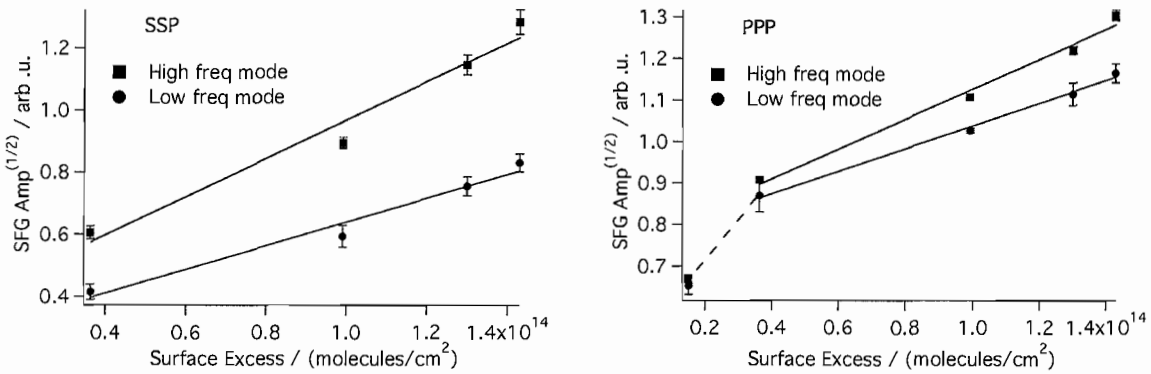

Figure 3.7. Square root of the fit amplitudes in the ssp (left) and ppp (right) polarization scheme plotted against the surface concentration which is calculated from the interfacial tension data. Each data point represents the center frequency for the low (●) or high (■) frequency mode at that particular surface concentration. The solid line is a linear fit to the data and the error bars are the standard deviation from fitting the pre-averaged individual sets of concentration spectra. Where error bars are not seen, the error is approximately the size of the data point. The dotted line is to illustrate the change in linearity below a surface coverage of $0.4\text{x}10^{14}$ molecules/cm^2.

When plotted and fit to a line, the amplitudes show a monotonic increase with respect to surface concentration, indicating that the increase in VSFS signal is due to the effect of increasing number density at the interface, and not a change in orientation as the monolayer is forming. The lowest concentration in ssp couldn't be reliably fit due to the low signal strength. When the ppp amplitudes are plotted in a similar fashion, roughly the same trend is observed with one exception, that the lowest concentration doesn't fit in with the overall linear trend. In Figure 3.7, it is seen that above $\approx$ $0.4\text{x}10^{14}$ molecules/cm^2 the trend is linear for both the low and high frequency modes in ssp and ppp. When inspecting the linear region of these plots, it is apparent that the slope of the higher frequency mode is larger than that of the lower frequency mode indicating that while both of the populations of molecules contributing to those modes

are increasing monotonically, the number density of the higher frequency population is growing at a faster rate than that of the lower frequency contributing population. Based on the polarization spectra this mode is most prominent in ssp which means the headgroup is in an upright orientation with the dipole more normal to the plane of the interface. Previous work shows increasing number density leads to increasing order in the monolayer[52], which in the case of carboxylate would fall in line with a headgroup that adopts a more upright configuration as surface concentration increases. This does not mean that the average orientation for each individual spectrally contributing species is changing, but because these two distinct regions can be resolved and fit as two separate peaks, it means that the ratio of one average orientation to the other is changing with respect to surface coverage. If the spectra were not resolved into two peaks and was instead a "continuum" of species that fit to one peak, then it is probable that the single fit mode would show a change in orientation as surface concentration increased due to that average orientation being spread over all species at the interface rather than two distinct regimes as we see here. The non-linearity for the lowest concentration ppp amplitude indicates that at very low surface coverage, there is a change in orientation as the surface number density increases but only up to the concentration of $\approx 0.4\text{x}10^{14}$ molecules/cm^2. Beyond this surface concentration the monolayer continues to form monotonically without any significant changes in overall orientation. This is not unexpected given that at very low surface coverage, monolayers are known to have larger areas per molecule and thus less conformational

order comes from decreased chain-chain interactions which would result in an initially floppy headgroup[48, 52].

Mode Assignment

From initial observations of the three polarization spectra in Figure 3.4 it is clear that there are at least two modes present. However, assignment of these modes is not straight forward due to the IR and Raman spectra of carboxylate surfactants which show not only the COO^- ν_s mode but also several CH bending, wagging and deformation modes[65] in this region. Initial guesses as to assignments might lead to assigning the high frequency mode to the carboxylate headgroup symmetric stretch and the low frequency mode to a CH wag. Experimentally, distinguishing these modes can be accomplished with the same VSFS experiments applied to a fully deuterated analog of Na-dodecanoate. The results of these studies can be seen in Figure 3.8 where it is clear that the entire width of the ppp spectrum and both modes in all three polarizations are due to the carboxylate headgroup. The only deuterated compound available for experiments was that of d23-K-dodecanoate. The change in counter ion from Na^+ to K^+ is the cause for the difference in amplitudes between the protonated and deuterated hydrocarbon chains as verified by the addition of a swamping amount of electrolyte to the Na-dodecanoate (spectra not shown) which causes the amplitudes to increase just as seen for the d23-K-dodecanoate spectra. Due to the isotopic substitution, there are no CH or CD modes to complicate the spectral region and

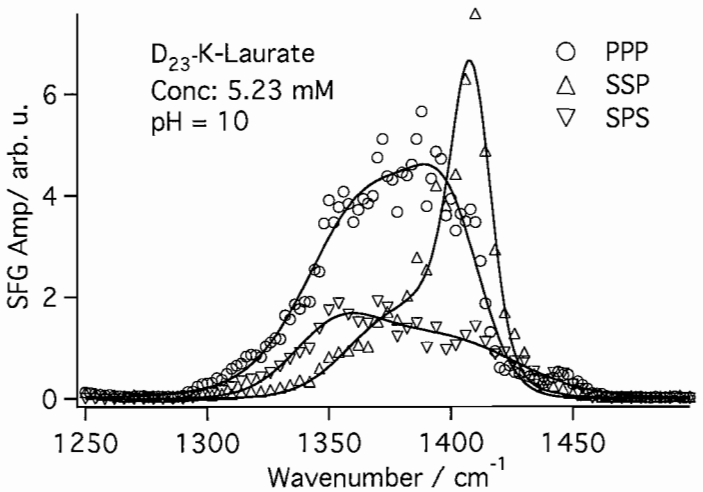

Figure 3.8. Polarization schemes ppp (○), ssp (△), and sps (▽) of K-dodecanoate with a fully deuterated chain at a concentration of 5.23 mM. Solid lines are two-peak fits to the data.

if any of the modes were CC modes, they would be shifted significantly enough to alter the spectra due to the substitution of the hydrogens. This indicates that not only is there a broad distribution of frequencies for the headgroup, but that these frequencies fall into two distinct frequency regions, one centered at $\approx$1365 cm^{-1} and one at $\approx$1405 cm^{-1}. It is proposed that several structural anomalies are occurring at the CCl_4-water interface that lead to the major differences in spectra between the oil-water interface and other interfaces such as the air-water and solid-liquid interface. The first major difference that has previously been shown is that the hydrocarbon chains of the surfactants are fully solvated and thus the chain-chain interactions are minimized to the extent that the monolayer becomes more disordered[48]. The second contribution to the spectral differences is the large area per headgroup due to the charge-charge repulsion. This large area per headgroup combined with the solvation

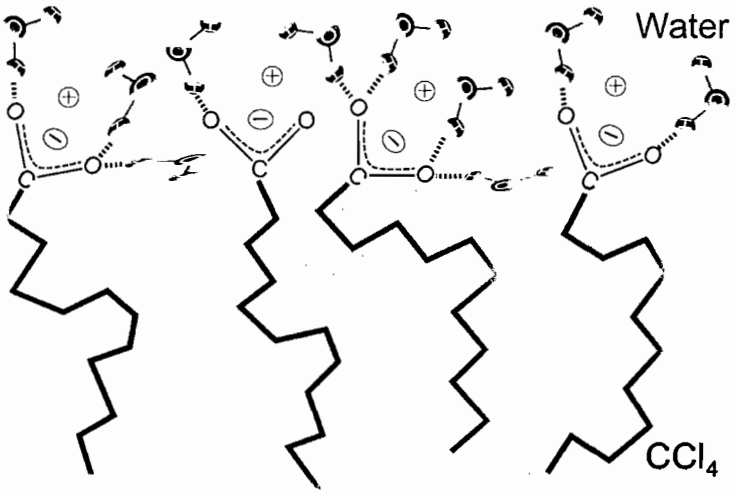

Figure 3.9. A representative cartoon showing the variety of structures and orientations of the headgroups at the oil-water interface.

of the chains allows the molecules at the interface to adopt a variety of orientations and conformations, which allows the headgroup to have a very broad distribution of angles at the interface that falls into two vibrational frequency regions. These orientations adopted by the headgroup are the leading cause as to why different ratios of the lower and higher vibrational frequency regions in the different polarization schemes are observed. Based on the distribution of frequencies in the spectra, the emerging picture is one where the headgroups exist in a variety of hydrogen bonding structures at the interface that are very different from each other. In one instance, there are headgroups which are only hydrogen bonded once, which leads to a very different vibrational frequency than that of a headgroup which is hydrogen bound four times (two on each oxygen). This is illustrated in Figure 3.9, which shows the different possible orientations and hydrogen bonding schemes of the headgroup.

Assigning the lower frequency peak to headgroups that have more hydrogen bonds leads to the orientation picture shown in Figure 3.9. Because this lower frequency peak is more prominent in the sps spectra, it means that the dipole of the headgroup is more in the plane of the interface than normal to it. Intuitively, one would typically think that a carboxylate headgroup with it's dipole normal to the interface would have the most opportunity to hydrogen bond due to both of its oxygens being pointed equally into the aqueous phase. However, MD simulations suggest that a large percentage of interfacial water molecules are not actually sum-frequency active because they lie in the plane of the interface[66, 67]. With this being the case, it is more likely that a carboxylate headgroup with one of it's oxygens near the plane of the interface would have more bonding opportunities with the "in plane" water molecules, which leads to the picture in Figure 3.9. This work provides seminal evidence of the relationship between headgroup orientation and hydrogen bonding for carboxylate surfactants, a topic for which there is little experimental evidence of.

The Effect of pH on Surfactants at the Interface

Studying pH affects on the interfacial carboxylate surfactants provides additional proof that the broad signal in the 1400 cm^{-1} region is due to the head group. Polarization spectra in ssp and ppp as a function of pH are shown in Figure 3.10 and 3.11. It is evident that as pH decreases, the entire contribution to the signal in both ssp and ppp decreases as well, providing additional support that the broad

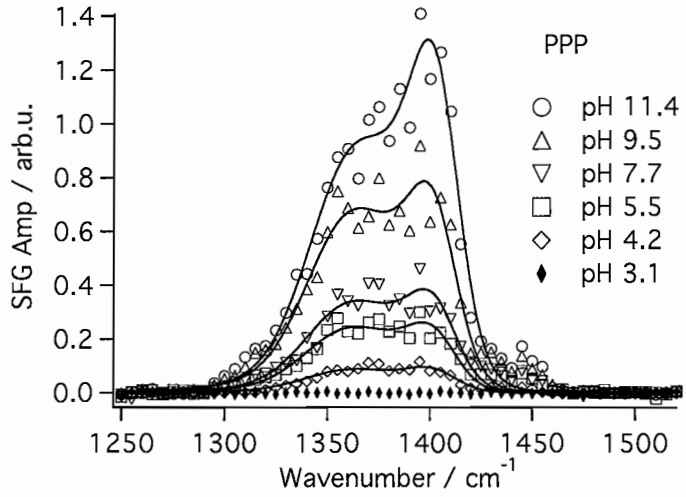

Figure 3.10. pH series spectra of Na-dodecanoate in ppp polarization from pH 3.1-11.4.

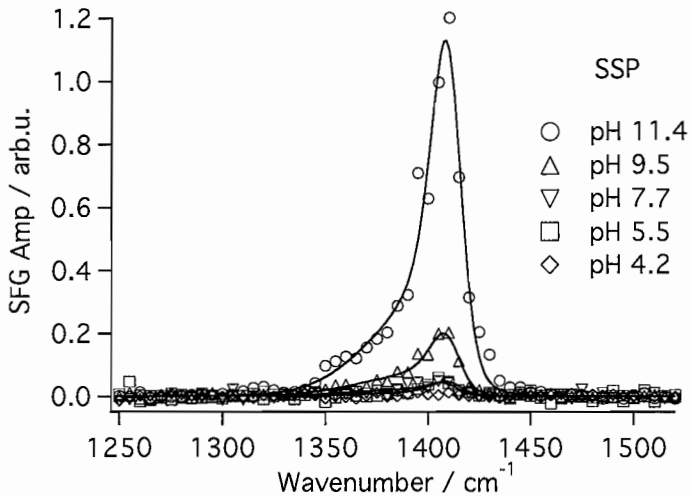

Figure 3.11. pH series spectra of Na-dodecanoate in ssp polarization from pH 4.2-11.4. Resolution of the modes in ssp is lower than in ppp, and the signal has essentially disappeared by pH 5.5.

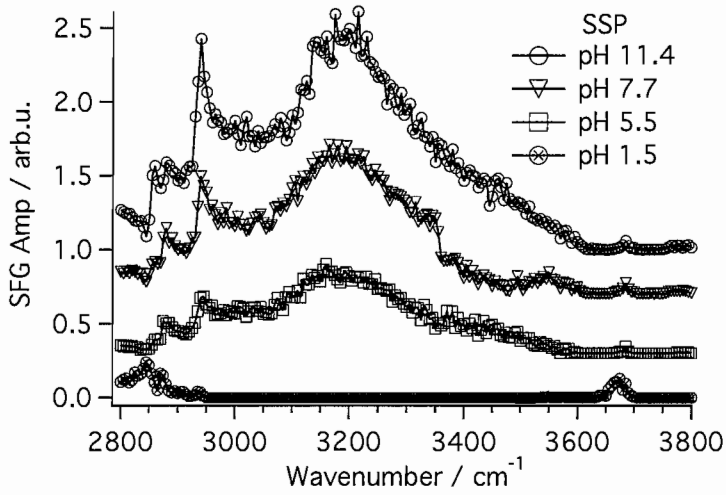

Figure 3.12. VSFS spectra of Na-dodecanoate ssp polarization in the water and CH region from pH 1.5-11.4.

spectral width is a result of the headgroup symmetric vibration. Combining the headgroup information from the mid-IR VSFS with VSFS spectra from the water region in Figure 3.12, it is observed that even at low pH there is still CH signal showing that surfactant is still present at the interface. At low pH, the surfactant is fully protonated as evidenced by the lack of signal in the 1400 cm^{-1} region, the presence of C=O signal at $\approx$1740 cm^{-1} in Figure 3.13, and the lack of water signal due to a fully neutralized CCl_4-water-surfactant interface. This supports the picture of a broad distribution of headgroup angles and hydrogen bonding stuctures drawn from the alkyl isotopic substitution studies. Additional evidence for the protonation and deprotonation exists in the pH spectra of the water region. At high pH, when the headgroup is deprotonated and charged, a field is created at the interface due to the double layer effect, which acts to align the water molecules at the surface.

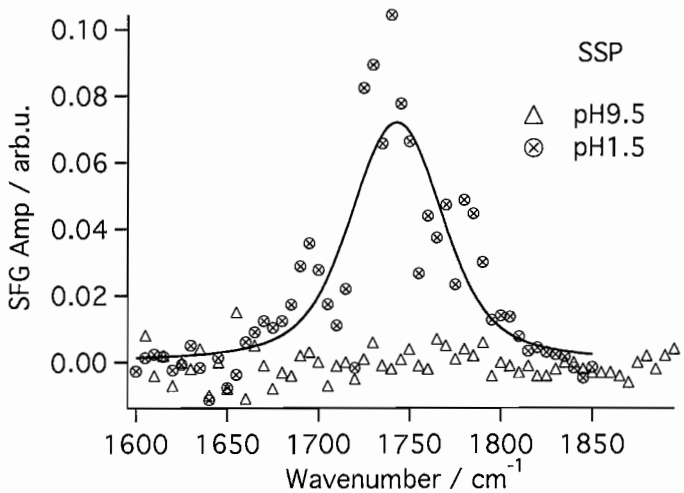

Figure 3.13. VSFS spectra of the carbonyl band at low and high pH. At a pH of 1.5, there is a small amount of signal assigned to the C=O, whereas at a pH of 9.5, there is not signal present due to the deprotonation of the headgroups in the monolayer.

This is manifested in the spectra by the large peak at 3200 cm^{-1} which is typically assigned to more highly coordinated water molecules with tetrahedral structure at the interface[68]. The data at low pH suggests the opposite picture where a majority of the headgroups are protonated, and thus there is little to no field at the interface due to charge neutrality, and hence the water signal at 3200 cm^{-1} is negligable. Evidence for the presence of surfactant at the interface at both high and low pH is given by the C-H modes in the 2800-3000 cm^{-1} region. Interestingly, it seems there is a propensity for the charged headgroup at the interface given its stronger signal relative to the weak C=O mode seen in Figure 3.13 corresponding to the protonated headgroup. Once again, due to the dependence of signal on both orientation and number density at the interface, it cannot be ruled out that the COOH headgroups are simply not well oriented and thus give much smaller signal, or that the carbonyl group is in the plane

of the interface, which would also yield no signal. In the water region ssp spectra, there is evidence for the C-O-H vibrational mode at 3550 cm^{-1} at pH 7.7 although there was no evidence of the C=O mode in any polarization combination at this pH, possibly providing further evidence that the C=O is oriented in the plane of the interface. In addition this small mode at 3550 cm^{-1} disappears at lower pHs. Given that this mode has been assigned to a very weakly bound C-O-H, indicative of a disordered head group, it is not surprising that there is little orientation of the C=O when taking into account the added effect of solvating the chains in the oil phase.

Considering the Hydrophobic Interactions of the Alkyl Chains

Another way to look at the broad widths, multiple peaks, and lower than normal vibrational frequencies of the headgroup is to consider the hydrophobic interactions of the surfactant alkyl chains and reconcile this with different types of interfaces. If the frequencies of the head group COO^- symmetric vibrational mode are considered at the solid-liquid, air-water, and CCl_4-water interface, an interesting trend is observed. In the upper table in Figure 3.14, it is shown that the vibrational frequency for the head group mode increases in energy as the length of the surfactant chain increases for the CaF_2-water interface. This increase in chain length is also associated with an increase in alkyl-water hydrophobic interactions and chain-chain interactions. At the CaF_2-water interface, the chains are not in their ideal environment and there is an energy cost associated with the forced solvation from the water. At very low

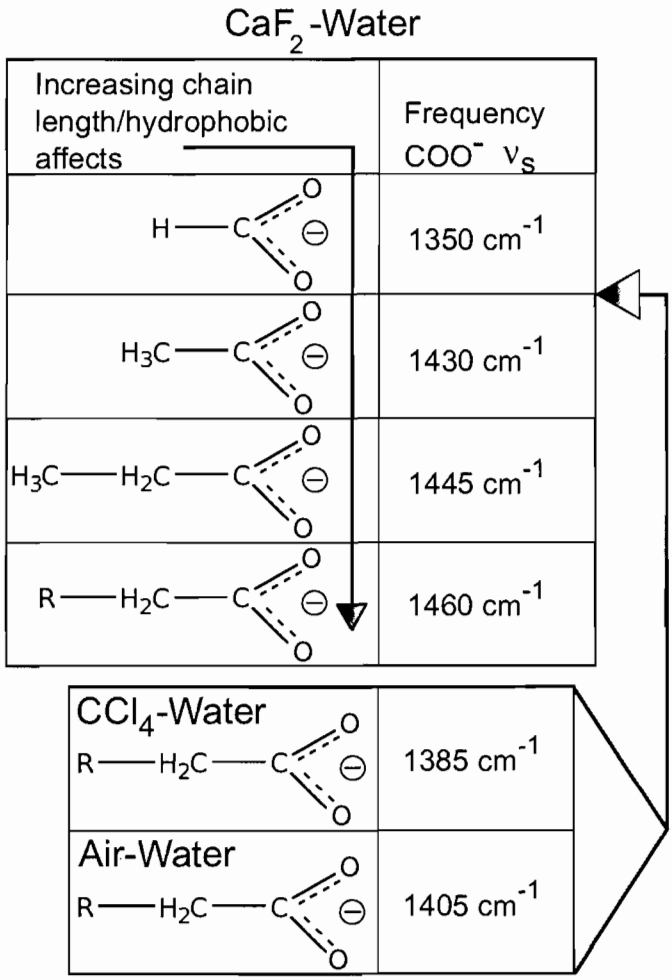

Figure 3.14. COO^- ν_s frequencies of carboxylate surfactants with increasing chain lengths at the CaF_2-water interface (top table) and the COO^- ν_s frequencies of Na-dodecanoate at the air-water and CCl_4-water interface (lower table). Clearly the trend is increased vibrational frequency with increased hydrophobic affects. The air-water and oil-water vibrational frequencies of a 12 carbon chain fall near the "very little hydrophobic affects" side of of the CaF_2 table. CaF_2 frequencies obtained from [41].

chain lengths such as the formate (top molecule in table), there are virtually no hydrophobic interactions occurring between the C-H and the water. However, as chain length increases, hydrophobic interactions increase and the energy of the carboxylate symmmetric vibrational mode is observed to increase. When the vibrational frequency of the carboxylate symmetric stretch at the air-water interface is compared with the CaF_2-water interface, the lack of hydrophobic interactions needs to be noted due to the fact that the chains are undoubtably sticking into the vapor phase and not into the water phase. There are still however strong chain-chain interactions which force a very ordered monolayer. Overall this situation correlates with a decrease in the vibrational energy of the headgroup. When the vibrational frequency of the COO^- is observed at the CCl_4-water interface, the headgroup vibrational frequency is shifted even closer to that of the formate at solid-liquid where there are little to no hydrophobic interactions. It is hypothesized that this is mainly due to the chains being solvated by the oil phase which is a "like" environment and instead of an energy loss like at the solid-liquid, there is an energy gain, and hence a lowering of the energy of the headgroup vibrational frequency. With these interfaces in mind, it is not surprising that the vibrational energy of medium chain length carboxylates at the CCl_4-water interface extends to much lower frequency than at the air-water interface and the solid-liquid interface for similar chain length carboxylate surfactants.

Conclusions

We have shown what is to our knowledge, the first mid-IR VSFS spectra of functional groups at the oil-water interface. Both the orientation and the hydrogen bonding are distinguishable with vibrational sum-frequency spectroscopy due to the different polarization combinations used and the frequency at which the vibrational modes are seen. These experiments have shown that the carboxylate head groups adopt a variety of orientations upon adsorption to the CCl_4-water interface due in part to the chains being solvated by the oil phase. This in turn leads to a variety of hydrogen bonding coordinations to the headgroup which affects the vibrational frequency of the headgroup modes. These experiments show that while information can be obtained from the CH modes as seen by many past studies, there is still a large amount of pertinent information to be gained by studying the spectroscopy of the headgroups. Combining both the mid-IR and the water/CH regions allowed a complete picture to be formed of the molecule at the interface. Due to the broad distribution of headgroup angles and hydrogen bonding structure, the CCl_4-water interface is an ideal place to study the binding of counter ions to the carboxylate headgroup and these effects could have interesting implications on the structure and bonding found in this current work.

CHAPTER IV

A STUDY OF THE BINDING OF METAL IONS TO CARBOXYLATE HEADGROUP SURFACTANTS

In this chapter, vibrational sum-frequency spectroscopy and surface tensiometry are used to study the binding of environmentally and biologically important metal ions with Na-decanoate at the CCl_4-water interface. The goal of this study was to understand the interfacial binding characteristics of metal ions. Infrared studies have often studied such systems, however, the technique is not surface specific, it cannot access the oil-water interface, and the way in which binding strengths are categorized is subject to scrutiny. Based on the conclusions from Chapter III, the carboxylate headgroup at the oil-water interface is an ideal model for studying metal binding due to the sensitivity of VSFS to the broad distribution of orientations observed. This work observes distinct changes in the headgroup vibrational region that are metal ion dependent, and thus the metal-carboxylate interaction can be probed directly based on frequency shifts and changes to the headgroup hydrogen bonding character. E. J. Robertson assisted in the acquisition of the interfacial tension data shown in this chapter.

Introduction

The importance of metal binding is widespread throughout chemistry and biology. One of the most extensive chelators of metals are carboxylate groups, which are present in familiar molecules such as EDTA, as well as being the primary headgroup in fatty acids and soaps. Environmentally, humic acids have a particularly high carboxylic acid content and aid in the transport of both toxins (such as heavy metals) and nutrients through the soil. There have been extensive studies modeling humic acid to understand the binding activities of metal ions[26, 69–78]. Metal ions are also present atmospherically in aqueous droplets and are known to catalyze sulfur oxidation and are thought to be involved in a number of other atmospheric reactions as well[79].

Metal ions also play an important role in a variety of biological processes. Zn^{2+} acts as a stabilizer for a collection of motifs known as zinc fingers, which contain 25-60 residues arranged around one or two Zn^{2+} ions and are important in the stabilization of small, folded polypeptide chains that interact with nucleic acids[80, 81]. In addition, metal ions, particularly transition metals, are required for catalysis in roughly one-third of all enzyme reactions[80]. The transition metal ions, such as Cu^{2+} and Mn^{2+} play a distinctly different role from monovalent ions like Na^{+} and K^{+}, which often act in a structural capacity rather than a catalytic one[80, 82, 83]. Also in contrast, monovalent ions tend to bind non-specifically and act to stabilize surface charge as a bulk electrolyte, whereas divalent metal ions have specific binding

to functional group such as phosphates, acting as superior shielding ions for large, highly structured biomolecules[80, 84]. Ca^{2+} and Mg^{2+} play important regulatory roles, signaling the switching process for metabolic reactions based on the flux of the ions through cell membranes[82]. The presence of metals is also known to have a structural effect on monolayers at the air-water interface, causing the monolayers to form a more condensed phase than in the absence of metal ions[85–93]. This has strong implications with regard to intracellular structure near membrane walls which are composed of fatty acids, phospholipids, and cholesterols.

Although bulk phase characteristics of metals binding to carboxylates has been extensively investigated, the importance of these events at interfaces is becoming increasingly clear as environmental and biological studies reveal more about the existence of metals in interfacial chemistry. While there have been a number of studies at the air-water interface pertaining to metal binding with surface active species, these have primarily been conducted with spectroscopies that are not surface specific and contributions from the bulk phase can have significant affects on the spectra[43, 63, 87, 91, 94, 95]. Previous surface specific VSFS work by Allen and coworkers probed the carboxylate headgroup of long chain surfactants at the air-water interface with $Na^{+}$and K^{+}, and found distinct differences between the binding and deprotonating ability of the two ions[32]. They did not however study any divalent ions to compare their results with. Huhnerfuss and coworkers completed a number of studies on metals binding with carboxylates at the air-water interface using IR

spectroscopy[43, 63, 95]. They categorized the types of binding based on the splitting between the symmetric and asymmetric stretching frequencies of the carboxylate headgroup. However, IR spectroscopy is not a surface specific technique and analysis of the split between asymmetric and symmetric peaks is controversial and the strength of the binding interactions is not definitive.

In this chapter, vibrational sum-frequency spectroscopy (VSFS) was used to study the interactions of alkali earth and transition metal ions with carboxylate surfactants by probing the carboxylate headgroup and alkyl CH vibrational modes at the CCl_4-water interface. Based on the vibrational frequencies of the carboxylate symmetric stretch, it was possible to identify the types and coordination of several alkali earth and transition metal ions with Na-decanoate adsorbed at the oil water interface. Recent experiments in this lab have shown the oil-water interface to be a unique environment for surfactant headgroups and the results proved the oil phase plays a large part in the distribution of orientations of the headgroup. By using VSFS in this study, the distribution of orientations of the headgroup is observed to change through vibrational frequency and peak widths depending on the metal that is bound to it. In addition, this work links the metal-headgroup interaction strength with the alkyl chain ordering using the methyl and methylene vibrational stretches.

Carboxylates at the Oil-Water Interface

The previous chapter showed that carboxylate surfactants adopt a wide distribution

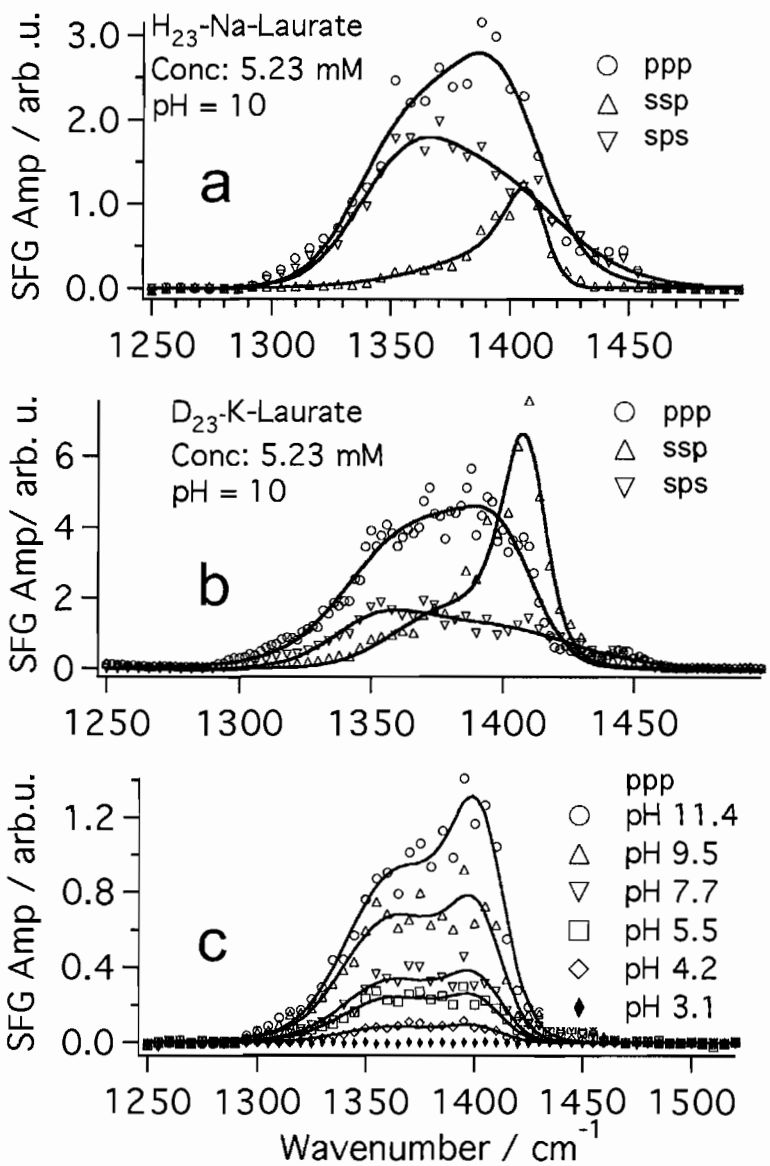

Figure 4.1. VSFS spectra of: a) H_{23}-Na-dodecanoate in ssp, sps, and ppp polarization schemes, b) D_{23}-K-dodecanoate in the ssp, sps, and ppp polarizations schemes, c) pH series of H_{23}-Na-decanoate in the ppp polarization scheme.

of orientations at the oil-water interface due to the large area per headgroup, the solvation of the chains via the oil phase, and the variety of possible hydrogen bonding structures of the headgroup at the interface. Figure 4.1a shows VSFS data in ssp, ppp,

and sps polarization schemes of the carboxylate headgroup symmetric stretch. The same spectra of a fully deuterated sample (Figure 4.1b) proved the entire width of all three polarization spectra were due to the carboxylate headgroup vibrations. Further proof of this was found in a pH series of Na-decanoate in ppp polarization (Figure 4.1c) where the full width of the modes is observed to decrease as the pH is lowered. As the headgroup is protonated to become a carboxylic acid, all the vibrational modes in the carboxylate region disappear. It was concluded that the VSFS spectra of the carboxylate region showed two vibrational modes in this region, one centered at approximately 1360 cm^{-1}, and the other at 1405 cm^{-1}. The two modes correspond to different hydrogen bonding structures of the headgroup at the interface. Although the spectra were fit with two modes, the hydrogen bonding exists in a continuum where lower frequency equates to a more hydrogen bound headgroup, and higher frequency is a less hydrogen bound headgroup. This is similar to the interpretations of VSFS water spectra where hydrogen bonding coordination number leads to shifts of 700 cm^{-1}or more[57, 96, 97]. The broad widths of the spectra and the distinguishable hydrogen bonded frequencies of the headgroups makes this an excellent case study for the binding of ions to the charged surfactants because any change in the headgroup hydrogen bonding structure, such as the ionic or covalent binding of metal ions, will be apparent in the VSFS spectral signatures. The ions used to perturb the carboxylate headgroup environment are Mg^{2+}, Ca^{2+}, Mn^{2+}, Ni^{2+}, Cu^{2+}, and Zn^{2+}. Tables 4.1 and 4.2 show the frequency shifts and amplitude changes observed in the ppp and

Table 4.1. Fit center frequency parameters for the metal ions with 1mM Na-decanoate in ppp polarization. Low and High refer to the relative frequencies of the modes observed. The initial frequencies are for 1 mM Na-decanoate at pH 5.5 and 0 mM in the table refers to the metal ion concentration.

Initial	Center Low	Center High
0 mM	1345±3	1400±2
Ion/Conc	Center Low	Center High
Mg 3 mM	1358±3	1410±1
Ca 3 mM	1357±2	1409±1
Mn 3mM	1357±2	1414±1
Ni 1.6 mM	1380±9	1420±1
Cu 0.2 mM	NA	NA
Zn 0.2 mM	NA	NA

Table 4.2. Fit amplitude parameters for the metal ions with 1 mM Na-decanoate in ssp polarization. Low and High refer to the relative frequencies of the modes observed. The initial amplitudes are for 1 mM Na-decanoate at pH 5.5 and 0 mM in the table refers to the metal ion concentration.

Initial	Amp Low	Amp High
0 mM	0.20±0.02	0.35±0.03
Ion/Conc	Amp Low	Amp High
Mg 3 mM	0.21±0.04	1.05±0.02
Ca 3 mM	0.18±0.06	1.21±0.02
Mn 3 mM	0.10±0.08	1.20±0.03
Ni 1.6 mM	0.10±0.07	1.12±0.09
Cu 0.2 mM	NA	NA
Zn 0.2 mM	NA	NA

ssp polarization spectra discussed throughout this chapter. Cu^{2+} and Zn^{2+} are not included in the tables due to their different binding characteristics which will be explained below. The ions will be discussed based on their respective groups, ie. alkali earth metals and transition metals.

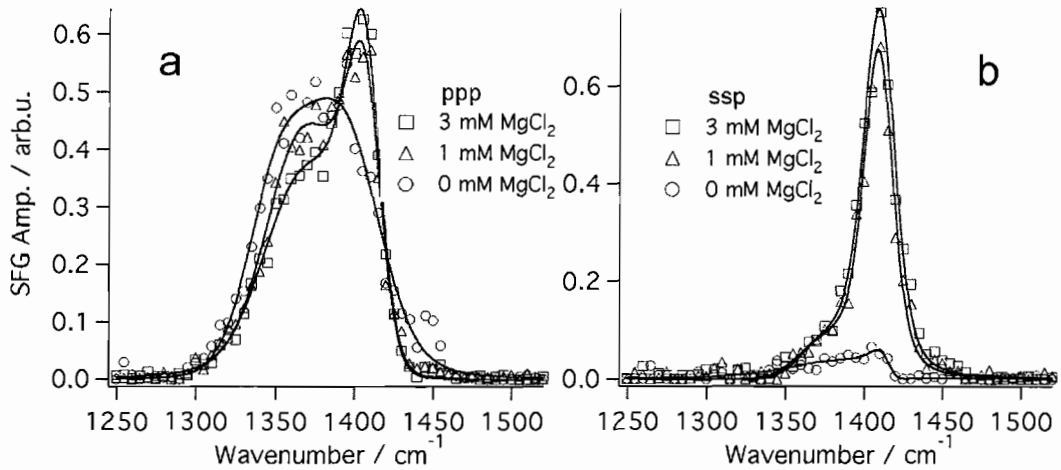

Figure 4.2. ppp (left) and ssp (right) VSFS spectra of $MgCl_2$ in the COO^- region. The solid lines are fits to the data.

Alkali Earth Metals

Alkali earth metals investigated in this study are Mg^{2+} and Ca^{2+}. Mg^{2+} and Ca^{2+} play important roles in structural stabilization in biological systems and have specificity in binding. X-ray crystallography has shown Mg^{2+} and Ca^{2+} form notable complexes with DNA and each ion generates a different crystal lattice structure[84, 98]. To model the binding of Mg^{2+} and Ca^{2+} to biomolecules, VSFS was used to probe the carboxylate headgroup of Na-decanoate in the presence of these aqueous salts. VSFS spectra were collected in ssp and ppp polarization for the carboxylate stretching region, and ssp in the CH stretching region (discussed later). Both salts affect the neat CCl_4-water-decanoate spectra in similar ways, although Ca^{2+} has slightly larger effects than Mg^{2+}. Figure 4.2 shows the effects of Mg^{2+} on a 1 mM Na-decanoate solution for both the carboxylate and CH stetching region. In the

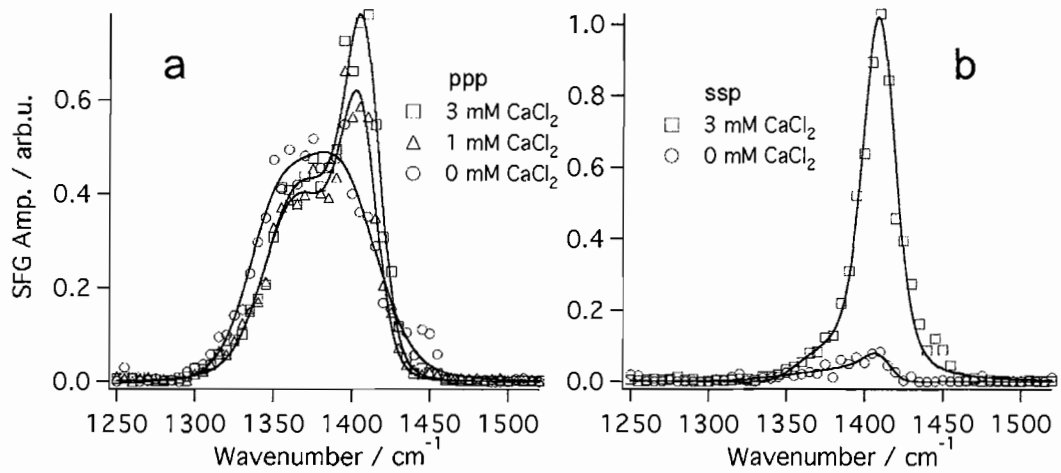

Figure 4.3. ppp (left) and ssp (right) VSFS spectra of $CaCl_2$ in the COO^- region. The solid lines are fits to the data.

carboxylate region (Figures 4.2a and b), ppp polarization spectra are observed to blue shift. As in the interpretation of water region VSFS spectra[99], blue shifting indicates a less hydrogen bound structure due to less damping of the oscillator from the H-bonds. In addition, the lower frequency component decreases in amplitude and the higher frequency component increases in amplitude. In ssp polarization, spectra show a significant increase in the 1410 cm^{-1} mode with the addition of salt. In Figure 4.3a and b, the same behavior is observed for Ca^{2+} additions to 1 mM Na-decanoate. In the case of Ca^{2+} and Mg^{2+} , it is shown that they both cause approximately equal amounts of blue shifting in the spectra, indicating they are disrupting the hydrogen bonding structure around the headgroup in an equivalent manner. In the process of an ion-headgroup interaction, water is excluded from the headgroup region and thus there would be fewer hydrogen bonding opportunities for the headgroup, which would act to shift the carboxylate headgroup symmetric stretch to higher frequencies. Both

of the divalent ions also induce a more ordered upright headgroup at the interface, indicated by the large increase in the higher frequency component in the ssp and ppp polarization spectra in Figures 4.2 and 4.3. The main difference between the effects of Mg^{2+} and Ca^{2+} ions is that Ca^{2+} induces a slightly larger increase in both the ssp and ppp polarization spectra. While both ions are known to have electrostatic interactions with the headgroup[89], the data demonstrates that Ca^{2+} has a slightly stronger interaction with the carboxylate headgroup than Mg^{2+}.

Transition Metals

While the previous section discussed the interactions of alkali earth metal ions with the carboxylate headgroups, the interactions were electrostatic in nature. To further the knowledge of divalent binding with relevance to both biological and environmental systems, binding of transition metals with carboxylates was investigated. Transition metals binding with organics are relavent to atmospheric chemistry as the presence of these ions can catalyze reactions at the interface of cloud droplets[79]. As discussed in the introduction, transition metals also play an important role biologically as structural stabilizers and additionally act in a catalytic capacity for enzyme reactions.

The transition metals used in this study were Mn^{2+} , Ni^{2+} , Cu^{2+} , and Zn^{2+}. The effects of the transition metals on the VSFS spectra are similar to what was seen in Mg^{2+} and Ca^{2+}, except the blue shifts, narrowing, and amplitude changes of the spectra are larger, indicating stronger interactions between the metals and

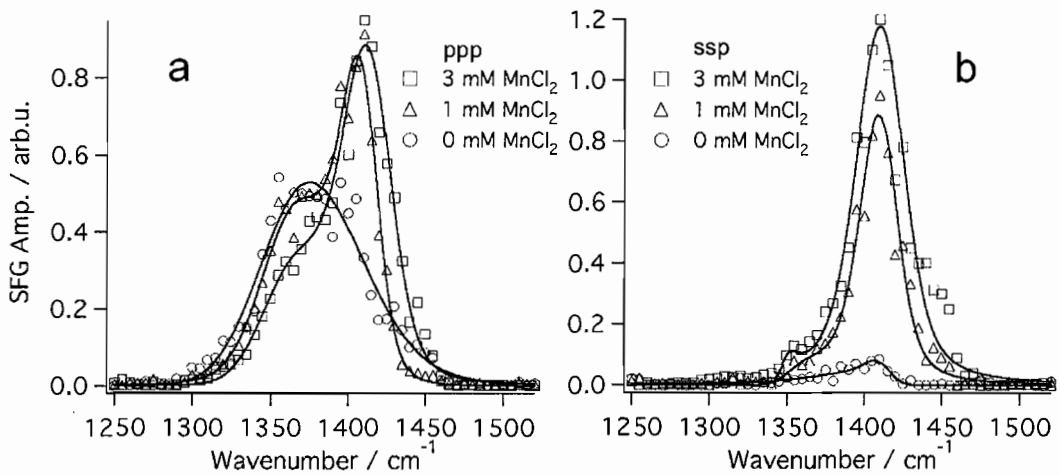

Figure 4.4. ppp (left) and ssp (right) VSFS spectra of $MnCl_2$ in the COO^- region. The solid lines are fits to the data.

the carboxylate headgroup. Figure 4.4 shows Mn^{2+} with 1 mM Na-decanoate in ppp (a) and ssp (b) polarizations for the carboxylate spectral region. In ppp, it is observed that the lower frequency component decreases in amplitude and blue shifts. The higher frequency component on the other hand increases in amplitude as it blue shifts. As with Mg^{2+} and Ca^{2+}, it is concluded that Mn^{2+} binds in an ionic manner and acts to narrow the distribution of orientations of the carboxylate headgroup. In ssp polarization, large increases in amplitude support the change in orientation showing that the higher frequency mode is gaining amplitude as increasing numbers of headgroups bind the cations. As in the interpretation of the Mg^{2+} and Ca^{2+} , this indicates less water is hydrogen bonded to the headgroup due to its exclusion from the headgroup region by the specific binding of the metal ions.

The next cation to be investigated was Ni^{2+}. Figure 4.5 contains VSFS spectra of $NiCl_2$ at an ionic strength of 400 μM in the presence of 1 mM Na-decanoate. Spectra

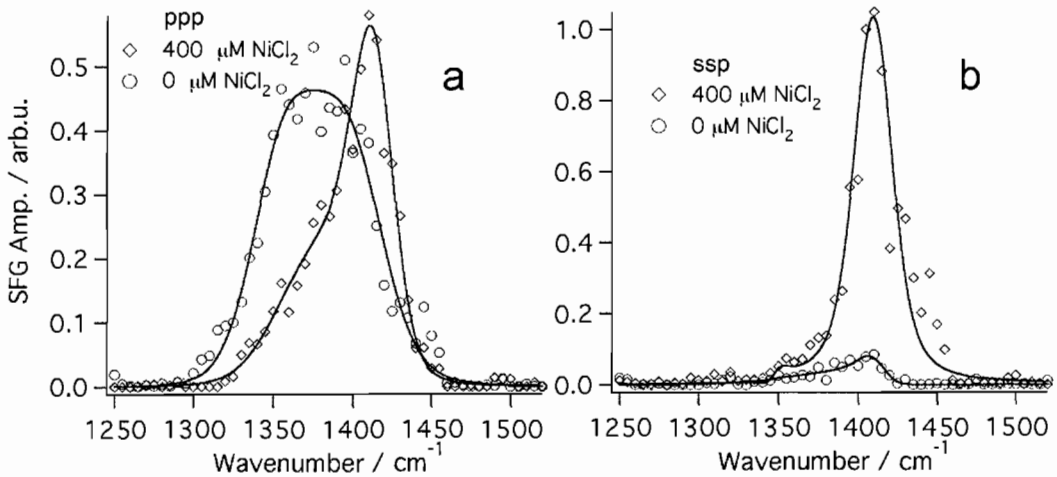

Figure 4.5. ppp (left) and ssp right) VSFS spectra of 400 μM $NiCl_2$ in the COO^- region. The solid lines are fits to the data.

show ppp (a) and ssp (b) polarization of the carboxylate region. Relative to the effective ionic strength, Ni^{2+} shows the most pronounced spectral shifts of the ions presented thus far. The lower frequency component is decreased significantly while the higher frequency component not only increases, but also blue shifts significantly to 1415 cm^{-1}. In ssp polarization, although the Ni^{2+} is at a bulk ionic strength six times less than that of the Mn^{2+} shown in Figure 4.4, it still gives roughly the same increase in amplitude over the neat 1 mM Na-decanoate ssp spectra. The induced shift and the amplitude increase both indicate that Ni^{2+} is by far the strongest bound ion introduced thus far. While Mg^{2+}, Ca^{2+}, and Mn^{2+} are known to bind with ionic character, Ni^{2+} is thought to bind with character between that of ionic and covalent monodentate[43, 92]. These results provide evidence that the binding strength of the Ni^{2+} with a carboxylate is much stronger than that of the other three ions. However, if the binding were monodentate in character, the spectra would be expected to shift

much more significantly than what is observed here. This expectation is due to the metal coordinating with one of the oxygens on the carboxylate resulting in the double bond character being primarily on the non-metal bound CO, and thus the frequencies observed for these modes would be much more similar to those of an unperturbed carboxylic acid, which are at 900-1250 cm^{-1} and $\approx$1750 $cm^{-1}$for the C-O-Me and C=O respectively[65].

In order to distinguish between ionic and covalent binding character, two ions were investigated that are thought to have stronger covalent binding characteristics with carboxylates, Cu^{2+} and Zn^{2+}. Due to solubility constraints these ions were studied at much lower concentrations than the ions above. However, the effects of these ions on the VSFS spectra of Na-decanoate even at low concentrations leave no doubt as to the ability to distinguish between ionic binding character and covalent binding character, specifically that of bi-dentate binding. Spectra of Cu^{2+} with 1 mM Na-decanoate in ppp and ssp polarization schemes are shown in Figure 4.6. In ppp (a), the spectral shape is similar to the neat carboxylate stretches between 1300 and 1400 cm^{-1}. However, a third mode clearly appears at 1450 cm^{-1} that was not present in any of the previous spectra. This mode is also assigned to the carboxylate symmetric stretch. Carboxylates bound to metal ions in a covalent bi-dentate fashion are known to produce multiple distinct vibrations within the carboxylate stretching region due to coupling between headgroups bound to the same metal ion[72, 82, 94]. The mode

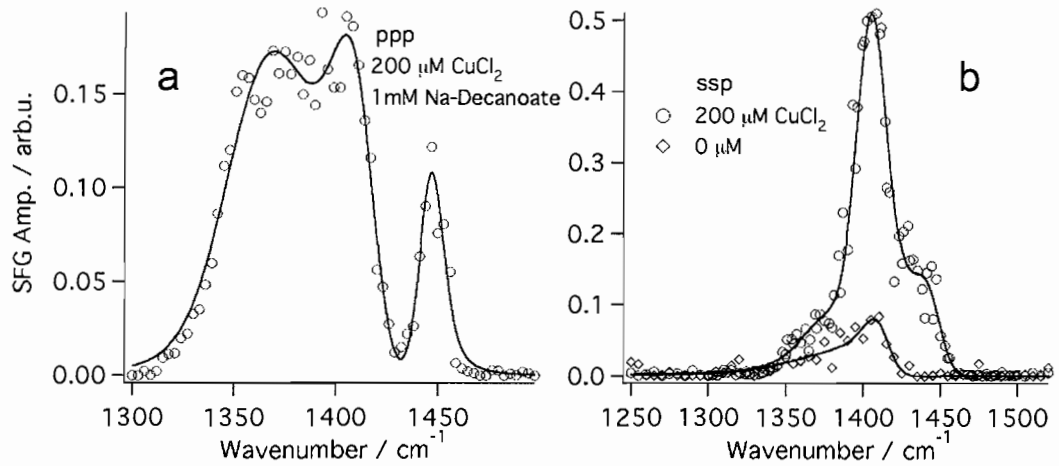

Figure 4.6. ppp (left) and ssp (right) VSFS spectra of $CuCl_2$ (I = 200 μM) and Na-decanoate (1 mM) in the COO^- region. The solid lines are fits to the data.

at 1450 cm^{-1} is attributed to the bound carboxylate headgroups where a Cu^{2+} ion is interacting in a bi-dentate manner with more than one carboxylate group.

Due to the drastically different results between Cu^{2+} and the other ions in the carboxylate stretching region, a study of Zn^{2+} was necessary to characterize the strength of binding between the covalently bound ions and the headgroup, as well as to provide a basis for the differences between the more weakly bound ions and the more strongly bound ions. Zn^{2+} has many important biological functions and warrants investigation into its binding characteristics. VSFS spectra of 0.5 mM Na-decanoate with 200 μM Zn^{2+} in ppp and ssp polarization of the carboxylate region are shown in Figure 4.7. The ppp Zn^{2+} spectra (a) show the same modes as seen observed for Cu^{2+} in Figure 4.6. There is a lower frequency component centered at 1360 cm^{-1}, a higher frequency component at 1400 cm^{-1}, and then an additional mode at 1450 cm^{-1} that isn't observed in the more weakly bound salt spectra. These

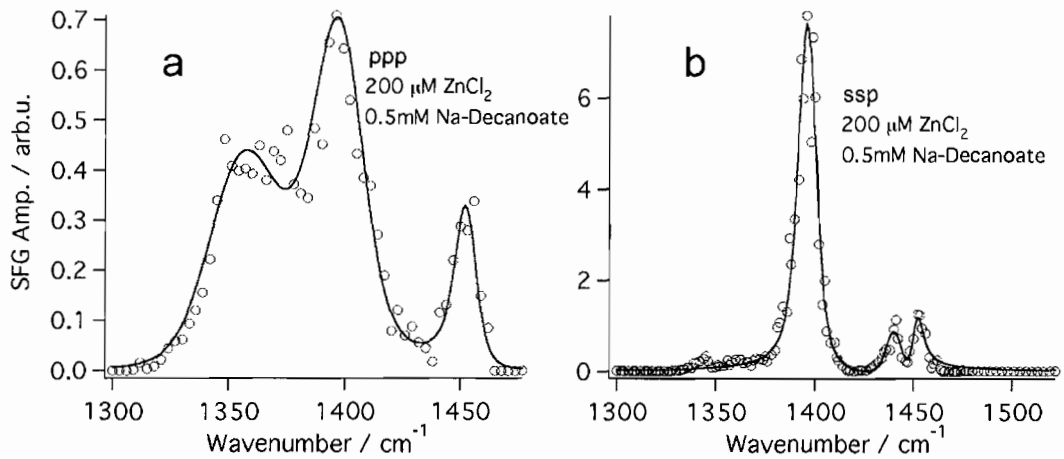

Figure 4.7. ppp (left) and ssp (right) polarization spectra of the COO^- vibrational region for $ZnCl_2$ (I = 200 μM) and Na-decanoate (0.5 mM). The solid lines are fits to the data.

modes are all assigned to carboxylate symmetric stretches. As in the case of Cu^{2+}, there is significant splitting of the frequencies. In the VSFS ssp polarization spectra of Zn^{2+} (b), significant splitting is also observed. There is a strong mode at 1395 cm^{-1}, and two weaker modes at 1435 cm^{-1} and 1450 cm^{-1}. Once again, these are all assigned to carboxylate symmetric stretching vibrations and the splitting of the modes is due to the vibrational coupling between multiple carboxylate groups bound to the same Zn^{2+} ion. Due to the complexity of the coupling between the carboxylate headgroup vibrations, it is not possible to characterize the binding strength of Zn^{2+} and Cu^{2+} relative to each other. However, it can clearly be stated that they both bind in a covalent bidentate manner, which is a much stronger interaction than any of the other ions presented in this chapter.

Alkyl Chain Conformations

Acquisition of VSFS spectra in the 2800-3000 cm^{-1} region allows the conformation of the alkyl chains to be linked with the interaction of the ions with the headgroup by tracking the CH_2 and CH_3 stretching vibrations. Spectra in ssp polarization are shown in Figure 4.8a-e for Mg^{2+}, Ca^{2+}, Mn^{2+}, Ni^{2+}, and Cu^{2+}. The spectra are fit to four vibrational modes. From low to high frequency, they appear at 2850, 2880, 2910, and 2940 cm^{-1}. These are assigned to the methylene symmetric stretch (ν_s CH_2), the methyl symmetric stretch (ν_s CH_3), the methylene fermi resonance (ν_{fr} CH_2), and the methyl fermi resonance (ν_{fr} CH_3) respectively in accordance with previous assignments in the literature[56, 100, 101]. Fitting the amplitudes of the peaks allows a direct assessment of the chain conformation. Methylene vibrations are only observed in VSFS when the cylindrical symmetry of the chain is broken via a gauche defect. In instances where methylene vibrations are observed, an order parameter may be calculated as the ratio of methyl/methylene amplitude as an internal method of comparing the ordering of the interfacial surfactant chains within a set of experiments[51, 53, 56].

The ratios of the methyl/methylene vibrations are shown in Figure 4.8f for each ion. The plot shows the ratio with respect to ionic strength, which allows the concentration of the ions to be factored into the induced ordering of the monolayer. Ca^{2+} and Mg^{2+} show the lowest ratio indicating that these two ions induce the lowest amount of monolayer ordering even though they are at the highest ionic strength

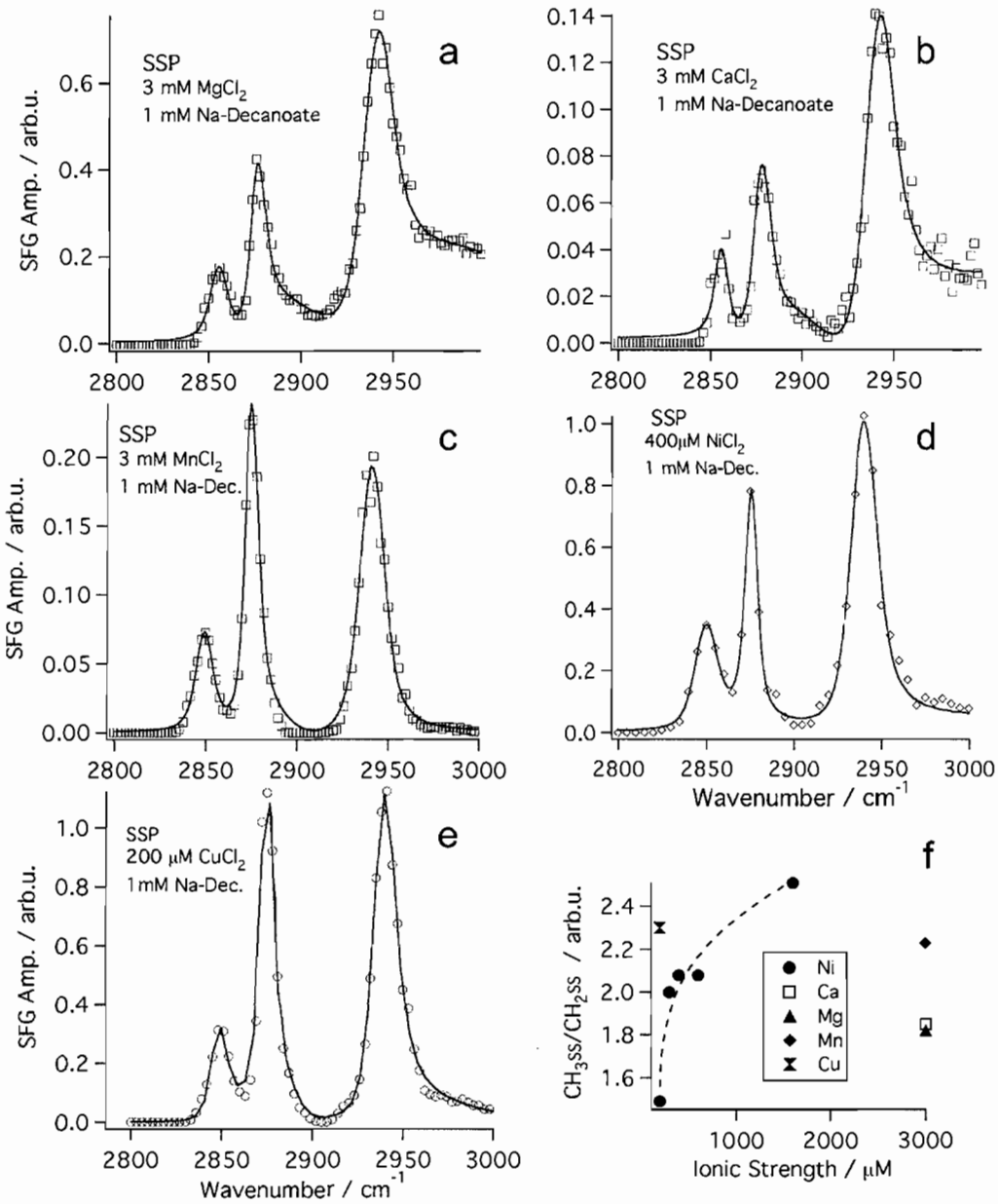

Figure 4.8. ssp polarization spectra of the CH vibrational region for the metal ions studied. The solid lines are fits to the data. Figure f shows the methyl/methylene ratio demonstrating the induced ordering of each of the ions at their respective ionic strengths.

used in this work. Mn^{2+} induces a significantly larger amount of ordering within the monolayer, followed by Ni^{2+}. In Figure 4.8f, Ni^{2+} is shown as a concentration series and more detail will be discussed in the following section. At half the ionic strength of Mn^{2+}, Ca^{2+}, and Mg^{2+}, Ni^{2+} induces more chain ordering. At only 200 μM, Cu^{2+} shows by far the largest enhancement in alkyl ordering for a given concentration, correlating well with it having the strongest headgroup interaction. Although Ni^{2+} does have a larger order parameter at 1.6 mM, this is a factor of eight greater in ionic strength. From the order parameters calculated, the alkyl chain conformations can be compared with the induced shifts of the headgroup vibrations. The alkyl ordering follows closely with the ion-headgroup interaction strength based on the headgroup vibrations and goes as $Cu^{2+} > Ni^{2+} > Mn^{2+} > Ca^{2+} \gtrsim Mg^{2+}$.

For further support of the binding trend that was found, interfacial tension data was acquired to observed the affects of the metal ions on the number density of the complexes at the interface. In Figure 4.9 the interfacial tension of the six ions along with Na-decanoate and the neat interface are shown. From the plot, it is clearly evident that each of the ions has a different effect on the adsorption of Na-decanoate to the interface. Ordering the ions in terms of increased adsorption, the trend goes as, $Ni^{2+} > Mn^{2+} > Ca^{2+} \gtrsim Mg^{2+}$. This follows closely with what was found from the VSFS data in the carboxylate and CH vibrational regions. The interfacial tension data also demonstrates that the increased ordering of the alkyl chains and the increased orientation of the headgroup observed in the VSFS data, are significantly altered due

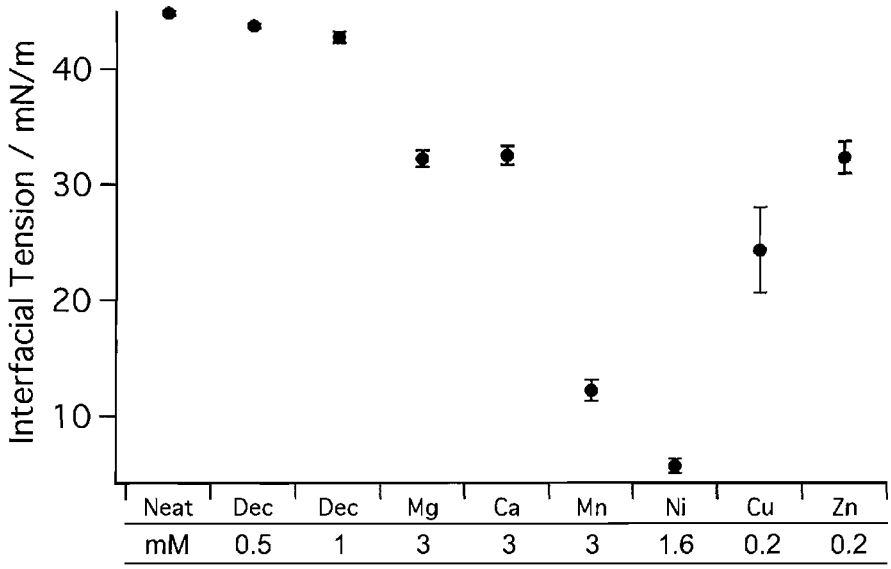

Figure 4.9. Interfacial tension measurements for the six ions at the CCl_4-water interface, as well as the interfacial tension of the two concentrations of Na-decanoate and the neat interface. Concentrations are those used in the VSFS experiments.

to an increase in the number density of the metal bound surfactant at the interface. It is concluded that increases in VSFS amplitude are a result of both a change in orientation and an increase in the number density at the interface. Cu^{2+} and Zn^{2+}, the two ions that were shown to be covalently bound in a bidentate fashion don't follow the trend, providing further proof that their interaction with the carboxylate headgroup is significantly different than the interaction of the other ions. According to the interfacial tension plot, Cu^{2+} and Zn^{2+} induce roughly the same amount of adsorption as Ca^{2+} and Mg^{2+} , which showed weak electrostatic interactions with the carboxylate headgroup. It is concluded that while Cu^{2+} and Zn^{2+} do not induce as much adsorption to the interface, they more heavily influence the orientation of

the surfactant molecules at the interface via the ordering of the alkyl chains and the orientation of the headgroups.

The binding strength of the ions based on the VSFS data fall into two categories. The first is the ions that bind electrostatically. From strongest to weakest based on the induced shift, the strength of the interaction is as follows: $Ni^{2+} > Mn^{2+} > Ca^{2+} \gtrsim Mg^{2+}$. Of the two ions that bind with more covalent character, $Zn \approx Cu$. The interaction of carboxylate with Zn^{2+} and Cu^{2+} is much stronger than that of the other ions as evidenced by the splitting of the vibrational modes, as well as by the induced ordering in the alkyl chains.

A Closer Inspection of $NiCl_2$

Of the six ions in this study, Ni^{2+} is unique because its binding characteristics are typically defined as being between what is categorized as ionic or covalent[43, 92]. The unique ability to look at the binding interactions directly at the interface in this study makes it possible to better characterize this interaction and definitively state whether Ni^{2+} is interacting in a covalent or ionic fashion. As discussed above, Zn^{2+} and Cu^{2+} gave distinct spectral signatures that indicated they were binding in a covalent bidentate fashion. In order to understand the binding nature of Ni^{2+}, a full concentration series was completed to observe the shifting of the vibrational modes. Figure 4.10 shows VSFS spectra of 1 mM Na-decanoate with $NiCl_2$ at concentrations from 50 μM to 1.6 mM in ppp and ssp polarizations. The ppp spectra show a blue

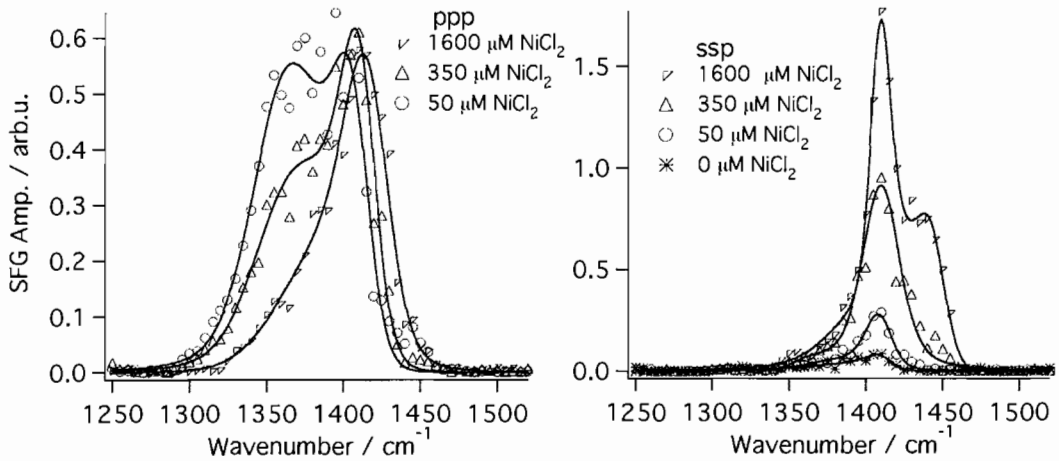

Figure 4.10. ppp and ssp polarization spectra of the COO^- region for the $NiCl_2$ concentration series. The solid lines are fits to the data. Some concentrations omitted for clarity.

shifting trend in the peaks and the low frequency component decreases significantly in amplitude as it blue shifts. In ssp polarization the carboxylate mode grows in amplitude and a shoulder appears on the high frequency side as concentration is increased. This shoulder alone is not conclusive evidence of bidentate binding although it is indicative of stronger binding. Cu^{2+} also showed a small shoulder at 1450 cm^{-1} in ssp, however, there was confirmation of this mode in ppp polarization with a significant peak at 1450 cm^{-1}. Ni^{2+} ppp polarization spectra don't show any peaks at 1450 cm^{-1}, and thus it is concluded that Ni^{2+} does not bind in a bidentate manner and its interaction is relegated to being electrostatic in nature given that monodentate binding has also been ruled out based on frequency locations. It is clear from the VSFS spectra of the carboxylate and CH region that Ni^{2+} does have stronger interaction that any of the other electrostatically interacting ions.

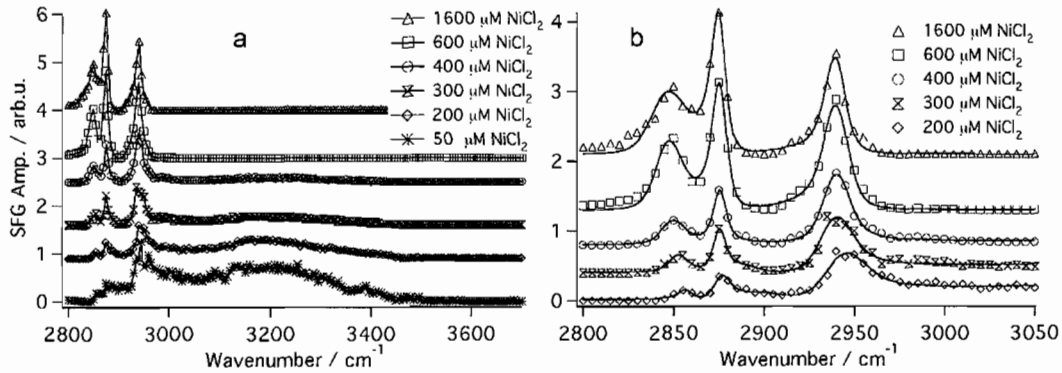

Figure 4.11. The water and CH vibrational region for the $NiCl_2$ concentration range investigated. The solid lines are fits to the data, which can be used to extract alkyl conformational changes over the concentration range. Spectra are offset for clarity.

To further investigate the effects of Ni^{2+} on the interfacial Na-decanoate molecules, the water and CH region were monitored as a function of Ni^{2+} concentration and are shown in Figure 4.11. As shown in Figure 4.8f, the concentration of Ni^{2+} has a large affect on the alkyl chain ordering. In addition, it was also shown that Ni^{2+} caused the largest drop in interfacial tension of 1mM Na-decanoate. In Figure 4.11, Ni^{2+} at 50 μM concentration results in the water spectrum adopting the shape of a typical charged surfactant at the interface. There are CH modes between 2800 and 3000 cm^{-1} and a broad water peak centered at 3200 cm^{-1} that is typically assigned to a highly coordinated water species at the interface. As the ionic strength of Ni^{2+} is increased, two regions of the spectra show significant change. The CH modes grow in amplitude and become more distinct as shown in Figure 4.11b. The Ni^{2+} concentration series is fit in the CH region and the methyl to methylene ratio is analyzed and plotted in Figure 4.8f. It is concluded that as Ni^{2+} concentration is increased, the ordering of

the alkyl chains increases. It is concluded that this is due to the increased adsorption at the interface as more Ni^{2+} ions are added to solution and bind with carboxylate surfactant. At 200 μM, the conformation of the alkyl chains is disordered. The conformation rapidly increases with increasing ionic strength and by 300 μM, the ordering within the monolayer has already surpassed that of Ca^{2+} and Mg^{2+} at 3 mM ionic strength. The second region in the spectra showing significant change is the broad water mode centered at 3200 cm^{-1}, which decreases to zero intensity as Ni^{2+} concentration increases. The electric field at the interface due to the double layer acts to orient these strongly coordinated water molecules and thus they contribute strongly to the VSFS spectra when the field is not neutralized[19, 20]. However, as more Ni^{2+} is added to solution, the field at the interface becomes negligable and the orientation of the water molecules within the interfacial region disappears leading to a loss of VSFS signal. In addition, the ions displace the water solvating the headgroup and thus the number density of water molecules within the interfacial region is also decreasing, further leading to a loss of VSFS signal. The neutralization of the interface is observed at a Ni^{2+} ionic strength around 400 μM. Relative to bulk concentrations, this means there is only one nickel ion present for every 7-8 surfactant molecules. However, at the interface, an excess of Ni ions is likely to exist due to the electrostatic attraction with the headgroups, and thus neutralization of the monolayer occurs at very low bulk concentrations of the ion.

Conclusions

In this work, it was found that metal ions have a strong effect on both the adsorption and orientation of carboxylate surfactants at the oil-water interface. It was also found that the binding strengths of the ions investigated varied greatly. Using VSFS to probe the symmetric carboxylate stretch and the alkyl chain modes, spectral shifts, splitting, and amplitudes clearly displayed the nature of the ion-headgroup binding, as well as the interaction strength. Of the six ions investigated, four were found to have electrostatic binding and two were found to bind with covalent bidentate character. The ions that were bound in an ionic manner were found to be ordered from strongest to weakest as, $Ni^{2+} > Mn^{2+} > Ca^{2+} \gtrsim Mg^{2+}$. This same trend was observed for the effect of the ions on the ordering of the alkyl chains within the interfacial surfactant layer. It was concluded this was due to the differing abilities of the ions to increase adsorption of the surfactant to the interface. In addition, Ni^{2+} was found to bind in with electrostatic character only, and not in a monodentate or bidentate fashion as has been previously suggested. Of the two covalent bidentate interacting ions studied here, it cannot be concluded which is a stronger binder than the other due to the wide array of effects bidentate binding can have on the carboxylate vibrational spectra. The effects of Cu^{2+} on the alkyl chains however are conclusive and it was found that the strong binding nature acts to strongly orient the alkyl chains, even though the interfacial tension did not show the magnitude of increased adsorption that ions such as Ni^{2+} and Mn^{2+} showed. This work provides conclusive evidence

of the interaction strengths between carboxylate surfactant headgroups and divalent metal ions, thus providing a way to define the type of interactions occurring between the ion and the headgroup.

CHAPTER V

STRUCTURED ADSORPTION OF POLYELECTROLYTES AT THE OIL-WATER INTERFACE

This chapter presents vibrational sum-frequency spectroscopy and surface tension studies of the adsorption of poly(acrylic acid) as a function of molecular weight, pH, concentration, and salt additions to gain a fundamental understanding of the structure of charged polymers at the CCl_4-water interface. Molecular weights used ranged from 1.8 kD - 1250 kD and the pH range investigated was 1.5 - 10. VSFS results indicated interesting similarities between all the molecular weights, whereas surface tensiometry found differences between them. Together, the two sets of results present a new dynamic picture of polyelectrolyte adsorption to the oil-water interface. In addition, a sharp transition pH was found that dictated whether adsorption to the interface would occur. This transition pH was found to be adjustable based on the addition of mono and divalent salts. E. J. Robertson assisted with the tensiometry.

Introduction

The study of macromolecular structures has become increasingly important due to their key involvement in biology. Within a single cell, the composition and size of the molecules that take part in intracellular processes and reactions is astoundingly

complex. While understanding of these processes has increased at a rapid pace over the last century, there is still much to be understood, particularly in the area of macromolecular conformation at interfaces due to the essential role of the interface in biological systems. One interface of particular interest is the oil-water interface. Unlike the air-water and solid-liquid interface, the oil-water interface is particularly relevant to biological systems because of the highly fluid nature of the two liquid phases, as well as the interplay between the polar and non-polar regions at the interface. The hydrophobic nature of the oil-water interface has often been used as a model for membranes and processes such as ion transfer across the interfacial region[102, 103]. The goal of this study is to make progress towards understanding macromolecular conformation at the oil-water interface by using a model polyelectrolyte that has a molecular composition with a number of similarities to important biomolecules.

Polyelectrolytes (PE) have captivated the interest of scientists and have been studied in great detail for multiple decades as evidenced by the quantity of literature on the subject. They have a wide variety of applications in industrial settings such as oil recovery and cleanup[104–106], water and soil remediation[106–110], electrical multilayer assemblies[111–115], complexation with nanoparticles[116, 117], fabrication of microwires[118], as well as a number of biological applications[119–125]. Notably, they also have many similarities to a number of naturally occurring molecules in environmental and biological systems, and thus can act as molecular models for

studying these complex systems in controlled experiments. Poly(acrylic acid) (PAA) has a simple structural repeat unit with a single carboxylic acid and is an ideal model for macromolecules of environmental and biological significance. Environmentally, humic substances have a high degree of carboxylic acid groups which act to chelate both nutrients and toxins for transport through soils and into water sheds[26, 69, 70]. A deeper understanding of the conformation of these types of macromolecules is of obvious importance given that where these macromolecular complexes end up within the soils and watersheds has important environmental implications regarding their cleanup or understanding of nutrient placement within the environment[126, 127]. Biologically, every amino acid contains a carboxylic acid making it one of the most abundant functional groups within biological systems. The equilibrium between a carboxylic acid and its anion is pH sensitive and has a large effect on the conformation of molecules containing these groups, as well as the solubility and interfacial activity of such molecules[33, 38].

While there have been several thorough studies on polyelectrolytes at air-water and solid-liquid interface in the presence of surfactants[128–132], the main focus of these studies was the properties of the surfactants at the interface. These studies systematically logged the large variety of adsorption regimes for a number of different surfactant-polymer systems. However, these studies did not observe polyelectrolytes at the interface by themselves, and the conclusions drawn on the increased surface activity of the surfactants was primarily attributed to polymer-surfactant interactions

in the interfacial region, when in fact, the interfacial activity of the polymer by itself could be a leading cause to the increased surface activity of the surfactant. Although some possibilities were proposed, there were no definitive conclusions as to the adopted conformation, or location of the polymer within the interfacial region in the presence of surfactants[132]. Due to some of these unanswered questions, it is necessary to take a step back and study polyelectrolytes at interfaces without the added presence of surfactants to gain a better understanding of their surface activity and conformations in order to learn how they are contributing to more complex systems. Early work by Katchalsky and Miller showed surface activity of PAA at the air-water interface using surface tension and observed interesting phenomena regarding the desorption characteristics of the poly-acid versus the monomeric acid[133]. Later work by Ishimuro and Ueberreiter confirmed the results of Miller, although between the two studies, the time scales to reach equilibrium were drastically different[134].

In this study, vibrational sum-frequency spectroscopy (VSFS) and interfacial tensiometry are used to investigate the adsorption and orientation of PAA at the CCl_4-water interface under the conditions of varying pH, metal salt additions, concentration, and molecular weight. The oil-water interface was chosen as an ideal model of a "soft"[135] interface and is representative of biological and environmental systems where the interfaces are often fluid in nature and the interfacial region is not well defined as in the solid-liquid or solid-air interface. PAA is chosen due to its simple repeat unit structure and similarity to biological and environmental molecules of

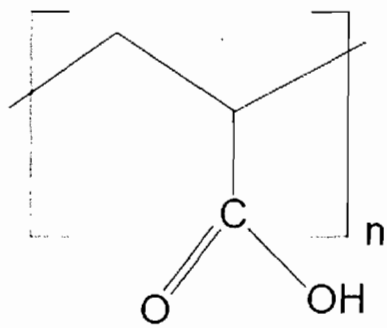

Figure 5.1. Poly(acrylic acid) repeat unit showing a single carboxylic acid functional group with a simple alkyl backbone.

interest. The repeat unit is shown in Figure 5.1. Both monovalent and divalent metal salts, specifically NaCl, $CaCl_2$, and $MgCl_2$ were chosen to investigate the binding properties at the interface and how these differ from what is known for bulk solution polyelectrolytes. This work addresses several different aspects of the adsorption of PAA at the CCl_4-water interface. The first to be covered will be adsorption of PAA as a function of molecular weight (MW), followed by the effects of concentration on adsorption. Next will be the effects of pH on adsorption and last will be how the addition of monovalent and divalent metal salts affect PAA adsorption to the interface.

Adsorption of PAA to the Oil-Water Interface

Figure 5.2 shows VSFS spectra and surface tensiometry of PAA (5 ppm, 450 kD, pH 2) at the CCl_4-water interface. The VSFS spectra from 1275-1900 cm^{-1}show a single peak at 1732 cm^{-1} which is assigned to the carbonyl mode of the carboxylic acid on the polymer. The VSFS data shows the existence of a layer of PAA at the

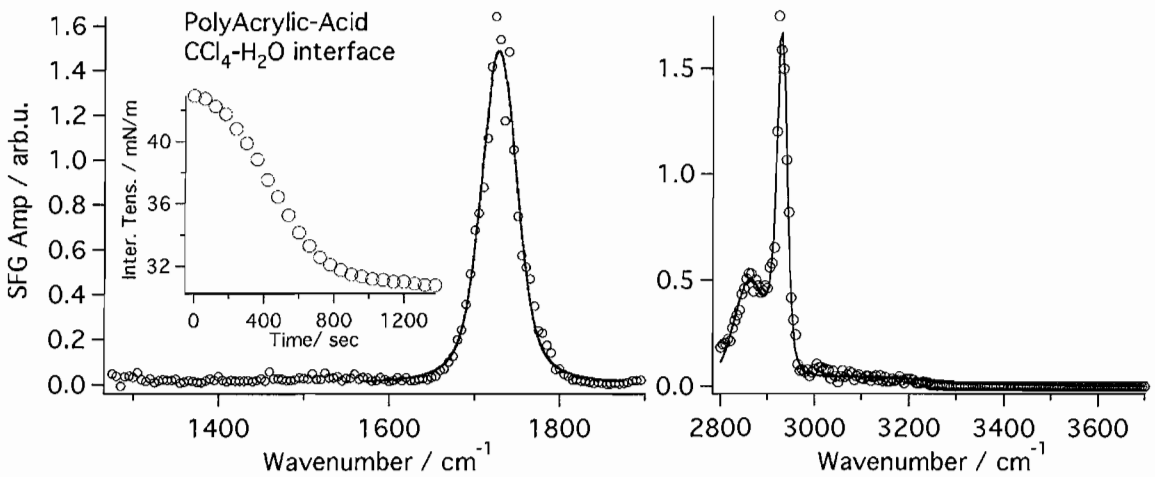

Figure 5.2. VSFS spectra of PAA (5ppm, 450kD, pH 2) at the CCl_4-water interface showing both the carboxylate and carbonyl stretching region. The solid line is a fit to the peak at 1732 cm^{-1}. The inset is an interfacial tension measurement of the same system using the pendant drop method.

oil-water interface that is adsorbed with its carboxylic acid groups and CH backbone groups strongly oriented. The CH and water region show one dominant CH peak at 2930 cm^{-1} and a small shoulder on the low frequency side at 2850 cm^{-1}. These are assigned to the asymetric and symmetric CH_2 vibrational stretches respectively. In addition to the CH modes, there is a small contribution from water in the interfacial region centered at 3000 $cm^{-1}$and this is assigned to water that is highly coordinated in the interfacial region. The tensiometry data shows a time dependent decrease in interfacial tension until an equilibrium value of $\approx$31 mN/m is reached, which support the conclusion of an adsorbed layer of PAA at the interface.

VSFS spectra of three different molecular weights(1800, 450,000, 1,250,000) of PAA were taken in the C=O and the water/CH vibrational frequency region. The data in Figure 5.3 shows a single peak centered at 1732 cm^{-1}, one dominant CH

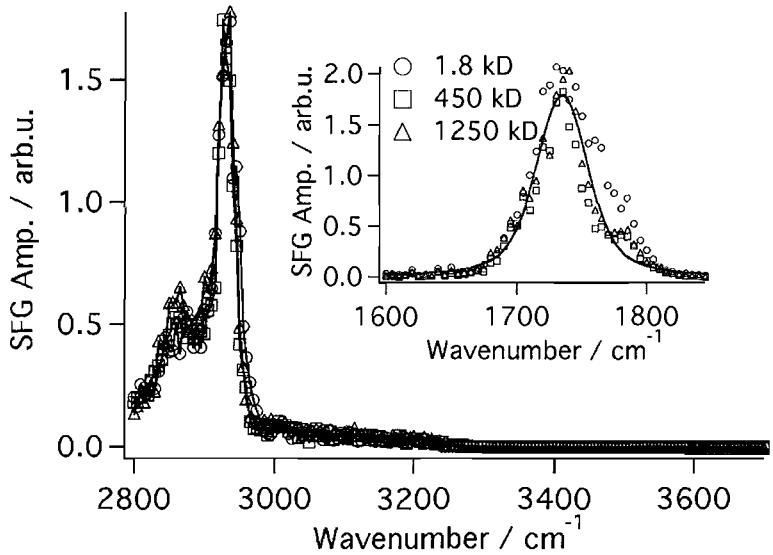

Figure 5.3. VSFS spectra of PAA in the C=O (inset) and water/CH region for three different molecular weights of the polymer.

mode at 2933 cm^{-1} with a small shoulder at $\approx$2852 cm^{-1}, and a small broad peak between 3000-3200 cm^{-1}. The peak at 1732 cm^{-1} is assigned to the C=O stretch of the acrylic acid group and the CH modes are assigned respectively to the asymmetric (2933 cm^{-1}) and symmetric (2852 cm^{-1}) vibrations of the CH_2 groups along the backbone of the polymer (frequencies obtained from fits to data). The small broad contribution to the spectrum from 3000-3200 cm^{-1} is typically associated with highly coordinated water molecules near the interface[136]. The spectra in Figure 5.3 show that the three molecular weights, despite the large size difference, give the same VSFS spectra in both the carbonyl and CH region. Each of the PAA MW spectra shown are taken starting at t=0 from when the interface is prepared resulting in no equilibration time. The data show that the adsorption and orientation of PAA at the interface is immediate and is independent of the polymer chain length. It is

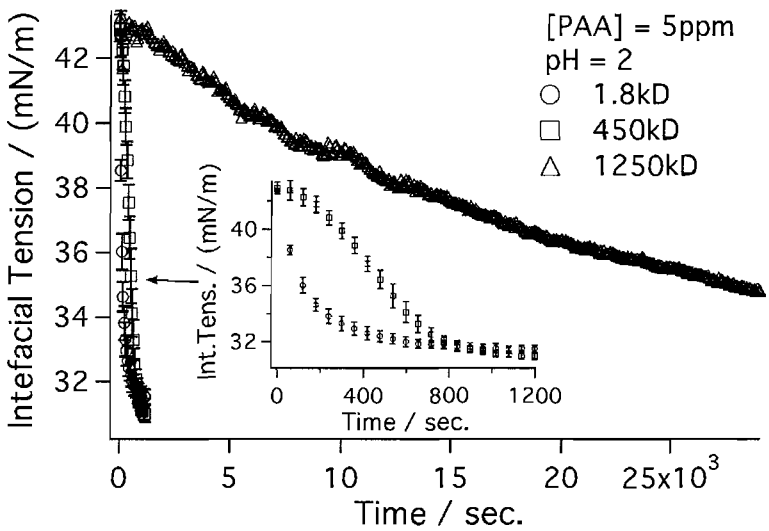

Figure 5.4.. Interfacial tension of 1.8, 450 and 1250 kD PAA as a function of time

well known that the gyroscopic radius of a polymer affects the time scale on which diffusion and conformation changes occur, and it would be expected that the different PAA molecular weights would result in different VSFS spectra as a function of time. In order to investigate this result further, interfacial tension measurements were conducted. Figure 5.4 shows interfacial tension measurements as a function of time for three molecular weights of PAA. The inset displays the 1.8 and 450 kD polymer measurements for clarity. These results show there is a significant time dependence in adsorption for the three molecular weights. The 1.8 and 450 kD PAA come to an equilibrium interfacial tension value in approximately 500 and 1000 seconds respectively, whereas the 1250 kD PAA is not seen to reach an equilibrium value even after a period of over seven hours. This data shows there is a time dependent component to the adsorption of these three PAA molecular weights.

The disparity between the surface tension and VSFS results can be reconciled by focusing on what each experimental technique is measuring. The interfacial tension measurements are only sensitive to number density at the interface, whereas the VSFS measurements are sensitive to both number density and orientation at the interface. From the properties measured by each technique, the differences between the results of the interfacial tension and the VSFS must be due to the orientation dynamics of the adsorbing polymer. The surface tension data indicates adsorption occurs over at least 10-20 minutes, or hours in the case of the high MW PAA. The VSFS data however demonstrates adsorption is immediate upon interface preparation. The two data sets together support the existence of an adsorption process with multiple steps. The initial step, observable via VSFS, is fast and adsorption and orientation of the polymer occurs immediately. This is followed by a slow, "loading" of the interface with more polymer that is not oriented, and is most likely randomly coiled. Due to the lack of orientation, it is not observable with VSFS, but is found in the interfacial tension measurments. The fact that both the C=O and CH vibrational regions give the same results with respect to MW and time, supports this initial fast step as it shows no reorientation of either the carboxylic acids or the backbone are occurring after the initial adsorption step.

Given that the data indicate a multiple step adsorption process, the picture of the interface that is formed consists of a monolayer of polymer that is highly oriented with a sub-interfacial region that is loaded with randomly coiled polymer. The field at

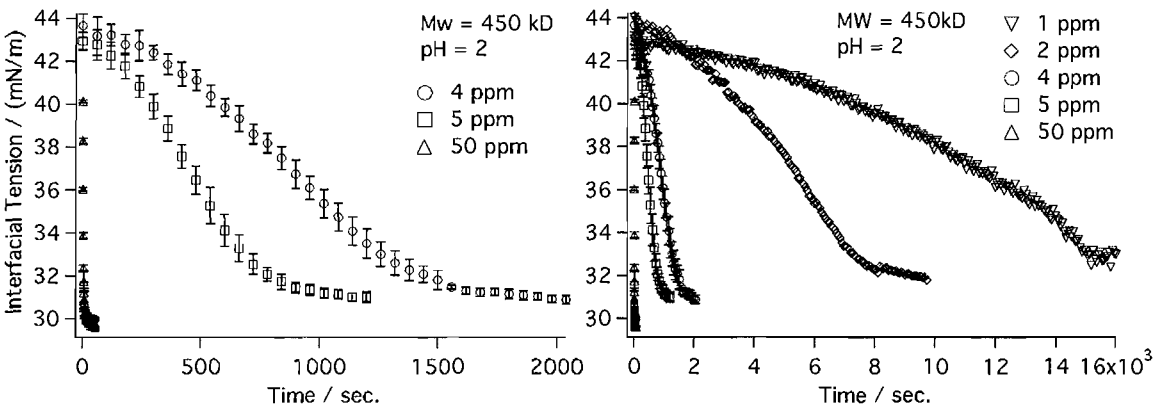

Figure 5.5. Interfacial tension of PAA as a function of time for five different concentrations.

the interface must therefore be strong enough to align the first layer of polymer, but lack the strength to align any additional polymer layers within the interfacial region. The additional randomly coiled polymer must be present though according to the interfacial tension data because there are additional long term adsorption processes which have large affects on the hydrogen bonding network of the interfacial region, which is shown by the falling interfacial tension long after VSFS equilibrium signal is reached.

Concentration Effects and Adsorption Time Dependence

VSFS and interfacial tensions measurements were made of 450 kD PAA at the CCl_4-interface as a function of bulk concentration. Each concentration was adjusted to pH 2, which ensured the polymer was in the protonated/neutral state for the experiments. The interfacial tension measurements (Figure 5.5) show that PAA

at a concentration of 50 ppm reaches equilibrium almost immediately, whereas 5 ppm requires ≈1000 seconds, and 4 ppm takes ≈1500 sec. At a concentration of 1 ppm PAA, the time required to reach equilibrium is greater than four hours. All concentrations appear to approach very similar interfacial tension values indicating that the surface coverage is not very different, even though a factor of ≈50 exists between the lowest and highest concentrations shown in Figure 5.5. In addition, between the fastest and slowest time to reach equilibrium, the time required to achieve surface coverage is different by a factor of ≈400 as shown in Figure 5.5. This shows that the bulk concentration has a large effect on adsorption time, but little effect on the surface coverage achieved at equilibrium, indicating that adsorption of the polymer to the interface is governed primarily by diffusion. Time dependent adsorption effects as a function of concentration aren't observed in the VSFS spectra until very low concentrations. For the VSFS spectra, instantaneous adsorption is observed down to approximately 1 ppm. However, the surface tension for 1 ppm as seen in Figure 5.5 is on the order of four hours. This supports the conclusion that there are multiple adsorption steps occurring. At 0.5 ppm PAA, VSFS spectra show noticeable time dependence and maximum signal is observed after approximately one hour. At 0.25 ppm PAA, VSFS spectra show an equilibration time of approximately two hours. Figure 5.6 shows spectra of 0.25 ppm PAA at the CCl_4-water interface over a period of approximately two hours. The solid lines in the figure are fits from a global routine designed to fit the entire time series to a single peak while holding all

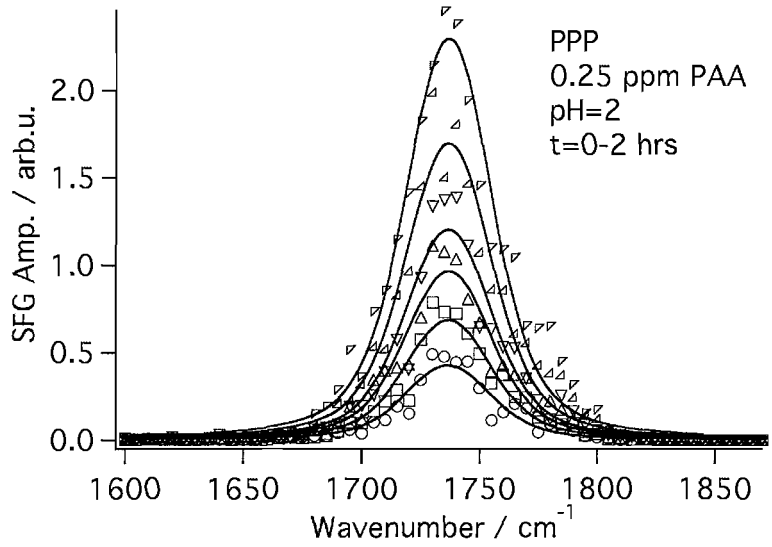

Figure 5.6. VSFS spectra of 0.25 ppm PAA at the CCl_4-water interface over a period of ≈2 hours.

parameters constant except for the amplitude. A steady increase in signal observed over this time period. As was the case for the VSFS and interfacial tension of the molecular weight series in the previous section, it is demonstrated that the interfacial tension and VSFS give different results for the time to maximum adsorption. The VSFS spectra show maximum adsorption in two hours for a sample of 0.25 ppm PAA whereas the interfacial tension is on the order of four hours for 1 ppm, which is four times the concentration of the time dependent VSFS data. The VSFS spectra of these very low PAA concentrations indicates that the adsorption of this first layer is limited by diffusion of PAA to the interface. The time resolution of the VSFS experiments used in these studies isn't small, however, diffusion limited adsorption is observed in these experiments below PAA concentrations of about 1 ppm. The multi-step adsorption process raises the interesting question of why the polymer continues

to adsorb to the interface after the first initial monolayer is quickly formed. First, it must be energetically favorable for this long time step to occur. However, the long time adsorption process only applies to polymer that isn't oriented, as it doesn't give VSFS signal. This leads to the conclusion that the polymer adsorbing on the long time scales is in a random coil, and thus presents a large two dimensional face area to the interface. If the interface is thought of as a two dimensional plane where there are a specific number of sites for the second layer to adsorb to, then conformational changes may have to occur within the randomly coiled polymer to build up this second layer. The conformation changes involved would still leave the polymer in a randomly coiled state, but this coiled state would have to conform to the available spaces in the sub interfacial region.

pH Effects on Adsorbed Polymer

Due to the acid-base equilibrium of the carboxylic acid functional group on the polymer, VSFS and surface tension were used to investigate the effects of pH and polymer charge density on adsorption. The main effect of pH on PAA in bulk solution is that as pH increases, the charge density on the polymer increases due to deprotonation of the carboxylic acid groups. In bulk solution, the increase in charge density causes the polymer to adopt an elongated conformation due to charge-charge repulsion between carboxylate functional groups along the backbone[137, 138].

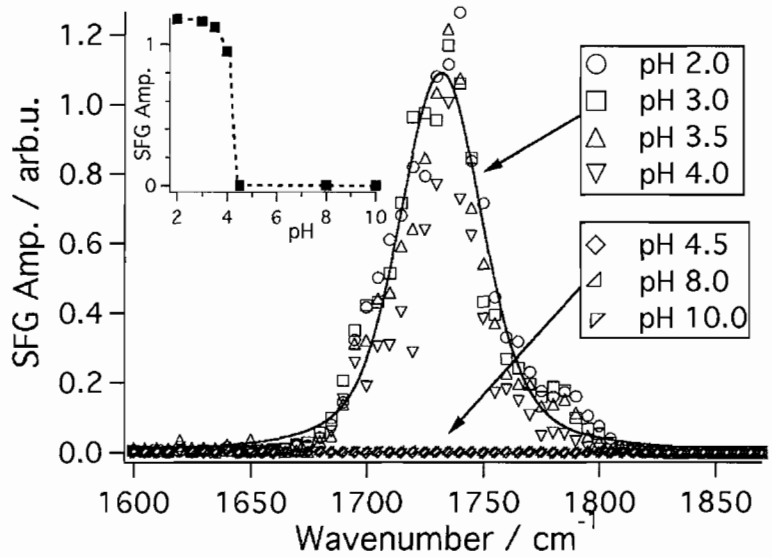

Figure 5.7. VSFS spectra of 5 ppm, 450 kD, PAA carbonyl vibration at 1730 cm^{-1} at the CCl_4-water interface. The solid line is from a global fit to the all the pH data. The inset shows the amplitudes retrieved from the global fit plotted against their respective pH. The dotted line in the inset is a guide for the eye.

Titrations in this lab show the pKa of PAA to be ≈6.5, which is in agreement with literature[139–141].

VSFS spectra of 5 ppm, 450,000 MW PAA at pH 2-10 are shown in Figure 5.7. In the main plot a single mode is centered at 1730 cm^{-1} for pH $\leq$ 4.0. However, as soon as the solution pH reaches 4.5, the VSFS signal decreases to zero intensity and this lack of signal is constant through pH 10. This demonstrates there is a sharp transition point between pH 4-4.5 where polymer desorption occurs. The transition is plotted in the Figure 5.7 inset, where the fit amplitudes are plotted with respect to their associated pH. The amplitudes are based on a global fitting routine applied to all the spectra between pH 2-4 simultaneously. This ensures a rigorous fit due to all parameters being held constant except the amplitudes. The plot inset shows

this sharp transition point for the desorption of PAA at the oil-water interface. The plotted amplitudes show a very slight nonlinear decrease in signal up to pH 4, then the curve plunges to zero and is constant above pH 4.5. According to titrations in this lab, the desorption process occurs at 20% deprotonation of the polymer in bulk, far below the known pKa. This sharp desorption point and the percent deprotonation agree well with early work by Katchalsky and Miller[133]. The surface pKa for weak acids such as carboxylic acid surfactants and phenols, is usually between 1-3 units higher than that of the bulk value[33, 38]. Following these guidelines, the surface pKa of PAA at the interface could be anywhere from 7.5 to 9.5. Given this information regarding the pKa range, the dynamic picture of the interface is one in which very little (much less than 1 in 5 carbonyl groups) accumulation of charge along the backbone is required to allow desorption of the polymer.

VSFS spectra of the water and CH region (Figure 5.8) provide supporting evidence for the sharp transition point for adsorption vs. desorption of PAA. From pH 2-3.5, identical water specta and CH modes are observed. There is no free OH water peak at 3665 cm^{-1} and only a very minor peak from 3000-3200 cm^{-1} due to a small amount of highly coordinated water in the interfacial region. The CH modes show strong orientation for the backbone of the polymer. At pH 4.0, the CH modes are nearly identical to those at lower pH. However, there is a small but distinguishable increase in the coordinated water mode between 3000-3200 cm^{-1} indicating a slight increase in orientation or number density of water molecules within this region. This is likely

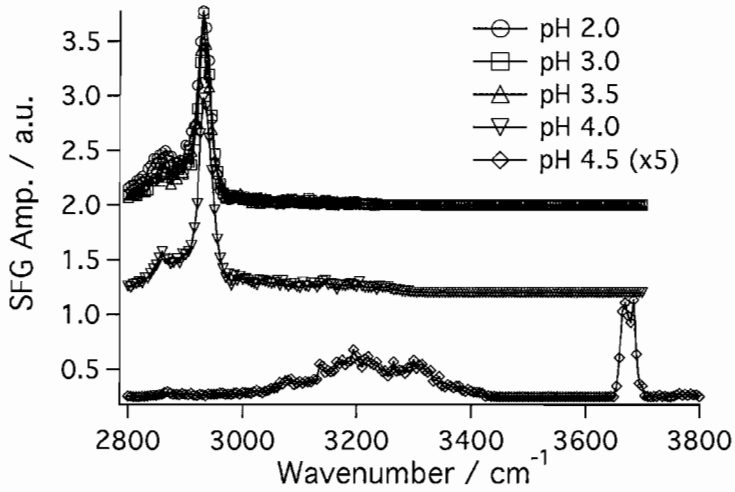

Figure 5.8.. VSFS spectra of the water and CH vibrational region from pH 2-4.5.

due to polymer rearrangement as the charge density along the polymer backbone increases, allowing more water into the interfacial region due to slight rearrangement. The increased charge also creates a larger field at the interface, which acts to align water molecules in the interfacial region, thus leading to increases in water VSFS signal. Analogous to the observations in Figure 5.7 between pH 4 and 4.5, drastic changes are observed in the water region spectrum when pH 4.5 is reached. This change is manifested as a complete lack of CH modes and a recovery of a near "neat" water interface with the presence of a free OH and coordinated water modes in the 3000-3400 cm^{-1} region, indicative of an interface where there is no polymer adsorbed.

For further support of these findings, interfacial tension measurements were made across the pH range of 1.5-10 and are shown in Figure 5.9. The interfacial tension measurements for pH 1.5-3 show identical findings. Each pH takes roughly 1200

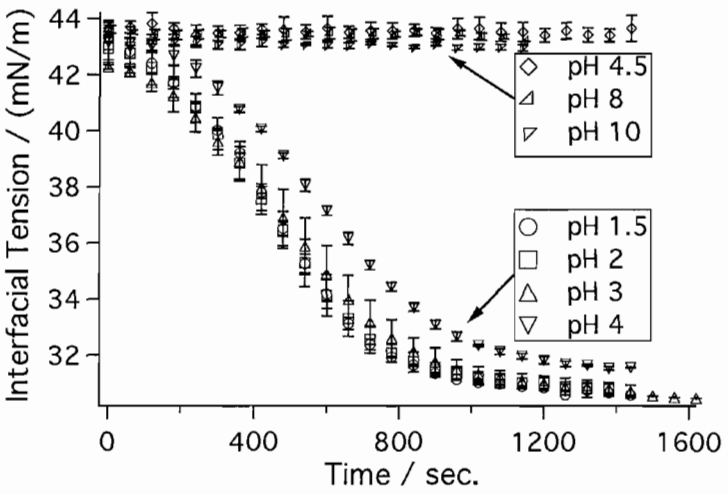

Figure 5.9.. Interfacial tension of PAA as a function of time for pHs 1.5-10.

seconds to reach an equilibrium interfacial tension value of 30-31 mN/m. The pH 4 solution shows approximately the same curve as the lower pHs, but is shifted slightly up, giving a higher final interfacial tension value of 32 mN/m. This corroborates the pH 4 VSFS data in the water region where the spectra for pH 4 show a small enhancement in the water peak. This also follows well with the inset plot in Figure 5.7 where the point associated with pH 4 shows a decrease in amplitude and is leading the curve towards zero. Figure 5.9 shows that when the pH reaches 4.5, adsorption of PAA no longer occurs and the interface retains its "neat" character. For pH 4.5-10, all the data points comprise a flat horizontal line at an interfacial tension of 44 mN/m, a value that matches that of the undisturbed CCl_4-water interfacial tension[21, 22]. These experiments provide support for the VSFS spectra that show

the polymer desorbs from the interface above a critical pH value of 4, and leaves a neat CCl_4-water interface in its absence.

From a thermodynamic perspective, the desorption of the polymer from the oil-water interface can be thought of in terms of the free energy of desorption, which dictates the energetic cost of moving a functional group from the interface into the bulk. The free energy of desorption for moving a carboxylic acid from the oil-water interface to the bulk water is about +1630 cal/mol[19]. However, deprotonating the acid group significantly lowers the free energy of desorption and thus charged portions of the chain are more easily solvated away from the interfacial region. Due to the polymer being only 20% (or less) deprotonated at the point of observed desorption, the deprotonation of only 1 in 5 carboxylic acids must lower the energy barrier enough to allow the entire length of the polymer to leave the interface.

As the pH of the solution is increased and charge accumulates along the length of the polymer, there are cooperative processes that allow a carboxylic acid group neighboring a charge to deprotonate more readily than an acid group that has little to no charge surrounding it[138, 142]. Due to these cooperative processes, an interfacial picture is proposed where the neutral parts of the polymer adsorbed to the interface decrease in size as the charged sections of the polymer increase in size until the free energy of desorption decreases enough for the entire polymer to become solvated. This is illustrated in Figure 5.10, which shows the interfacial region at low and high pH. At low pH, the figure depicts the proposed structure of trains adsorbed to the interface

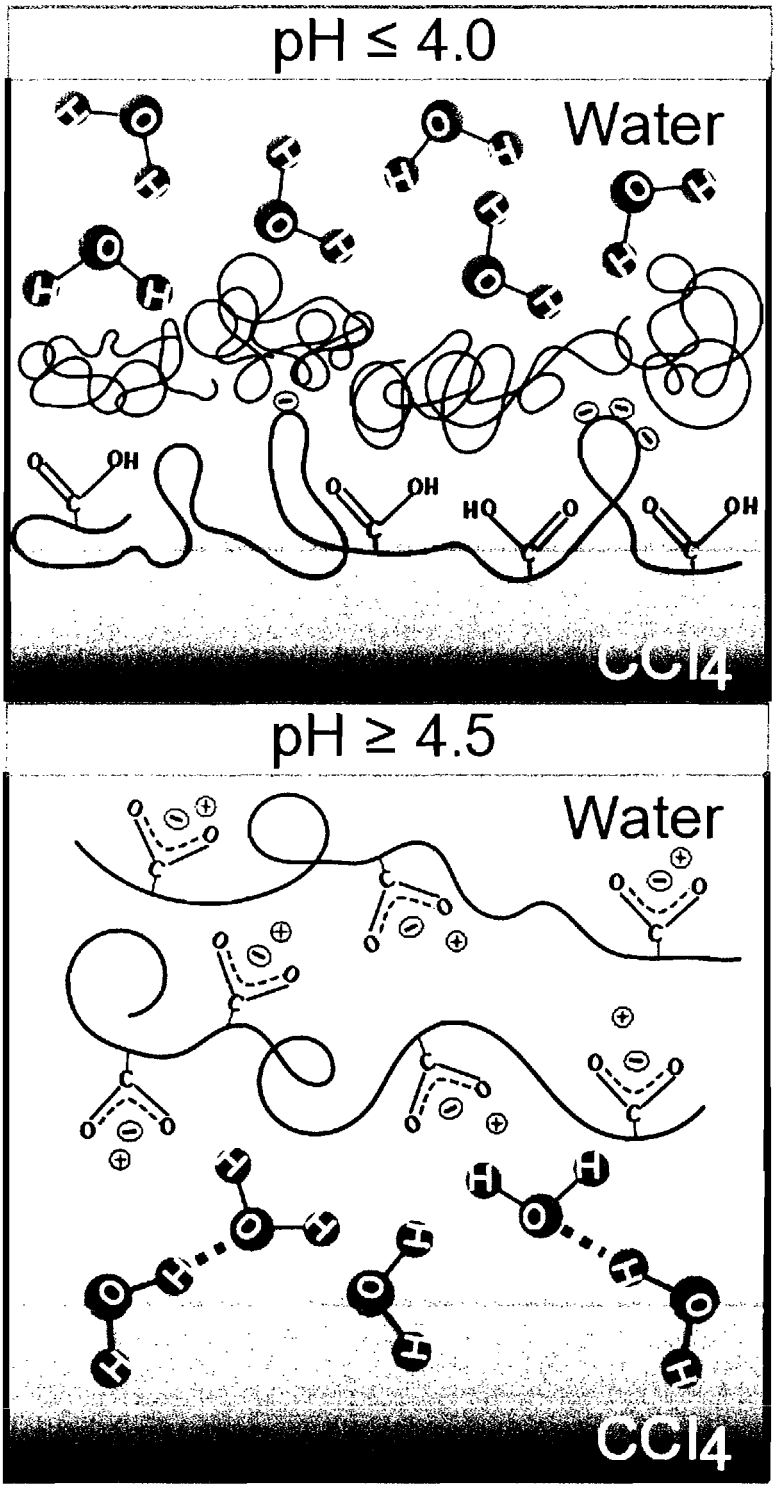

Figure 5.10. A depiction of the interfacial region above and below the critical pH.

while loops with charge are solvated into the aqueous solution, consistent with current proposed theoretical pictures[135, 143]. These loops would be smaller at low pH and increase in size as the critical pH of desorption is approached and charge density increases. Just above the oriented polymer at the interface is the randomly coiled polymer that is evidenced by the longer adsorption process in the interfacial tension measurements. This polymer, as seen in the cartoon, has no orientation associated with it, and the time scale on which it adsorbs is much longer than that of the oriented polymer right at the interface. Once the critical pH is reached, the interfacial picture is described by the lower panel, where water structure dominates the interfacial region much like what is seen in a neat CCl_4-water VSFS spectra. The polymers are desorbed from the interface and the charged functional groups act to keep the polymer in a stretched out conformation due to charge-charge repulsion[137, 138].

One intriguing result from these studies is that only the neutral (protonated) functional groups are observed at the interface. As described above, it is energetically more favorable for an uncharged molecule to adsorb to the interface[19]. It is also known for bulk solutions of neutral PAA that the polymer adopts a random coil because there aren't any forces requiring it to be in an uncoiled structure[138]. Interfacial structure of the polymer is unknown, although some models have been proposed[135, 143]. Despite the lack of charge-charge repulsion forces at low pH, these studies suggest that PAA is not in a random coil at the interface due to the strong orientation of the carbonyl and CH groups. If the polymer was in a random

coil at the interface then signal from the carbonyl groups would cancel due to a lack of net orientation. Instead, there must be an organized structuring of the polymer at the interface that allows net orientation. Two possible structures could occur to satisfy what is observed in the spectroscopy. The first is that the polymer could have organized, oriented trains adsorbed at the interface interrupted by loops or coils protruding into the water phase. The second possibility is that the polymer is lying fully stretched out along the plane of the interface with its carbonyls oriented into the water phase. In either case, as the pH (and charge density) increases, the charged carboxylate functional groups do not have a net orientation as signal was not observed in the 1400 cm^{-1} region. The accumulated charge on the chain must therefore either be contained in the loops/coils that are solvated by the water, or, the charged carboxylates must be positioning themselves to have net opposing orientations along the backbone of the polymer chain, which would also be a minimum energy conformation for two charged groups, and would lead to a cancellation of VSFS signal.

Effects of Salt on Adsorption

The previous section showed desorption of PAA occurs only above a critical pH value. It was proposed that this critical pH value corresponded to the existence of a minimum charge requirement along the backbone of the polymer that would make it energetically favorable to be solvated away from the interface. In this section, mono

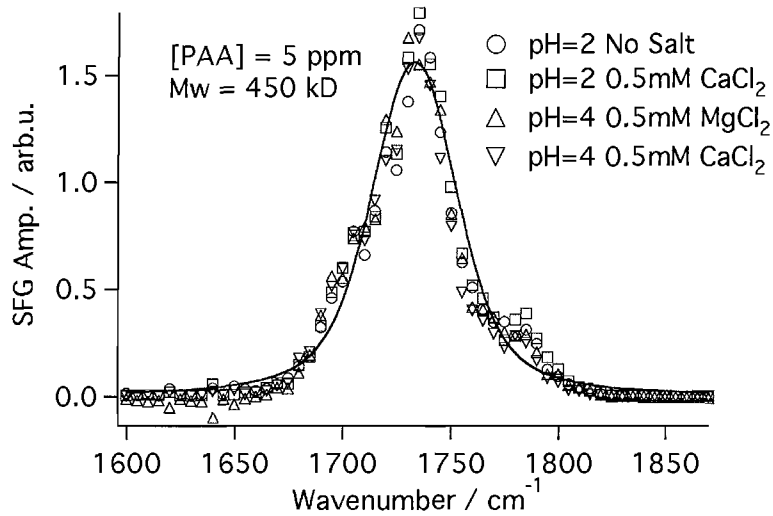

Figure 5.11. VSFS spectra of PAA (5 ppm, 450 kD) with Mg^{2+} and Ca^{2+} at the CCl_4-water interface below the critical pH of desorption. No increase in resonant amplitude is observe when salt is added to the solution.

and divalent metal ions were used in conjunction with the previous experiments to observe adsorption above the critical pH value to gain a better understanding of the orientation and adsorption properties of PAA. Previous work has shown that carboxylated poly-acids binds stronger to Ca^{2+} than Mg^{2+}, whereas sulfonated poly-acids show no difference in the binding behavior between the two divalent ions[144, 145].

To establish a baseline of maximum adsorption at the interface below the critical pH in the presence of salt, VSFS spectra were obtained at two pH values as shown in Figure 5.11. It is seen that at pH 2 and pH 4, the addition of Ca^{2+} or Mg^{2+} has no affect on the amplitude of the carbonyl stretch with respect to the spectra with no salt added. This indicates that maximum adsorption of PAA occurs below the

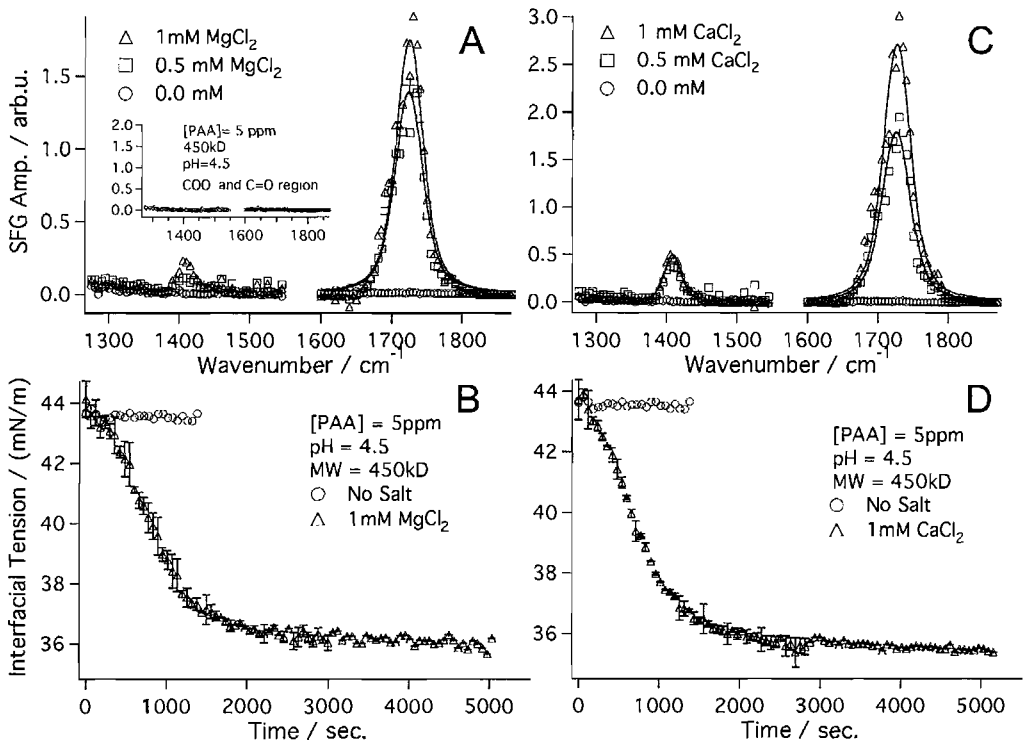

Figure 5.12. VSFS (top) and interfacial tension measurements (bottom) of Mg^{2+} (left) and Ca^{2+} (right) binding with PAA. The inset in the top left panel shows the two spectral regions with PAA at 5 ppm and pH 4.5 with no salt added.

critical pH and the addition of salt doesn't change the orientation or the amount of PAA adsorbed at the interface.

Figure 5.12 shows VSFS and interfacial tension measurements for Mg^{2+} and Ca^{2+} ions binding to PAA at a pH of 4.5, which is just above the critical pH of desorption. VSFS of Mg^{2+} at a concentration of 0.5 and 1 mM are shown In Figure 5.12A. It is observed that with the addition of Mg^{2+}, there is an enhancement in the VSFS signal at both 1730 cm^{-1} and at 1410 cm^{-1}. The 1410 cm^{-1} peak was not introduced in prior sections because it wasn't observed until salt was present in the system. This peak is assigned to the carboxylate symmetric vibration and is comparable to literature

assignments of this mode[65]. The inset in Figure 5.12A shows the same PAA solution without the addition of salt and it is evident, as shown in the previous section, that adsorption of PAA is not taking place. The addition of Mg^{2+} forces adsorption and orientation of PAA at the oil-water interface by binding to the charged carboxylate groups on the polymer. This is supported by the interfacial tension measurements shown in Figure 5.12B. For reference, the interfacial tension is shown at pH 4.5 without added Mg^{2+} and it is seen to be a flat line near that of the neat CCl_4-water interface[21, 22]. When 1mM Mg^{2+} is added to the solution, the interfacial tension is observed to fall and reach an equilibrium value of 36 mN/m after 2000 seconds. In the case of Ca^{2+}, the VSFS spectra (Figure 5.12C) show very similar results to those of Mg^{2+}, with the exception of an almost two fold increase in signal over the Mg^{2+}. The increased amplitude in the Ca^{2+} vs. Mg^{2+} VSFS spectra is observed for both the carbonyl mode and the carboxylate mode. The interfacial tension measurements for Ca^{2+} in Figure 5.12D show identical results to those containing Mg^{2+} with a final equilibrium interfacial tension of $\approx$36 mN/m. In addition, both Mg^{2+} and Ca^{2+} give identical adsorption times for the interfacial tension measurements. As in previous sections, the VSFS showed a much faster adsorption time than what was given by the tensiometer measurements. This further supports a multiple step adsorption process consisting of a fast initial adsorption of stretched out highly oriented polymer, followed by a slow loading of the interfacial region by randomly coiled polymer. The tensiometer measurements give identical results for both Ca^{2+} and Mg^{2+}, but the

VSFS gives a large increase in spectral amplitude for Ca^{2+} vs. Mg^{2+}. The difference in these results shows that Ca^{2+} induces a much stronger orientation in the carboxylate and carbonyl groups than the Mg^{2+}, but it does not induce more adsorption to the interface. This indicates that the carboxylate-Ca^{2+} interaction is stronger than that of carboxylate-Mg^{2+}. Furthermore, this suggests that Ca^{2+} has a greater ability to screen the carboxylate anionic charge, which would in turn produce a stronger orientation of the carboxylate groups and result in a stronger VSFS signal.

Support for the adsorbtion of PAA to the interface in the presence of salt is found in VSFS spectra of the water OH and CH stretching region as shown in Figure 5.13. For reference, the PAA VSFS spectra at pH 4.5 without salt is also shown in Figure 5.13. This shows a near neat water spectrum, indicating a lack of adsorption of PAA. In the presence of salt, the water spectra change dramatically, showing large CH stretching modes in the 2800-3000 cm^{-1} region along with water modes in the 3000-3200 cm^{-1} region, indicating as previously discussed, strong adsorption and orientation of PAA. As shown in the carbonyl and carboxylate region in Figure 5.12, the CH region shows Ca^{2+} to give enhanced signal over Mg^{2+}, although the difference between the Ca^{2+} and Mg^{2+} CH modes is smaller. This is likely due to the backbone CH group orientation having less dependence on the salts than the carboxylates, which are actually being bound by the salts. In addition to the CH modes, the broad water mode decreases slightly in intensity relative to the CH modes when going from 0.5 to 1 mM salt for both the Ca^{2+} and the Mg^{2+}. This indicates increasing the salt

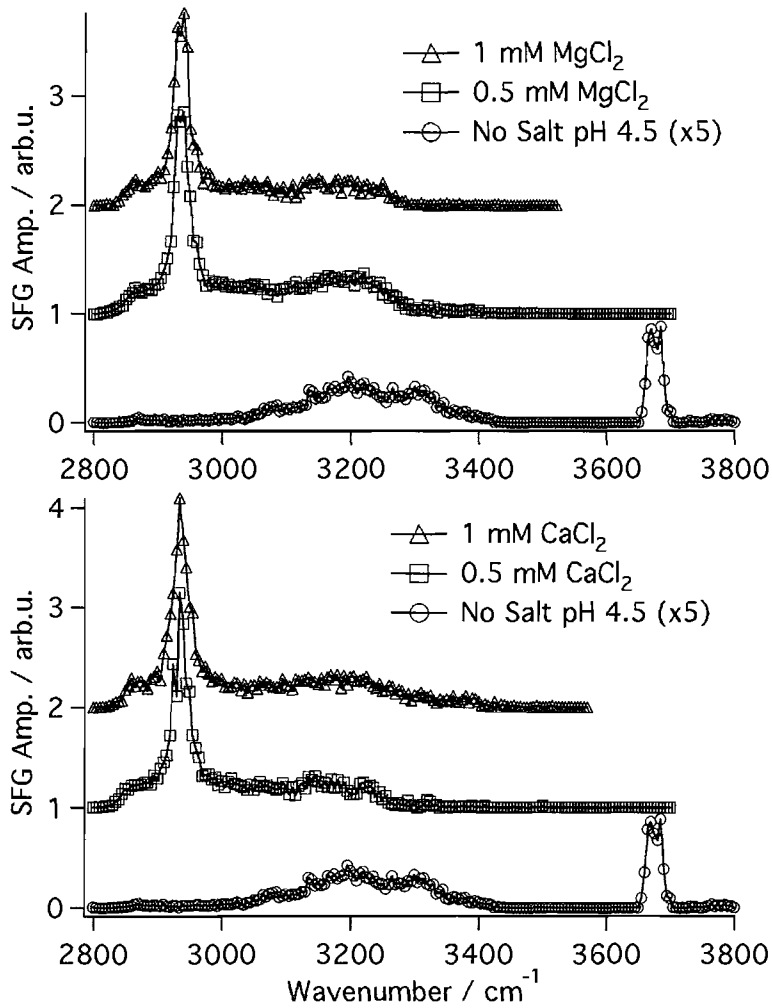

Figure 5.13.. VSFS of the water and CH region for Mg and Ca binding with PAA

concentration leads to fewer oriented water molecules in the interfacial region. This is due to charge neutralization of the polymer carboxylate anions via the binding of the cations, which acts to decrease the field strength that was a result of the anions at the interface.

Divalent salts generally have stronger binding to polyelectrolytes than monovalent salts[138]. This is due to the ability of the larger divalent ions to penetrate into the

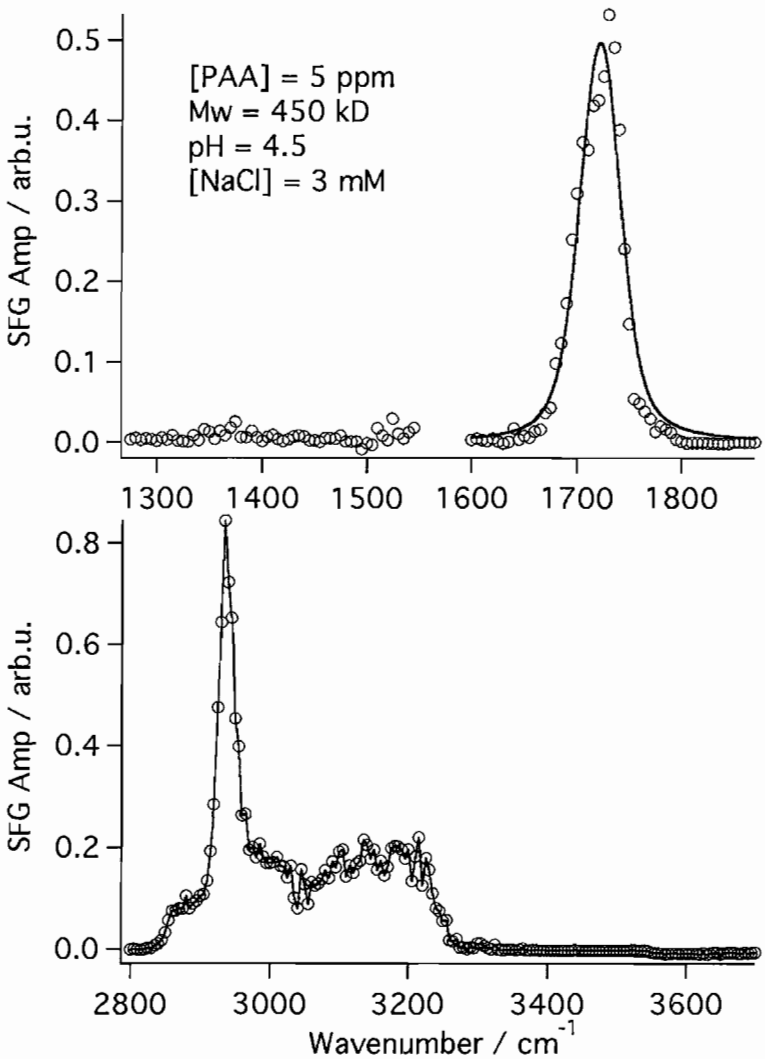

Figure 5.14. VSFS spectra of PAA (5 ppm, 450 kD) with NaCl (3 mM) at the CCl_4-water interface.

cylindrical symmetry of the polymer better than smaller monovalent ions[138]. To test the increased adsorption ability of PAA in the presence of divalent ions, and in particular the better binding ability of Ca^{2+} versus Mg^{2+}, Na^+ was added to PAA solutions to observe differences in adsorption characteristics. In Figure 5.14, it is observed that Na^+ does induce adsorption of PAA, however, based on the amplitudes

and presence of vibrational modes, it clearly does not drive PAA to the interface as strongly as Ca^{2+} or Mg^{2+}. From the carbonyl region, it is clear that Na^{+} does aid in adsorption, but the Na^{+} is not as effective at screening the charged carboxylate groups from one another because there is no signal observed from the carboxylate functional groups, indicating the carboxylates are still randomly oriented to produce a net cancellation of their contribution to $\chi^{(2)}$. This shows that monovalent ions at equivalent ionic strengths to divalent ions do not screen the charge of the carboxylate ion enough to allow orientation of this group at the oil-water interface. Due to the lack of screening provided by the Na^{+}, the charged groups must either be adopting opposing orientations along the backbone of the chain, or still be solvated as loops into the water phase. Further evidence of the decreased ability of Na^{+} to screen the carboxylates is found in the water region in Figure 5.14. There is increased water signal relative to the CH modes in Na^{+} than in either of the divalent ions, indicating the field at the interface is stronger due to a lack of screening of the charged carboxylates on the polymer.

From the data, it is clear that the addition of salt increases adsorption of PAA at a solution pH where there would otherwise be no adsorption. In addition, below the critical pH, maximum adsorption and orientation of the polymer occurs without any additional salt. Above the critical pH however, where there is initially no adsorption of PAA, divalent metal salts can induce both adsorption and strong orientation in both the carbonyl groups and the carboxylate groups, whereas monovalent salts only

induce orientation in carbonyl group. This is primarily due to the ability of the ions to screen the charges from one another along the backbone. For the divalent salts, the minimum energy conformation is no longer one of charges taking opposite sides of the chain or being randomly oriented, but rather one of the charged groups being oriented along the backbone in plane with the uncharged carboxylic acid groups. However, for the monovalent salts the charged carboxylates are not screened from each other and charge-charge repulsion still dominates the determination of the orientation of the carboxylate groups along the backbone.

Conclusions

In summary, the first experiments determining the adsorption and orientation characteristics of a polyelectrolyte at the neat oil-water interface using vibrational sum-frequency spectroscopy and interfacial tension measurements have been shown. This was accomplished by monitoring the carbonyl, carboxylate, methylene, and water vibrational modes with supplemental data coming from interfacial tension measurements using the pendant drop method. It was found that poly(acrylic acid) adsorbs to the interface under a very specific set of conditions, either below a critical pH, or in the presence of salt if above the critical pH. It was also shown that adsorption occurs as a multi-step process with a very fast initial adsorption which contains highly oriented polymer at the interface, followed by a slow loading of the subsurface region with additional poly(acrylic acid) that is not oriented and most likely in a random

coil. It was also found that variations in MW over a large range has little affect on the fast initial adsorption step, but does have a large affect on the long time scale buildup of polymer at the interface.

The implications of this work are two-fold. First, the fluid nature of interfacial biochemistry necessitates the study of biomolecules in an environment that mimics *in-vivo* conditions. The oil-water interface is an excellent way to probe these important systems, and this work shows how the interface can be used to this purpose. While many polyelectrolytes and biomolecules are well characterized in bulk solution, the conformation, adsorption properties, and dynamics can be quite different at the interface as shown in this work. The sharp transition for adsorption versus desorption at a critical pH demonstrates the differences between molecular properties in the bulk phase versus at the interface, particularly in the case where it was expected that neutral polyelectrolyte be in a random coil. This was clearly shown to not be the case at the oil-water interface, indicating that some of the same differences may be observed for biomolecules, particularly in areas where conformational changes may be taking place, such as with protein folding, or enzyme reactions. The second implication of this work is in the area of polyelectrolyte complexation. As previously stated, there exist a large number of studies on the complexation of polyelectrolytes with surfactants and nanoparticles. These complexes are often found to be surface active. However, the reason for the surface activity is often attributed to the complexed surfactant or particle. This work shows that the polyelectrolyte could

be responsible for the increased surface activity of such complexes, given that PAA is extremely surface active by itself. Where solution conditions weren't favorable for PAA adsorption, it was found that very small quantities of ions led to a large increase in surface activity, indicating that the binding of surfactants or particles to the polymer could be increasing the surface activity of the polymer. This work provides an important avenue of investigation for polymers at the oil-water interface and opens the door to studying macromolecules in an environment that is fluid on both sides of the interface, mimicking the true nature of biological and environmental systems.

CHAPTER VI

CONCLUSIONS

This dissertation described three independent research projects, each focusing on an aspect of adsorbates at the oil-water interface. The goal of the research was to further the understanding of significant chemical interfacial systems and open the door for future research on macromolecular assemblies at the oil-water interface using VSFS. Chapters III–V discuss carboxylic acid based surfactants, metal binding with the surfactants, and polymer adsorption. All the projects presented were able to define an interfacial picture that was previously unknown.

Na-dodecanoate was found to have a broad distribution of orientations at the oil-water interface, something not found at the air-water or solid-liquid interface. This was due to the variety of hydrogen bonding environments coordinating the headgroup, where the number of solvating water molecules that were directly hydrogen bonded to the headgroup had a strong effect on the orientation of the headgroup at the interface. It was concluded this unique distribution of orientations was due to the solvating effects of the oil phase on the alkyl chains. These results have not been observed at air-water due to the strong chain-chain interactions that occur at that interface, which force the chains and the headgroups to adopt a more narrow distribution of orientations.

From the conclusions drawn in chapter III about the interfacial structure of Na-dodecanoate, it was obvious that the oil-water interface was an ideal environment to study the binding of metal ions with carboxylate headgroups. The broad peak widths from the orientation and hydrogen bonding distribution were ideally sensitive to small changes in the headgroup binding and solvating structure. It was shown that a wide variety of divalent metal cations have very different effects on the orientation of the headgroup and the hydrogen bonding network. Mg^{2+} and Ca^{2+} were shown to have very similar effects on the headgroup and were bound in an electrostatic fashion. Mn^{2+} and Ni^{2+} were shown to have much stronger electrostatic interactions with the carboxylate headgroup, with the latter being the strongest interaction observed with electrostatic character. Cu^{2+} and Zn^{2+} were observed to have very different affects on the VSFS spectra. They did not narrow the distribution as much as Mn^{2+} and Ni^{2+} , but rather split the peaks significantly, a phenomenon indicative of covalent bi-dentate binding interactions. Thus the ions could be ordered in terms of their interaction strength with the carboxylate headgroup.

Finally, in chapter V, the knowledge from working with carboxylate surfactants was applied to macromolecules to study models of complex biological processes using poly(acrylic acid). PAA was found to desorb very quickly at a sharp transition pH. Below this transition pH, adsorption was constant, and above there was no adsorption of PAA. When adsorption did occur, it was found that the carboxylic acids of the polymer oriented strongly into the water phase and the CH groups along the backbone

were also very ordered. It was concluded the polymer was stretched out along the plane of the interface with the possibility of loops sticking into the water phase. It was also found that the adsorption process contained interesting dynamics. There was a fast initial adsorption step where polymer was strongly oriented, followed by a slow adsorption to the interfacial region of randomly coiled polymer that showed no increase in VSFS signal, but was apparent in the interfacial tension measurements. The addition of mono and divalent salts to PAA strongly altered the adsorption dependent pH properties and it was discovered that even at a pH above the critical pH of desorption, that PAA would adsorb strongly if salt was present. In addition, divalent salts were demonstrated to bind and orient the polymer significantly stronger than monovalent salts.

This dissertation shows vibrational sum-frequency spectroscopy is a powerful technique for advancing the knowledge of interfacial chemistry on a molecular level. The oil-water interface is inherently difficult to access with spectroscopic measurements and the experiments shown here have furthered our understanding of this complex and often unique environment. It is hopeful that this research will open the door to future studies of more biologically complex molecules at the oil-water interface, an environment that has particular relevance due to it's fluid nature across the interface.

BIBLIOGRAPHY

[1] Cacase, M. G.; Landau, E. M.; Ramsden, J. J. *Q. Rev. Biophys.* **1997**, *30*, 241.

[2] Morgan, P. W. *J. Macromol. Sci. Chem.* **1981**, *15*, 683.

[3] Millich, F.; Carraher, C. E.; Preston, J. *Interfacial Synthesis*; M. Dekker: New York, 1977.

[4] Boker, A.; Lin, Y.; Chiapperini, K.; Horowitz, R.; Thompson, M.; Carreon, V.; Xu, T.; Abetz, C.; Skaff, H.; Dinsmore, A. D.; Emrick, T.; Russell, T. P. *Nature Mat.* **2004**, *3*, 302–306.

[5] Rosen, M. J.; Wang, H.; Shen, P.; Zhu, Y. *Langmuir* **2005**, *21*, 3749–3756.

[6] Shannon, M. A.; Bohn, P. W.; Elimelech, M.; Georgiadis, J. G.; Marinas, B. J.; Mayes, A. M. *Nature* **2008**, *452*, 301–310.

[7] Bloembergen, N.; Pershan, P. S. *Phys. Rev.* **1962**, *128*, 606.

[8] Zhu, X. D.; Suhr, H.; Shen, Y. R. *Phy. Rev. B* **1987**, *35*, 3047.

[9] Guyot-Sionnest, P.; Hunt, J. H.; Shen, Y. R. *Phys. Rev. Lett.* **1987**, *59*, 1597.

[10] Donaldson, D. J.; Vaida, V. *Chem. Rev.* **2006**, *106*, 1445.

[11] Walker, D. S.; Richmond, G. L. *J. Phys. Chem. C* **2008**, *112*, 201–209.

[12] Lobau, J.; Wolfrum, K. *J. Opt. Soc. Am. B* **1997**, *14*, 9687–9690.

[13] Shen, Y. R. *Pure Appl. Chem.* **2001**, *73*, 1589–1598.

[14] Shen, Y. R. *The Principles of Nonlinear Optics*; Wiley: New York, 1984.

[15] Lambert, A.; Davies, P. B.; Neivandt, D. J. *Appl. Spect. Rev.* **2005**, *40*, 103–145.

[16] Bain, C. D. *J. Chem. Soc. Faraday Trans.* **1995**, *91*, 1281–1296.

[17] Bain, C. D.; Davies, P. B.; Ong, T. H.; Ward, R. N. *Langmuir* **1991**, *7*, 1563–1566.

[18] Moore, F. G.; Becraft, K. A.; Richmond, G. L. *Appl. Spectrosc.* **2002**, *56*, 1575–1578.

[19] Davies, J. T.; Rideal, E. K. *Interfacial Phenomena*, 2nd ed.; Academic Press: New York, 1963.

[20] Rosen, M. J. *Surfactants and Interfacial Phenomena*, 3rd ed.; Wiley: New Jersey, 2004.

[21] Freitas, A. A.; Quina, F. H.; Carroll, F. A. *J. Phys. Chem. B* **1997**, *101*, 7488–7493.

[22] Apostoluk, W.; Drzymala, J. *J. Colloid Interface Sci.* **2003**, *262*, 483–488.

[23] Oss, C. J. V. *Interfacial Forces in Aqueous Media*, 2nd ed.; CRC Press: Boca Raton, 2006.

[24] Naughton, M. A.; Dintzis, H. M. *Proc. Nat. Acad. Sci.* **1962**, *48*, 1822–1830.

[25] Checover, S.; Marantz, Y.; Nachliel, E.; Gutman, M.; Pfeiffer, M.; Tittor, J.; Oesterhelt, D.; Dencher, N. A. *Biochemistry* **2001**, *40*, 4281–4292.

[26] Rebhun, M.; Meir, S.; Laor, Y. *Environ. Sci. Technol.* **1998**, *32*, 981–986.

[27] Stathi, P.; Louloudi, M.; Deligiannakis, Y. *Environ. Sci. Technol.* **2007**, *41*, 2782–2788.

[28] Buschmann, J.; Kappeler, A.; Lindauer, U.; Kistler, D.; Berg, M.; Sigg, L. *Environ. Sci. Technol.* **2006**, *40*, 6015–6020.

[29] Kido, M. C.; Blower, P. G.; Richmond, G. L. *J. Phys. Chem. B* **2007**, *111*, 13703–13713.

[30] Russell, L. M.; Maria, S. F.; Myneni, S. C. B. *Geophys. Res. Lett.* **2002**, *29*, 1–4.

[31] Saxena, P.; Hildemann, L. M. *J. Atmos. Chem.* **1996**, *24*, 57.

[32] Tang, C. Y.; Allen, H. C. *J. Phys. Chem. A* **2009**, *113*, 7383–7393.

[33] Miranda, P. B.; Du, Q.; Shen, Y. R. *Chem. Phys. Lett.* **1998**, *286*, 1–8.

[34] Tyrode, E.; Johnson, C. M.; Rutland, M. W.; Day, J. P.; Bain, C. D. *J. Phys. Chem. C* **2007**, *111*, 316–329.

[35] Johnson, C. M.; Tyrode, E.; Kumpulainen, A.; Leygraf, C. *J. Phys. Chem. C* **2009**, *113*, 13209–13218.

[36] Gericke, A.; Huhnerfuss, H. *J. Phys. Chem.* **1993**, *97*, 12899–12908.

[37] Gurau, M. C.; Kim, G.; Lim, S.; Albertorio, F.; Fleisher, H. C.; Cremer, P. S. *Chem. Phys. Chem.* **2003**, *4*, 1231–1233.

[38] Rao, Y.; Subir, M.; McArthur, E. A.; Turro, N. J.; Eisenthal, K. B. *Chem. Phys. Lett.* **2009**, *477*, 241–244.

[39] Becraft, K. A.; Richmond, G. L. *J. Phys. Chem. B* **2005**, *109*, 5108–5117.

[40] Konek, C. T.; Musorrafiti, M. J.; Al-Abadleh, H. A.; Bertin, P. A.; Nguyen, S. T.; Geiger, F. M. *J. Am. Chem. Soc.* **2004**, *126*, 11754–11755.

[41] Schrodle, S.; Moore, F. G.; Richmond, G. L. *J. Phys. Chem. C* **2007**, *111*, 8050–8059.

[42] Winter, N.; Vieceli, J.; Benjamin, I. *J. Phys. Chem. B* **2007**, *112*, 227–231.

[43] Kutscher, J.; Gericke, A.; Huhnerfuss, H. *Langmuir* **1996**, *12*, 1027–1034.

[44] Johann, R.; Vollhardt, D.; Mohwald, H. *Coll. Surf. A* **2001**, *182*, 311–320.

[45] Johnson, C. M.; Tyrode, E.; Baldelli, S.; Rutland, M. W.; Leygraf, C. *J. Phys. Chem. B* **2005**, *109*, 321–328.

[46] Tyrode, E.; Johnson, C. M.; Baldelli, S.; Leygrad, C.; Rutland, M. W. *J. Phys. Chem. B* **2005**, *109*, 329–341.

[47] McFearin, C. L.; Richmond, G. L. *J. Phys. Chem. C* **2009**, *113*, 21162–21168.

[48] Watry, M. R.; Richmond, G. L. *J. Am. Chem. Soc.* **2000**, *122*, 875–883.

[49] Schlossman, M. L.; Tikhonov, A. M. *Annu. Rev. Phys. Chem.* **2008**, *58*, 153–177.

[50] Tikhonov, A. M.; Schlossman, M. L. *J. Phys. Chem. B* **2003**, *107*, 3344–3347.

[51] Conboy, J. C.; Messmer, M. C.; Richmond, G. L. *J. Phys. Chem.* **1996**, *100*, 7617–7622.

[52] Conboy, J. C.; Messmer, M. C.; Richmond, G. L. *Langmuir* **1998**, *14*, 6722–6727.

[53] Conboy, J. C.; Messmer, M. C.; Richmond, G. L. *J. Phys. Chem. B* **1997**, *101*, 6724–6733.

[54] Walker, R. A.; Gruetzmacher, J. A.; Richmond, G. L. *J. Am. Chem. Soc.* **1998**, *120*, 6991–7003.

[55] Walker, R. A.; Gragson, D. E.; Richmond, G. L. *Coll. Surf. A* **1999**, *154*, 175–185.

[56] Walker, R. A.; Conboy, J. C.; Richmond, G. L. *Langmuir* **1997**, *13*, 3070–3073.

[57] McFearin, C. L.; Beaman, D. K.; Moore, F. G.; Richmond, G. L. *J. Phys. Chem. C* **2009**, *113*, 1171–1188.

[58] Conboy, J. C.; Richmond, G. L. *J. Phys. Chem. B* **1997**, *101*, 983–990.

[59] Calvez, E. L.; Blaudez, D.; Buffeteau, T.; Desbat, B. *Langmuir* **2001**, *17*, 670–674.

[60] Kanicky, J. R.; Shah, D. O. *Langmuir* **2003**, *19*, 2034–2038.

[61] *Critical Micelle Concentrations of Aqueous Surfactant Systems*; Mukerjee, P., Mysels, K. J., Eds.; U.S. Dept. of Commerce: National Bureau of Standards: Washington, DC, 1971.

[62] Umemura, J.; Cameron, D. G.; Mantsch, H. H. *J. Phys. Chem.* **1980**, *84*, 2272–2277.

[63] Gericke, A.; Huhnerfuss, H. *Thin Solid Films* **1994**, *74*, 245.

[64] Gericke, A.; Mendelsohn, R. *Langmuir* **1996**, *12*, 758–762.

[65] Colthrup, N. B.; Daly, L. H.; Wiberley, S. E. *Introduction to Infrared and Raman Spectroscopy*; Academic Press: New York, 1964.

[66] Hore, D. K.; Walker, D. S.; Mackinnon, L.; Richmond, G. L. *J. Phys. Chem. C* **2007**, *111*, 8832–8842.

[67] Hore, D. K.; Walker, D. S.; Richmond, G. L. *J. Am. Chem. Soc.* **2008**, *130*, 1800–1801.

[68] Gragson, D. E.; Richmond, G. L. *J. Phys. Chem. B* **1998**, *102*, 569–576.

[69] Saito, T.; Koopal, L. K.; Nagasaki, S.; Tanaka, S. *Environ. Sci. Technol.* **2005**, *39*, 4886–4893.

[70] Ramos, M. A.; Fiol, S.; Lopez, R.; antelo, J. M.; Arce, F. *Environ. Sci. Technol.* **2002**, *36*, 3109–3113.

[71] Kretzschmar, R.; Sticher, H. *Environ. Sci. Technol.* **1997**, *31*, 3497–3504.

[72] Alvarez-Pueblo, R. A.; Calahorro, C. V.; Garrido, J. J. *Langmuir* **2004**, *20*, 3657–3664.

[73] Robertson, A. P.; Leckie, J. O. *Environ. Sci. Technol.* **1999**, *33*, 786–795.

[74] Christl, I.; Kretzchmar, R. *Environ. Sci. Technol.* **2007**, *41*, 1915–1920.

[75] Rey-Castro, C.; Mongin, S.; Huidobro, C.; David, C.; Salvador, J.; Garces, J. L.; Glaceran, J.; Mas, F.; Puy, J. *Environ. Sci. Technol.* **2009**, *43*, 7184–7181.

[76] Christl, I.; Milne, C. J.; Kinniburgh, D. G.; Kretzchmar, R. *Environ. Sci. Technol.* **2001**, *35*, 2512–2517.

[77] Porasso, R. D.; Benegas, J. C.; van den Hoop, M. A. G.; Paoletti, S. *Environ. Sci. Technol.* **2002**, *36*, 3815–3821.

[78] Teot, A. S.; Daniels, S. L. *Environ. Sci. Technol.* **1969**, *3*, 825–829.

[79] Weschler, C. J.; Mandich, M. L.; Graedel, T. E. *J. Geophys. Res.* **1986**, *91*, 5189–5204.

[80] D. Voet, C. W. P., J. G. Voet *Fundamentals of Biochemistry: Life At The Molecular Level*, 2nd ed.; John Wiley and Sons, Inc., 2006.

[81] Berg, J. M. *Annu. Rev. Biophys. Biophys. Chem.* **1990**, *19*, 405–421.

[82] Cotton, F. A.; Wilkinson, G.; Murillo, C. A.; Bochmann, M. *Advanced Inorganic Chemistry*, 6th ed.; John Wiley and Sons, Inc.: New York, 1999.

[83] Karlin, K. D.; Cruse, R. W.; Gultneh, Y.; Farooq, A.; Hayes, J. C.; Zubieta, J. *J. Am. Chem. Soc.* **1987**, *109*, 2688–2679.

[84] Sreedhara, A.; Cowan, J. A. *Biometals* **2002**, *15*, 211–223.

[85] Yazdanian, M.; Yu, H.; Zografi, G.; Kim, M. W. *Langmuir* **1992**, *8*, 630–636.

[86] Liu, M.; Kira, A.; Nakahara, H.; Fukuda, K. *Thin Solid Films* **1997**, *295*, 250–254.

[87] Du, X.; Liang, Y. *J. Phys. Chem. B* **2001**, *105*, 6092–6096.

[88] Kunda, S.; Datta, A.; Hazra, S. *Chem. Phys. Lett.* **2005**, *405*, 282–287.

[89] Datta, A.; Kmetko, J.; Yu, C. J.; Richter, A. G.; Chung, K. S.; Bai, J. M.; Dutta, P. *J. Phys. Chem. B* **2000**, *104*, 5797–5802.

[90] Ye, S.; Noda, H.; Nishida, T.; Morita, S.; Osawa, M. *Langmuir* **2004**, *20*, 357–365.

[91] Ren, Y.; Iimura, K.; Kato, T. *Langmuir* **2001**, *17*, 2688–2693.

[92] Du, X.; Liang, Y. *Langmuir* **2000**, *16*, 3422–3426.

[93] Moskovits, M.; Suh, J. S. *J. Am. Chem. Soc.* **1985**, *107*, 6826–6829.

[94] Lu, Y.; Miller, J. D. *J. Colloid Interface Sci.* **2002**, *256*, 41–52.

[95] Huhnerfuss, H.; Neumann, V.; Stine, K. J. *Langmuir* **1996**, *12*, 2561–2569.

[96] Ji, N.; Ostroverkhov, V.; Tian, C. S.; Shen, Y. R. *Phys. Rev. Lett.* **2008**, *100*, 0906102–1–4.

[97] Gragson, D. E.; Richmond, G. L. *J. Phys. Chem. B* **1998**, *102*, 3847–3861.

[98] Minasov, G.; Tereshko, V.; Egli, M. *J. Mol. Bio.* **1999**, *291*, 83–99.

[99] Moore, F. G.; Richmond, G. L. *Acc. Chem. Res.* **2008**, *41*, 739–748.

[100] Watry, M. R.; Richmond, G. L. *Langmuir* **2002**, *18*, 8881–8887.

[101] Tyrode, E.; Johnson, C. M.; Rutland, M. W.; Claesson, P. M. *J. Phys. Chem. B* **2007**, *111*, 11642–11652.

[102] Luo, G.; Malkova, S.; Yoon, J.; Schultz, D. G.; Lin, B.; Meron, M.; Benjamin, I.; Vanysek, P.; Schlossman, M. L. *J. Electro. Chem.* **2006**, *593*, 142–158.

[103] Benjamin, I. *Annu. Rev. Phys. Chem.* **1997**, *48*, 407–451.

[104] Taylor, K. C.; Nasr-El-Din, H. A. *J. Petrol. Sci. Eng.* **1998**, *19*, 265–280.

[105] Goddard, E. D. *J. Oil Chemists Soc.* **1995**, *71*, 1–16.

[106] Luthy, R. G.; Selleck, R. E.; Galloway, T. R. *Environ. Sci. Technol.* **1977**, *11*, 1211–1217.

[107] Rulison, C. *Water Soluble Polymers*; Plenum Press: New York, 1998.

[108] Rivas, B. L.; Pooley, S. A.; Pereira, E. D.; Maureira, A. *Macromol. Symp.* **2006**, *245*, 116–122.

[109] Bassaid, S.; Chaib, M.; Bouguelia, A.; Trari, M. *Reac. Func. Poly.* **2008**, *68*, 483–491.

[110] Morlay, C.; Cromer, M.; Vittori, O. *Wat. Res.* **2000**, *34*, 455–462.

[111] Kett, P. J. N.; Casford, M. T. L. .; Yang, A. Y.; Lane, T. J.; Johal, M. S.; Davies, P. B. *J. Phys. Chem. B* **2009**, *113*, 1559–1568.

[112] Kim, J.; Cremer, P. S. *J. Am. Chem. Soc.* **2000**, *122*, 12371–12372.

[113] Guzman, E.; Ritacco, H.; Ortega, F.; Svitova, T.; Radke, C. J.; Rubio, R. G. *J. Phys. Chem. B* **2009**, *113*, 7128–7137.

[114] Jaber, J. A.; Schlenoff, J. B. *Curr. Op. Coll. Inter. Sci.* **2006**, *11*, 324–329.

[115] Sukhishvili, S. A.; Granick, S. *J. Am. Chem. Soc.* **2000**, *122*, 9550–9551.

[116] Ulrich, S.; Laguecir, A.; Stoll, S. *Macromolecules* **2005**, *38*, 8939–8949.

[117] Wang, Y.; Zhang, Y.; Du, W.; Wu, C.; Zhao, J. *J. Colloid Interface Sci.* **2009**, *334*, 153–160.

[118] Lu, X.; Yu, Y.; Chen, L.; Mao, H.; Wang, L.; Zhang, W.; Wei, Y. *Polymer* **2005**, *46*, 5329–5333.

[119] Allahyarov, E.; Lowen, H.; Gompper, G. *Phys. Rev. E* **2003**, *68*, 061903.

[120] Das, R.; mills, T. T.; Kwok, L. W.; Maskel, G. S.; Millett, I. S.; Doniach, S.; Finkelstein, K. D.; Herschlag, D.; Pollack, L. *Phys. Rev. Lett.* **2003**, *90*, 188103.

[121] Cooper, C. L.; Dubin, P. L.; Kayitmazer, A. B.; Turksen, S. *Curr. Op. Coll. Inter. Sci.* **2005**, *10*, 52–78.

[122] Jewell, C. M.; Lynn, D. M. *Curr. Op. Coll. Inter. Sci.* **2008**, *13*, 395–402.

[123] Wiedmer, S. K.; Cassely, A.; Hong, M.; Novotny, M. V.; Riekkola, M. L. *Electrophoresis* **2000**, *21*, 3212–3219.

[124] He, J.; Niu, Z.; Tangirala, R.; Wang, J. Y.; Wei, X.; Kaur, G.; Wang, Q.; Jutz, G.; Boker, A.; Lee, B.; Pingali, S. V.; Thiyagarajan, P.; Emrick, T.; Russell, T. P. *Langmuir* **2009**, *25*, 4979–4987.

[125] Kwon, H. J.; Gong, J. P. *Curr. Op. Coll. Inter. Sci.* **2006**, *11*, 345–350.

[126] Ma, J.; Jiang, J.; Pang, S.; Guo, J. *Environ. Sci. Technol.* **2007**, *41*, 4959–4964.

[127] Avena, M. J.; Koopal, L. K. *Environ. Sci. Technol.* **1998**, *32*, 2572–2577.

[128] Duffy, D. C.; Davies, P. B.; Creeth, A. M. *Langmuir* **1995**, *11*, 2931–2937.

[129] Windsor, R.; Neivandt, D. J.; Davies, P. B. *Langmuir* **2001**, *17*, 7306–7312.

[130] Zhang, J.; Thomas, R. K.; Penfold, J. *Soft Matt.* **2005**, *1*, 310 318.

[131] Penfold, J.; Thomas, R. K.; Taylor, D. J. F. *Curr. Op. Coll. Inter. Sci.* **2006**, *11*, 337–344.

[132] Taylor, D. J. F.; Thomas, R. K.; Penfold, J. *Adv. Coll. Inter. Sci.* **2007**, *132*, 69–110.

[133] Katchalsky, A.; Miller, I. *J. Phys. Chem.* **1951**, *55*, 1182–1194.

[134] Ishimuro, Y.; Ueberreiter, K. *Coll. Polymer Sci.* **1980**, *258*, 928–931.

[135] Netz, R. R.; Andelman, D. *Phys. Rep.* **2003**, *380*, 1–95.

[136] Scatena, L. F.; Brown, M.; Richmond, G. L. *Science* **2001**, *292*, 908–912.

[137] Katchalsky, A.; Eisenberg, H. *J. Polym. Sci.* **1951**, *6*, 145–154.

[138] Oosawa, F. *Polyelectrolytes*; Marcel Dekker, Inc.: New York, 1971.

[139] Porasso, R. D.; Benegas, J. C.; van den Hoop, M. A. G. *J. Phys. Chem. B* **1999**, *103*, 2361–2365.

[140] Borkovec, M.; Koper, G. J. M.; Piguet, C. *Curr. Op. Coll. Inter. Sci.* **2006**, *11*, 280–289.

[141] Benegas, J. C.; Cleven, R. F.; van den Hoop, M. A. *Anal. Chim. Acta* **1998**, *369*, 109–114.

[142] Garces, J. L.; Koper, G. J. M.; Borkovec, M. *J. Phys. Chem. B* **2006**, *110*, 10937–10950.

[143] Dobrynin, A. V.; Rubinstein, M. *Prog. Polym. Sci.* **2005**, *30*, 1049–1118.

[144] Mattai, J.; Kwak, J. C. *Macromolecules* **1986**, *19*, 1663–1667.

[145] Morawetz, H. *J. Polym. Sci. B* **2002**, *40*, 1080–1086.